

AFIT/GM/ENP/98M-12

IMPROVING CAPE CANAVERAL'S DAY-2
THUNDERSTORM FORECASTING USING
MESO-ETA NUMERICAL MODEL OUTPUT

THESIS

Christian S. Wohlwend, Second Lieutenant, USAF

AFIT/GM/ENP/98M-12

Approved for public release; distribution unlimited

19980409038

The views expressed in this thesis are those of the author and do not reflect the official policy or position of the Department of Defense of the U.S. Government.

AFIT/GM/ENP/97M-12

IMPROVING CAPE CANAVERAL'S DAY-2 THUNDERSTORM
FORECASTING USING MESO-ETA NUMERICAL MODEL OUTPUT

THESIS

Presented to the Faculty of the Graduate School of Engineering

of the Air Force Institute of Technology

Air University

Air Education and Training Command

In Partial Fulfillment of the Requirements for the

Degree of Master of Science in Meteorology

Christian S. Wohlwend, B.S.
Second Lieutenant, USAF

March 1998

Approved for public release; distribution unlimited

IMPROVING CAPE CANAVERAL'S DAY-2 THUNDERSTORM
FORECASTING USING MESO-ETA NUMERICAL MODEL OUTPUT

Christian S. Wohlwend, B.S.

Second Lieutenant, USAF

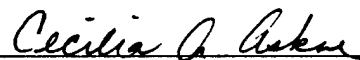
Approved:



Lt Col Michael K. Walters
Chairman, Advisory Committee

5 MAR 98

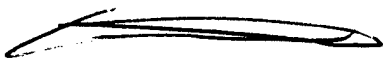
Date



Lt Col Cecilia A. Askue
Member, Advisory Committee

5 Mar 98

Date



Lt Col Glen P. Perram
Member, Advisory Committee

6 Mar 98

Date

Table of Contents

	Page
Acknowledgments.....	iii
Table of Contents.....	iv
List of Figures.....	vii
List of Tables.....	xi
Abstract.....	xii
1. Introduction.....	1
1.1 Overview.....	1
1.2 Background.....	3
1.2.1 Usefulness to the Air Force.....	3
1.2.2 Thunderstorm Generation.....	3
1.2.3 The NPTI.....	4
1.2.4 The Meso-Eta Model.....	5
1.3 Research Objectives.....	5
1.4 Research Approach.....	7
1.5 Summary of Results.....	9
2. Theoretical and Experimental Background.....	11
2.1 Overview.....	11
2.2 Thunderstorm Generation and Case Studies on Florida's East Coast.....	11

2.2.1 Sea Breeze Studies.....	12
2.2.2 Flow Regime Research.....	13
2.3 NPTI Prediction Technique.....	14
2.4 Numerical Modeling.....	17
2.4.1 Overview of the Meso-Eta Model.....	17
2.4.2 Meso-Eta's Operational Evaluation.....	21
2.5 Statistical Methods.....	22
3. Methodology.....	31
3.1 Overview.....	31
3.2 Data Acquisition.....	31
3.3 Meso-Eta Processing and NPTI Calculation.....	33
3.3.1 Meso-Eta Processing.....	33
3.3.2 NPTI Calculations.....	34
3.4 Statistical Calculations.....	38
3.5 Case Study Procedures.....	39
4. Results and Analysis.....	42
4.1 Overview.....	42
4.2 NPTI with Meso-Eta Results.....	42
4.3 NPTI Over Extended Period Results.....	47
4.4 Case Study Results.....	61
5. Conclusion and Recommendations.....	116
5.1 Overview.....	116

5.2 Conclusion.....	116
5.3 Recommendations.....	117
Appendix A. Code for NPTI Algorithm with Meso-Eta inputs.....	119
Appendix B. Example Control Card for Meso-Eta Variable Extraction.....	123
Appendix C. NPTI with Meso-Eta Data.....	149
Appendix D. Climatological Statistical Results.....	150
Appendix E. Example Output from the NPTI Code.....	153
Appendix F. Entire Climatological Statistic Results.....	157
Appendix G. Example Output from the NPTI Code.....	169
Bibliography.....	171
Vita.....	173

List of Figures

Figure	Page
Figure 1: Map of Florida showing the location of Cape Canaveral.....	2
Figure 2: Arakawa Semi-staggered E grid.....	18
Figure 3: Two-By-Two Contingency Table.....	23
Figure 4: Tangential Lambert Conformal Mapping.....	36
Figure 5: Graph of Accuracy Measures versus the Threshold Percentage.....	52
Figure 6: Graph of Bias versus Threshold Percentage.....	52
Figure 7: Graph of Accuracy Measures versus the Threshold Percentage, May.....	53
Figure 8: Graph of Bias versus Threshold Percentage, May.....	53
Figure 9: Graph of Accuracy Measures versus the Threshold Percentage, June.....	54
Figure 10: Graph of Bias versus Threshold Percentage, June.....	54
Figure 11: Graph of Accuracy Measures versus the Threshold Percentage, July.....	55
Figure 12: Graph of Bias versus Threshold Percentage, July.....	55
Figure 13: Graph of Accuracy Measures versus the Threshold Percentage, August.....	56
Figure 14: Graph of Bias versus Threshold Percentage, August.....	56
Figure 15: Graph of Accuracy Measures versus the Threshold Percentage, September..	57
Figure 16: Graph of Bias versus Threshold Percentage, September.....	57
Figure 17: Attributes diagram for the four independent years.....	59
Figure 18: Meso-Eta 500-mb Geopotential Heights for 22 September 1997.....	65

Figure 19: 500-mb Winds Over Florida, 22 September.....	66
Figure 20: 700-mb Winds Over Florida, 22 September.....	67
Figure 21: 850-mb Winds Over Florida, 22 September.....	68
Figure 22: 1000-mb Winds Over Florida, 22 September.....	69
Figure 23: 500-mb Q-vectors Over Florida, 22 September.....	70
Figure 24: 500-mb Q-vector Divergence Over Florida, 22 September.....	71
Figure 25: 500-mb Temperature, 22 September.....	72
Figure 26: 700-mb Temperature, 22 September.....	73
Figure 27: 850-mb Temperature, 22 September.....	74
Figure 28: 1000-mb Temperature, 22 September.....	75
Figure 29: 1000-mb Dew Point Temperature, 22 September	76
Figure 30: 700-mb Relative Humidity, 22 September.....	77
Figure 31: 850-mb Relative Humidity, 22 September.....	78
Figure 32: 1000-mb Relative Humidity, 22 September.....	79
Figure 33: Surface Map with Radar Overlay, 22 September.....	80
Figure 34: GOES East IR Satellite Image, 22 September.....	81
Figure 35: Meso-Eta 500-mb Geopotential Heights for 23 September 1997.....	82
Figure 36: 500-mb Winds Over Florida, 23 September.....	83
Figure 37: 700-mb Winds Over Florida, 23 September.....	84
Figure 38: 850-mb Winds Over Florida, 23 September.....	85
Figure 39: 1000-mb Winds Over Florida, 23 September.....	86

Figure 40: 500-mb Q-vectors Over Florida, 23 September.....	87
Figure 41: 500-mb Q-vector Divergence Over Florida, 23 September.....	88
Figure 42: 500-mb Temperature, 23 September.....	89
Figure 43: 700-mb Temperature, 23 September.....	90
Figure 44: 850-mb Temperature, 23 September.....	91
Figure 45: 1000-mb Temperature, 23 September.....	92
Figure 46: 1000-mb Dew Point Temperature, 23 September.....	93
Figure 47: 700-mb Relative Humidity, 23 September.....	94
Figure 48: 850-mb Relative Humidity, 23 September.....	95
Figure 49: 1000-mb Relative Humidity, 23 September.....	96
Figure 50: Surface Map with Radar Overlays, 23 September.....	97
Figure 51: GOES East IR Satellite Image, 23 September.....	98
Figure 52: Meso-Eta 500-mb Geopotential Heights for 24 September 1997.....	99
Figure 53: 500-mb Winds Over Florida, 24 September.....	100
Figure 54: 700-mb Winds Over Florida, 24 September.....	101
Figure 55: 850-mb Winds Over Florida, 24 September.....	102
Figure 56: 1000-mb Winds Over Florida, 24 September.....	103
Figure 57: 500-mb Q-vectors Over Florida, 24 September.....	104
Figure 58: 500-mb Q-vector Divergence Over Florida, 24 September.....	105
Figure 59: 500-mb Temperature, 24 September.....	106
Figure 60: 700-mb Temperature, 24 September.....	107
Figure 61: 850-mb Temperature, 24 September.....	108

Figure 62: 1000-mb Temperature, 24 September.....	109
Figure 63: 1000-mb Dew Point Temperature, 24 September.....	110
Figure 64: 700-mb Relative Humidity, 24 September.....	111
Figure 65: 850-mb Relative Humidity, 24 September.....	112
Figure 66: 1000-mb Relative Humidity, 24 September.....	113
Figure 67: Surface Map with Radar Overlays, 24 September.....	114
Figure 68: GOES East IR Satellite Image, 24 September.....	115

List of Tables

Table	Page
Table 1: Summary of Statistical Results.....	10
Table 2: NPTI Contingency Results.....	43
Table 3: Accuracy Measures, Bias, and χ^2 Test Results.....	44
Table 4: Skill Score Results.....	45
Table 5: Skill Scores Involving Other Reference Techniques.....	47
Table 6: Accuracy Measures and Bias for the 38 Percentile Threshold Level.....	48
Table 7: Accuracy Measures and Bias for the 50 Percentile Threshold Level.....	49
Table 8: Skill Score for the 50 and 38 Percentile Threshold Level Statistics.....	50
Table 9: The Brier Score and Ratio Skill Score statistics.....	58
Table 10a: Observed Relative Frequency per Forecast Probability Group.....	59
Table 10b: Observed Relative Frequencies for 50-95 Percent.....	59

Abstract

The 45th Weather Squadron (WS) is responsible for the protection of billions of dollars worth of Air Force and NASA equipment from weather hazards. They produce a seven day planning forecast as one tool to support the space launch community.

Improving this forecast can potentially save millions of dollars of government funds.

This research focuses on the feasibility of improving the day-two thunderstorm forecast by applying Meso-Eta numerical forecasts to the Neumann-Pfeffer Thunderstorm Index (NPTI). The NPTI is currently used by the 45th WS for same-day thunderstorm probability forecasting utilizing the morning radiosonde as input. The perfect prognosis assumption was used when assessing the value of this technique.

NPTI thunderstorm probabilities were calculated using input variables extracted from the day-two Meso-Eta . The NPTI output was verified against coincident thunderstorm observations taken at Cape Canaveral Air Station. Accuracy and bias statistics were used to calculate a forecasting skill score versus persistence. Statistically significant positive skill scores were produced, indicating that the proposed method is a potentially useful forecasting tool for day-two thunderstorm probability forecasting.

The skill of the same-day NPTI was also compared against persistence forecasts using a 20 year climatological data set. This comparison shows that the NPTI has marginal skill compared to persistence, particularly during northeast wind regimes.

I. Introduction

1.1 Overview

Since the advent of the computer, numerical models have been used to forecast the synoptic scale weather pattern. Improving the value of the output to forecasters and their customers is a major goal in the field of meteorological research. This research project involved analyzing possible improvements to operational forecasting of thunderstorms 24 hours in advance using Meso-Eta model output at Cape Canaveral Air Station (CCAS). It concentrated on applying the Neumann-Pfeffer Thunderstorm Index (NPTI) with Meso-Eta model output to analyze the value of using this combination to predict thunderstorms for the 24 hour forecast of the 45th Weather Squadron's seven day outlook (Neumann 1971). If the NPTI and Meso-Eta outperform persistence, they may be employed operationally by forecasters of the 45th Weather Squadron. The squadron is located at Cape Canaveral Air Station and Patrick Air Force Base (PAFB), Florida, and supports the United States Air Force (USAF) and the National Aeronautics and Space Administration (NASA) space launch programs (Roeder et al. 1997). See Figure 1 for the geographic location. Their forecasters are the primary customers of the results presented by this research. The hypothesis tested was that the Meso-Eta model has the ability to provide forecasted soundings which are comparable enough to the actual atmosphere for the NPTI to have a positive skill score versus persistence, thereby making it a valuable tool to forecasters.

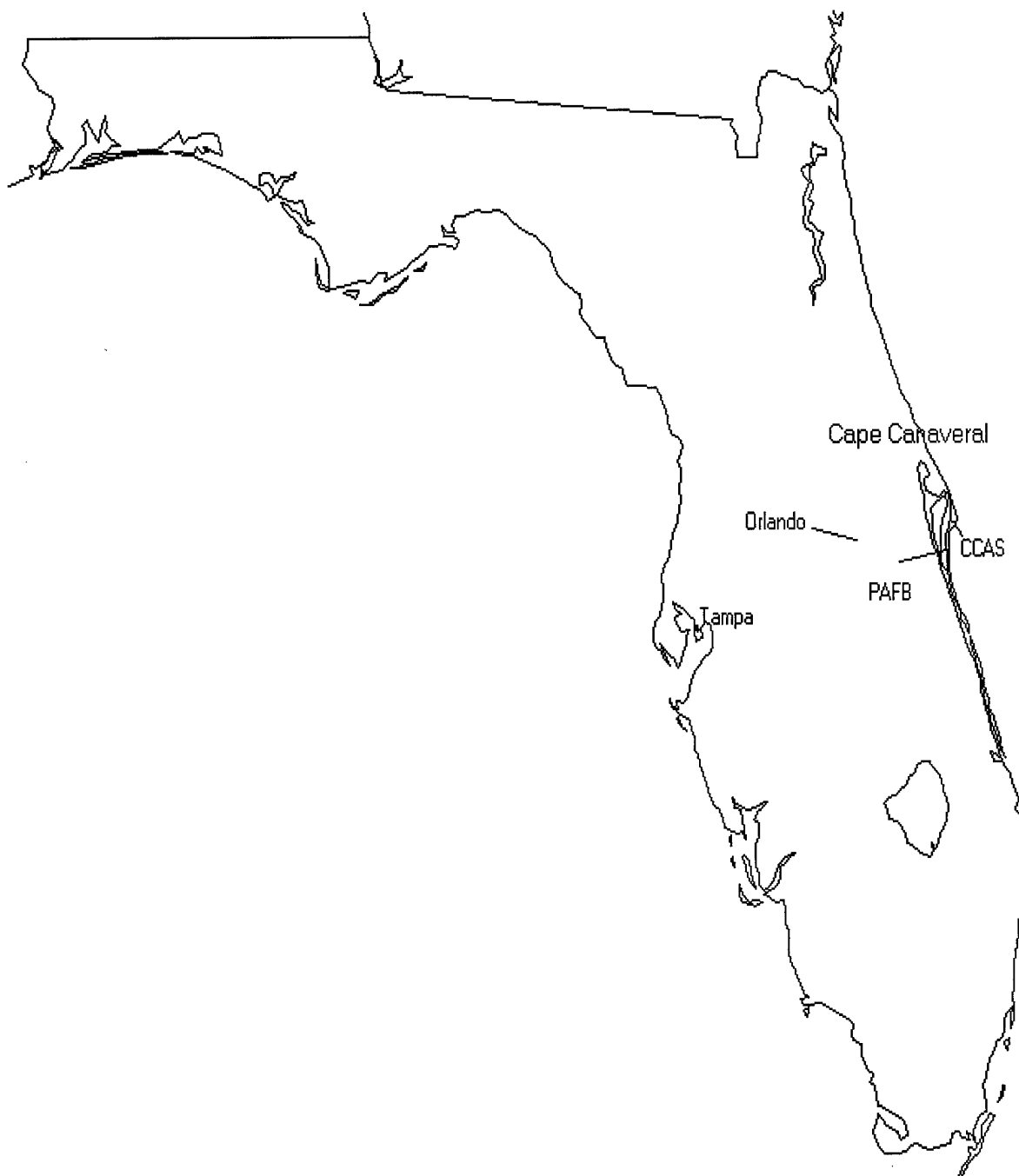


Figure 1. Map of Florida showing the location of Cape Canaveral. The general geographic features are shown with Cape Canaveral, the Air Force installations, and the major central Florida cities indicated.

1.2 Background

1.2.1 Usefulness to the Air Force. Cape Canaveral is on the central east coast of Florida and is home to the USAF's Cape Canaveral Air Station and NASA's Kennedy Space Center (KSC). The 45th Weather Squadron produces a seven day weather outlook that is used by these organizations for planning purposes. They also provide nowcasts in support of all space launch and shuttle landing missions. The 45th Weather Squadron is responsible for the protection of \$7 billion worth of government property from weather damage. This number does not include the enormous cost of the space vehicles or the close to \$1 million the government must spend to scrub a space shuttle launch. With over 30% of all space launch attempts being scrubbed or postponed due to weather, a better forecast would save taxpayer money (Roeder et al. 1997). The objective of this research was to improve the thunderstorm forecasting for day two of the seven day outlook by applying the NPTI with Meso-Eta model output. Improving their ability to forecast convective storms and lightning which hinder space launch missions will enable the operators to be primed for significant weather during the launch window. Due to the high cost of launching crafts into orbit it is very valuable for the space launch community to select the day with the highest probability for success.

1.2.2 Thunderstorm Generation. The major weather events during the summer months at KSC are thunderstorms. Due to its location in the lower subtropics with warm and moist conditions, Florida has more thunderstorms overall than anywhere else in the United States (Cetola 1997). A convective storm requires three main properties are present for formation: moisture, instability, and lift (Bluestein 1993). The complex

relationship between the synoptic patterns, mesoscale phenomena like the sea and river breezes, and the warm, moist atmosphere at Cape Canaveral provide the perfect location for convection to occur (Cetola 1997). The abundance of thunderstorms creates quite a challenge for forecasters to provide adequate predictions of days that meet the stringent space launch and shuttle landing criteria.

1.2.3 The NPTI. Forecasters supporting the space mission are currently using the Neumann-Pfeffer Thunderstorm Index to analyze daily morning soundings to predict the probability of thunderstorm occurrence (Neumann 1971). This index was developed from 1968 to 1971 through a statistical analysis of data over Cape Canaveral from 1951 to 1969. A statistical regression was performed to obtain an equation for the probability of thunderstorms with inputs to the index of regional climatology, the wind velocity at 850 mb and 500 mb, the relative humidity (RH) in the 800-mb to 600-mb layer, and the Showalter Stability Index (Neumann 1970). The Showalter Stability Index is an indicator of the static stability present in the atmosphere over one location, and is useful for predicting storms in regions with deep moist layers where convection is likely to occur (Bluestein 1993). The complete NPTI outputs a probability of convective storms and a “yes” or “no” forecast of thunderstorm occurrence. The NPTI is used to predict daily occurrence of thunderstorms utilizing the morning’s radiosonde sounding as input, but applying model generated soundings from the Meso-Eta to the NPTI had never been attempted. That is why this research tested the validity of applying the index with Meso-Eta model output for the 24 hour forecasted sounding of the 1500 UTC model run.

1.2.4 The Meso-Eta Model. The Meso-Eta is a numerical model that is run operationally by the Mesoscale Modeling Branch of the National Centers for Environmental Prediction's (NCEP) Environmental Modeling Center. This model is run at a 29-km horizontal resolution. The output is provided in the original 29-km format or the Advanced Weather Interactive Processing System (AWIPS) 40-km resolution, both of which are transmitted in GRIdded Binary (GRIB) format (NASA CR-205409 1997). The model output data necessary to perform a NPTI analysis is provided in both model output formats. There are 50 eta surfaces in the vertical, which are adjusted pressure surfaces with step-mountain topography. To obtain AWIPS format output the eta surfaces are then interpolated by NCEP to constant pressure surfaces that extend from 1000 mb to 50 mb in 25 mb increments plus special surface, 2-m, and 10-m levels (NASA CR-205409 1997). Other models may also provide valuable data for predicting thunderstorms, but the Meso-Eta's high resolution is the primary reason it was chosen to test the NPTI's forecasting ability. T. L. Black's 1994 paper, "The New NMC Mesoscale Eta Model: Description and Forecast Examples" from *Weather and Forecasting*, provides more information on the eta vertical coordinate and the Meso-Eta model.

1.3 Research Objectives

The Neumann-Pfeffer Thunderstorm Index is the current tool used by the 45th Weather Squadron for thunderstorm forecasting. It was specially designed for use at the Cape Canaveral launch facilities using multiple regression techniques (Neumann 1971).

That is why this research was restricted to using only the NPTI to get probabilities for convection, and not other prediction techniques which utilize stability indices.

The weather squadron has certain criteria that must be met for the warnings and advisories it issues. They include thunderstorms within 10 nautical miles (n mi) of PAFB, lightning within 5 n mi of PAFB, KSC, or CCAS, lightning within 25 n mi of CCAS, and many wind, rain, hail, funnel cloud, and temperature warnings all of which can be associated with severe thunderstorms (Roeder et al. 1997). These are important criteria to remember when trying to predict thunderstorms near Cape Canaveral.

As discussed earlier, other numerical models may prove valuable in predicting thunderstorms. Forecasters have the ability to choose from several different models in trying to provide an accurate prediction. The Air Force, Navy, and the NCEP all run models which try to predict the weather. Some of these models are grid point numerical models like the Eta, others are spectral models that use spherical harmonics (Haltiner and Williams 1980). This research used the high resolution grid point model of the Meso-Eta to provide a determination of the ability of this numerical model and the NPTI to predict convective storms over the Space Coast. Model output necessary to analyze the NPTI's prediction abilities was collected for August and September, 1997. This period is the later half of the primary convective season in eastern Florida, which extends from May through September (Neumann 1968). The sample size was adequate for a preliminary study to examine the ability of the Meso-Eta model to predict thunderstorms 24 hours in advance using the NPTI; however, a larger sample size will provide more information for the statistical analysis. After the NPTI's thunderstorm occurrence predictions were

obtained, they were statistically compared with the actual occurrence of thunderstorms at the station, or in the vicinity of the station, and a case study was performed to look for weather phenomena that may contribute to successful or unsuccessful forecasts. This research will conclude with the model supported NPTI's potential operational value to the 45th Weather Squadron's forecasters.

1.4 Research Approach

This research project used the model output at the levels described by Neumann to calculate the NPTI (1970). The perfect prog, or "perfect prognosis", assumption was necessary to directly input the model data into the algorithm. This assumption uses the variables calculated by the numerical model and assumes that they were perfectly forecast (Wilks 1995). To use the Meso-Eta variable in the algorithm a NCEP program was used which enables the user to extract data from the model output. Then, FORTRAN 77 code was written which would make the data usable in the NPTI algorithm. This code calculated the Showalter Stability Index and the NPTI using the model data as input. The output from the NPTI included a ten by ten grid of probability of thunderstorm occurrence and a yes or no thunderstorm forecast. This forecast was verified against the actual observations taken at CCAS and PAFB for the same time frame. A statistical analysis was conducted to confirm if the model is able to skillfully forecast day-two thunderstorm occurrence. The statistical analysis consisted of 2x2 contingency tables with accuracy and bias measures (Wilks 1995). A skill score was used to test the method against persistence (Wilks 1995). Persistence is a forecasting technique that uses today's

weather as the forecast for tomorrow. To determine the dependence or independence between the forecasts and observations in the contingency tables a χ^2 test was performed (Everitt 1992). The case study involved looking at the relationship between the dynamic weather events that day and forecasting ability. These case studies will add to the forecaster's ability to utilize this prediction tool. To increase the value of the case study the NPTI was run on approximately 20 years of upper air soundings taken at Cape Canaveral and scrutinized for the presence of any predictor or general trends in the algorithm which may make the NPTI less accurate under certain situations. This information was then used as a comparison tool in the case study of the NPTI output. The two case studies involved checking the synoptic and mesoscale events present in the model for any indication into why the NPTI incorrectly forecast the thunderstorm prediction for that day. A final comparison reviewed the incorrectly forecasted days, September 22, 23, and 24, for similar predictors for the missed forecast that may later be employed in interpreting the NPTI's forecast.

The results will show if the current NPTI applied to forecasted soundings from model output of the Meso-Eta models are accurate enough in predicting thunderstorms to be a useful tool for operational forecasters. A statistically significant skill in predicting thunderstorms means that forecasters potentially have another tool to use in their endless struggle to try to predict the chaotic behavior of Earth's atmosphere. An inconclusive result may indicate that this model and index do not provide the necessary accuracy to be useful indicators; however, other models and other indices may prove to be more useful in the future. On the other hand, inconclusive results may also indicate that a larger

sample size is need to obtain a valuable conclusion. The case study results provide more information into the biases and true forecasting ability of this combination. Whatever the conclusion, the 45th Weather Squadron has a first step in the direction of using numerical models as automated decision aides in forecasting the thunderstorms that plague warm season space launch.

1.5 Summary of Results

The NPTI applied with Meso-Eta output was tested for its ability as a forecasting technique for day two of the seven day planning forecast. To objectively verify its performance, a forecasting skill score versus persistence was developed. The findings of this research showed that the NPTI can be used with Meso-Eta output to produce a forecast which is able to outperform persistence.

The results from the NPTI algorithm indicated that it was able to predict a majority of the thunderstorms during the test period. Of the 32 day sample tested in this thesis, only five days were improperly forecast. Only one day was underforecast, which is defined as a thunderstorm occurrence that was not forecast; conversely, four days were overforecast. Even with the small sample size, the observations were found to be dependent on the forecasts through the χ^2 test. The statistics showed an accuracy level which exceeded the accuracy of persistence in all the measures except the probability of detection. Table 1 shows the accuracy and bias statistics along with their comparative skill score shown as a percent above or below the forecasting ability of the reference forecasting method of persistence. The hit rate (HR) describes the ability of the NPTI to

predict correct yes and no thunderstorm forecasts. The skill score of HR shows that overall the NPTI has the ability to provide an adequate forecast. The NPTI also provides a far better false-alarm rate (FAR) than persistence. The FAR, coupled with the good inverse false-alarm rate (FARN), show that the NPTI makes a lower percentage of mistakes than persistence. It is clearly visible, however, that the NPTI algorithm is much better at predicting days without thunderstorms than persistence. This can be seen through the huge difference in skill scores for threat score (TS) and inverse threat score (TSN) which is the ability of the algorithm to forecast clear days. The lower skill score of TS shows that it has some problems forecasting days with thunderstorm occurrence. The very low skill score for the probability of detection (POD) and the extremely high skill score for the inverse probability of detection (PODN) also indicate this. The NPTI also has a noticeable bias to underforecast. This could be a factor of the sample size or of the NPTI's algorithm not being designed for use with model output. Whatever the case, it can be seen that there is some potential in this method as a forecasting tool and further study into its ability is recommended.

Table 1. Summary of Statistical Results for NPTI with Meso-Eta inputs

	HR (%)	TS (%)	TSN (%)	POD (%)	POD N (%)	FAR (%)	FAR N (%)	Bias
NPTI	84.38	79.17	61.54	82.61	88.89	5	33.33	0.8696
Skill Score vs. persistence	13.37	3.43	26.58	-56.5	53.98	61.66	12.22	N/A

II. Theoretical and Experimental Background

2.1 Overview

Forecasting thunderstorms is a subject that has long been studied by meteorologists. This chapter will review the methods used by previous research into this phenomenon and theoretical concepts that apply to this project. The subjects addressed are thunderstorm generation and case studies of previous research, prediction techniques, numerical modeling, and the statistical methods applied to this research.

2.2 Thunderstorm Generation and Case Studies on Florida's East Coast

Thunderstorm generation involves the combination of synoptic scale and mesoscale features in a region that is primed for convection. All convective storms follow the basic principle that warmer air rises. The synoptic and mesoscale features that help to generate convection all involve the increasing of moisture, the instability of the region, and the forcing mechanisms associated with upward vertical motion. On Florida's East Coast, many of these factors exist on a very regular basis during the summer months. The most difficult indicator to successfully forecast is the forcing mechanism, which can include upper level flow, jetstreak circulations, and any type of frontal system.

This section focuses on some of the previous research work performed in the area of thunderstorm generation over the east coast of Florida to illustrate how flow regimes and breeze circulations affect thunderstorm generation. The interaction of the land/sea

interface creates thermally direct circulations known as the sea, river, and lake breezes that exist over this part of Florida and are an important forcing mechanism for thunderstorms. The other important phenomenon is the flow regime over this coastal location. The general direction of the low level wind field indicates the intensity and ability of convection to occur.

2.2.1 Sea Breeze Studies. The sea breeze interaction with the synoptic scale pattern and air over the landmass helps to induce convective storms. The low level convergence created by the sea breeze was found to occur at just the right time to coincide with the onset of afternoon convection (Byer and Rodebush 1948). This process of sea breeze dynamics was later numerically modeled three-dimensionally by Pielke (1974). This gave great insight into the features of the sea breeze circulation and the associated convergence. Recent work has been conducted on the climatology of the sea breeze over Cape Canaveral (Cetola 1997). This particular work adds knowledge of this forcing mechanism for the Cape Canaveral region. Cetola's research found that an onshore sea breeze was likely for any day with large scale flow that was not out of the northeast. It also found that river breezes tended to occur only when the large scale flow was weak. Convective storms occurred on 53 percent of days with a sea breeze, and were most common for days when the synoptic flow was from the southwest. It is important to note this when relating thunderstorm generation to flow regimes. Another important factor is the location of the convergence-generated convection with respect to the sea breeze front. In general, convergence occurred along the leading edge of the penetration of the sea breeze; however, a trailing convergence line was also found to exist behind the

sea breeze front under special situations. This trailing convergence zone is generated because the shape of Cape Canaveral induces northwesterly and southwesterly sea breezes which converge along an east-west running line instead of north-south like the sea breeze frontal convergence zone. This phenomenon was only noticeable on days with weak large scale flow (Cetola 1997). This knowledge will help to better predict the time and location of convergence and the duration of the convective outbreak.

2.2.2 Flow Regime Research. The direction of the large scale flow is important when trying to determine the potential for thunderstorm occurrence. One study performed for Cape Canaveral on this subject was done by Bauman, Kaplan, and Businger (1997) to help nowcast for easterly flow regimes. Using a sample data set of four days during the Convection and Precipitation/Electrification Experiment conducted in July and August of 1991, they were able to draw some interesting conclusions about the effects of different forcing mechanisms during easterly flow over Cape Canaveral (Bauman et al. 1997). It is especially difficult to forecast convective storms during an easterly flow regime since they can produce days with weather that varies from clear skies to organized thunderstorms. Generally onshore flow (easterly) creates less intense convection than the offshore flow because of the strength of convergence zones. Three types of days were classified for the easterly flow regime. They were the "active" days with weak synoptic scale forcing that resulted in strong sea breeze forcing along the convergence zones, the "passive" days with little convection which was generated by the existence of the sea breeze front with the synoptic pattern changing, and the "suppressed" days with stable lapse rates and low moisture which hindered convection. The

southwesterly flow contained a deep layer of moisture and accounted for nearly 66 percent of all lightning strikes at CCAS during this experiment. This research showed that not only did the low level flow regime matter to thunderstorm generation, but the synoptic scale pattern was also important. It found that the transverse circulations around the left entrance and exit regions of a jetstreak which create upward and downward vertical motion respectively aided in the convection (Bauman et al. 1997).

2.3 NPTI Prediction Technique

The more automated prediction techniques try to incorporate the most important factors involved in the process of thunderstorm generation. Some of these factors are used in the calculation of the NPTI. The 800-mb to 600-mb layer average relative humidity is a measure of the moisture above the marine layer and is an indicator of the level of static stability. The Showalter Stability Index is a good measure of the static stability present above the extremely moist marine layer. This is because the index uses the location of the lifted condensation level above 850 mb to calculate the parcel temperature at 500 mb if the parcel were lifted moist adiabatically. The 850-mb wind direction and speed indicate the flow regime that exists on the synoptic scale in the lower levels. This will show the general position of high and low pressure regions in relation to CCAS. The 500-mb wind shows the same results for the upper levels of the atmosphere. Finally, the climatology of the region describes an historical percent chance of thunderstorms during the summer season.

The index was created by Neumann in 1971 using a multiple regression technique that took into account nonlinear interactions between the variables. Data was used from Cape Canaveral soundings for the 13 years between 1957 and 1969 to obtain the resulting regression equations (Neumann 1971). A systematic study of over 250 variables including the winds, temperature, relative humidity, derived quantities like thickness, shear, layer means, and stability indexes, and climatology was conducted to determine the correlation between these factors and the occurrence of thunderstorms. The results included nine variables that had a large enough correlation to thunderstorm occurrence to investigate further. Those nine variables included the components of the 850-mb and 500-mb winds, the 800-mb to 600-mb mean relative humidity, the Showalter stability index, the day number, the 900-mb temperature and the 1000-mb to 850-mb thickness. Of these nine variables, all but the last two were included in the final probability equation. During the study it was discovered that the constants of the regression to the probability equation were dependent on the month of the year. Therefore, separate constants were calculated for the five warm season months, May through September. The final probability equation (Eq. 1) ended up being a linear combination of the five main factors:

$$P = C1 + C2 \cdot f(X1) + C3 \cdot f(X2) + C4 \cdot f(X3) + C5 \cdot f(X4) + C6 \cdot f(X5) \quad (1)$$

where, C_n , are the constants and:

X_1 = 850-mb wind in knots

X_2 = 500-mb wind in knots

X_3 = Mean relative humidity in the 800-mb to 600-mb layer

X_4 = Showalter stability index

X_5 = Day number

are the variables in the functions. The functions are regressions of the nonlinear dependence of each of the variables. The first function (Eq. 2) is the relationship of the winds at both 500 mb and 850 mb.

$$\begin{aligned} f(X) = & A_1 + A_2 \cdot u + A_3 \cdot v + A_4 \cdot u \cdot v + A_5 \cdot u^2 + A_6 \cdot v^2 + A_7 \cdot u^3 \\ & + A_8 \cdot u^2 \cdot v + A_9 \cdot u \cdot v^2 + A_{10} \cdot v^3 \end{aligned} \quad (2)$$

where the constants, A_n , are different regression constants than those from the overall probability equation. The second function (Eq. 3) provides similar calculations for the mean layer relative humidity again using different regression constants:

$$f(X_3) = B_1 + B_2 \cdot X_3 + B_3 \cdot X_3^2 + B_4 \cdot X_3^3. \quad (3)$$

The last two equations (Eq.4) are the Showalter stability index regression and the day number climatology regression. Both of these regressions resulted in quadratic equations with different constants:

$$f(X) = D_1 + D_2 \cdot X + D_3 \cdot X^2. \quad (4)$$

Where X is either X4 or X5 and the constants are varied depending upon the regression factor and the month. The final result was six simple equations that could use the data from the mornings sounding to predict a probability of thunderstorms (Neumann 1971).

2.4 Numerical Modeling

NCEP's Meso-Eta model was developed during the early 1990's from the lower resolution Eta model which has been operational at NCEP since the mid-1980's. The model includes dynamical and physical aspects that calculate the synoptic and mesoscale features of the weather over its area of operation. The forecasting ability of the model was reviewed by the Applied Meteorology Unit of the 45th Weather Squadron to test its functionality in forecasting weather phenomena at CCAS and KSC (NASA CR-205409 1997). Through their research, the biases and inaccuracies of the model output can be accounted for during the analysis process of the NPTI's performance using Meso-Eta model output.

2.4.1 Overview of the Meso-Eta Model. The Meso-Eta model derives its name from the high resolution of the grid and the vertical coordinate used in the model. The eta coordinate (Eq. 5) is an adjusted pressure surface designed to remain relatively horizontal, even in rough terrain. The surface is the level where eta

$$\eta = \left(\frac{p - p_t}{p_{sfc} - p_t} \right) \cdot \left[\frac{p_{ref}(z_{sfc}) - p_t}{p_{ref}(0) - p_t} \right] \quad (5)$$

is constant. In this equation p is the pressure, p_t is the pressure at the top of the domain, p_{sfc} is the surface pressure with z_{sfc} being the height of the lower boundary, and p_{ref} is

the pressure at a reference state which is a function of height above sea level. There are 50 vertical levels present in the model with increased resolution near the surface, which gradually reduces with height. An exception exists in the tropopause region, which has a bit greater resolution for better location of the boundary (Black 1994). Most of the prognostic variables are carried at the middle of each layer and calculated using the defined variables on each surface (Black 1994). The 29-km horizontal resolution allows the model to identify some mesoscale patterns. However, it is important to note that at least four grid points and usually six are required to accurately represent a wave in the model due to aliasing errors (Haltner and Williams 1980). The result of this fact is that the shortest wave accurately resolvable by the model is between 90 km and 150 km. The model uses a semi-staggered Arakawa E grid with different mass and velocity positions (Black 1994). In Figure 2, the H represents a mass point and the V represents a velocity point with d being the distance between adjacent H or V points. The value of d defined to be the 29-km model resolution.

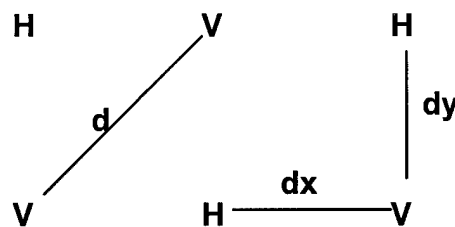


Figure 2. Arakawa Semi-staggered E grid.

To accommodate for rough terrain the model uses a method called step-mountain topography which finds an average level for the terrain over each horizontal grid space (Black 1994). The domain that is covered by this model includes all of the contiguous

United States as well as large portions of Canada and Central America on a tangential Lambert conformal grid mapping with the tangent line intersecting at 25N and the true meridian at 95W (Dey 1996). The AWIPS version of the model output was used in this research. NCEP interpolates the original 29 km output to a 40 km grid for easier dissemination in GRIB format (Black 1994). The model is run twice daily at NCEP with the initialization valid at the 0300 UTC and 1500 UTC with a six hour data ingestion around the initialization time.

Temperature, specific humidity, horizontal components of the wind, surface pressure, and turbulent kinetic energy are the major variables calculated by the model (Black 1994). To begin this procedure the model is initialized three hours prior to the model run by interpolating data from the spectral Aviation (AVN) model to the Meso-Eta horizontal and vertical grids which is combined with all the available data from the Global Assimilation System. This "first guess" undergoes a multi-variate Optimum Interpolation analysis to calculate the initial variables for the model run. This second step is repeated an hour and half later to update for new information; then the model is run. One of the problems with the initialization of the model that must be remembered when using the Meso-Eta is the need for a "run-up" time for the cloud model. This part of the model is not initialized using cloud water or ice; therefore, it requires time to reach saturation before precipitation will occur (Staudenmaier 1996b). This means that some physical effects are not fully developed in the early forecast hours of the model output.

The model includes some of the dynamics and physics that create the observed weather. They involve the use of the equations of motion, the continuity equation, and

others that take into account vertical motion and water and ice conservation. To limit gravity wave formation a forward-backward scheme is used (Black 1994). In order to calculate vertical advection a centered difference in space and Euler-backward time scheme is used for all quantities except specific humidity since physical aspects like precipitation and evaporation hinder its adjustment through strictly dynamical calculations. A piecewise linear method that calculates the moisture physics at each step overcomes the creation of false minima and maxima is used instead. Some of the important aspects of the physics in the model, which apply to this research, are the calculation of convective and grid scale precipitation as well as a cloud model (Black 1994). These are important because their presence as physical processes which affect the nature of the atmosphere being modeled are necessary in order to have accurate variables for input into the NPTI. It is essential to understand what aspects of the atmosphere are being modeled, so that an objective and informed look can be taken at the generation process of the input variables for the NPTI algorithm. The convective precipitation routine uses a parameterization scheme called the Betts-Miller cumulus parameterization (Staudenmaier 1996a). Model profiles are used to determine the type of convection possible and the physics involved. The model uses an explicit cloud water parameterization scheme, which uses the mixing ratios of water and ice to calculate the grid-scale precipitation (Staudenmaier 1996a). Of course, the most important aspect of the model for this research is whether it will be able to use all of the physics and dynamics schemes to accurately calculate the inputs to the NPTI and its thunderstorm prediction algorithm.

2.4.2 *Meso-Eta's Operational Evaluation.* The Applied Meteorological Unit's (AMU) contracted report about the usefulness of the Meso-Eta for supporting the weather needs of the space program provided valuable information about the model's general trends (NASA CR-205409 1997). The report discussed the verification of the model using both an objective and a subjective approach to diagnosing its strengths and weaknesses. The objective verification concluded that the model produces forecast soundings for the summer months which are generally drier and more stable than actually observed and misrepresents the height of the tropopause at CCAS (NASA CR-205409 1997). A statistically negative bias of the convective available potential energy and a positive bias of the lifted index, both of which indicate drier and more stable soundings, showed this. However, the results of their objective verification did not conclude whether the model was more accurate during the warm or cool season over east central Florida. They did notice that the errors were equally distributed by wind regime, easterly or westerly flow, during the four month study period; therefore, they did not stratify results based on the wind regime. The subjective verification, which included multiple case studies involving sea breeze circulations and thunderstorms, had more conclusive results about the ability of the model during these periods. They were able to see that the model still did not have the resolution necessary to incorporate the small mesoscale features of the sea, river, and lake breeze circulations, thunderstorm outflow boundaries, and other small features which are important for thunderstorm prediction over the Space Coast. The subjective case studies of warm season phenomena revealed that the thermally driven sea breezes were predicted by the model roughly 50 percent of the time

they were observed. They also showed that the Meso-Eta is able to predict organized convection, especially in the late afternoon, but cannot predict individual thunderstorm cells (NASA CR-205409 1997). These drawbacks in the model's performance aided in the research of the NPTI's performance, especially when dealing with thunderstorm probability acceptance criteria. The AMU's research helps to justify the lower threshold percentage for a 'yes' or 'no' forecast used in this research.

2.5 Statistical Methods

Statistics are essential to providing an adequate demonstration of the effectiveness of any forecasting technique. In order to define the forecasting value of the NPTI applied with the Meso-Eta model output, two-by-two contingency tables were used with bias, hit rate, threat score, probability of detection, and false-alarm rate for measures of accuracy. A forecasting skill score was also calculated to compare this method versus 24 hour persistence. The skill score tests the performance of this proposed tool for forecasting thunderstorms against persistence forecasting. To check the dependence between the forecast and the observations a χ^2 test was used. This test will indicate if the observations and the forecasts are related, which is necessary in order to prove that the contingency square was not created by random events, thereby giving the statistics validity.

		Observed		
		Yes	No	
Forecast	Yes	a	b	a + b
	No	c	d	c + d
		a + c	b + d	N = a+b+c+d

Figure 3. Two-By-Two Contingency Table

The contingency table, shown in Figure 3, takes into account all outcomes of a forecast test. The result of a perfect forecast would have $a + d = n$ with $b=c=0$ (Wilks, 1995). This would mean that the forecast perfectly matched the observations taken. However, very few forecasts are that accurate; therefore, we need to use tests that show the accuracy and bias of the forecast. These include hit rate (Eq. 6), which is the measure of how many forecasts were correct compared to the total number of forecasts (Wilks 1995). It can be calculated by:

$$HR = \frac{a + d}{N} \cdot 100 . \quad (6)$$

This equation describes the overall forecasting ability of the algorithm. Another measure of accuracy is the threat score (Eq. 7) or critical success index. This accuracy statistic measures the ability of the forecast to get correct “yes” forecasts. In the case of predicting thunderstorms, it is important for the operator to know when a “no” forecast is

believable. Therefore, the threat score can be redefined to calculate correct “no” forecasts as well (Eq. 8), which is the definition of the inverse threat score. These two threat scores can be calculated using the equations:

$$TS = \frac{a}{a + b + c} \cdot 100 \quad (7)$$

for a “yes” forecast, and

$$TSN = \frac{d}{b + c + d} \cdot 100 \quad (8)$$

for a “no” forecast. These statistics tell a forecaster what percent of “yes” or “no” forecasts are believable. These results are particularly important when looking at a case in which either the “no” or “yes” forecast dominates the forecast period. The probability of detection (Eq. 9) tells us the number of “yes” forecasts versus the number of “yes” observations. In mathematical terms, that is the $p(y_1 | o_1)$, which is the probability of thunderstorm occurrence, o_1 , given that it was forecast, y_1 . The calculation of this statistic involves using the following equation:

$$POD = \frac{a}{a + c} \cdot 100 \quad (9)$$

There is also a probability of detection for non-thunderstorm days (Eq. 10), which compares the number of “no” forecasts to the total number of “no” observations. This probability is called the inverse probability of detection and defined by the following equation:

$$PODN = \frac{d}{b + d} \cdot 100 \quad (10)$$

These statistics can be thought of as the individual hit rate for the "yes" or "no" forecast. Two other important quantities show the percentage of times the "yes" or "no" forecast failed. These measures are known as the false-alarm rate (Eq. 11) and the inverse false-alarm rate (Eq. 12). They let the forecaster know what percentage of "yes" and "no" forecasts are incorrect. They are represented by the equations

$$FAR = \frac{b}{a+b} \cdot 100 , \quad (11)$$

and

$$FARN = \frac{c}{c+d} \cdot 100 . \quad (12)$$

Now that the accuracy measures of the forecast have been discussed, the overall bias of the forecasting technique must be determined. To get this general feeling about the ability of the method we will use the fraction of "yes" forecasts to "yes" observations (Wilks 1995). The bias (Eq. 13) can be calculated from the following equation:

$$BIAS = \frac{a+b}{a+c} \cdot 100 \quad (13)$$

All of the accuracy and bias equations are shown in their percent probability form instead of a zero to one probability form. This form is used for all the statistics used in this research.

After the different measures of accuracy and bias have been calculated, they need to be compared to the reference forecasting method of persistence. Persistence forecasting involves taking the weather that is occurring today and forecasting that for tomorrow. Persistence is a good reference forecasting method because it represents a

minimal skill forecast. If a forecast method cannot outperform persistence, then it is not necessary to further consider that method. In order to test the NPTI's success versus persistence, all of the accuracy and bias measures will be calculated for the persistence method. Then a forecast skill score (Eq. 14) will be calculated for the NPTI versus persistence (Wilks 1995).

$$SS = \frac{A - A_{ref}}{A_{perf} - A_{ref}} \cdot 100 \quad (14)$$

In equation 12, A is a standard accuracy measure that is calculated for the forecast method and the reference method, which in this case is persistence. The variable A_{perf} is the value of the perfect forecast for the accuracy measure. Therefore, a positive skill score will show the percent improvement over the reference method of persistence, whereas, a negative skill score indicates that persistence is the more accurate method. This skill score will be calculated for each of the accuracy measures used in this research to get the broadest idea of the value of the NPTI forecasts.

Three other statistics were calculated to further the understanding of the algorithm's performance: the Heidke Skill Score, the Kuipers Skill Score, and the Brier Score (Wilks 1995). The Heidke Skill Score (Eq. 15) uses the hit rate as its accuracy measure, and compares versus the reference of a random forecast that has the same marginal distributions as the actual verification data set. This skill score has the same properties as a regular skill score, and can be calculated using the equation

$$HSS = \frac{2(ad - bc)}{(a + c)(c + d) + (a + b)(b + d)} \cdot 100 \quad (15)$$

The Kuipers Skill Score (Eq. 16), also known as the Hanssen-Kuipers discriminant, Kuipers' performance index, or the true skill score, is similar to a regular skill score using the hit rate as its accuracy measure with a reference random forecast which is restricted to be unbiased. This skill score can be calculated using the equation

$$KSS = \frac{ad - bc}{(a + c)(b + d)} \cdot 100 . \quad (16)$$

These two statistics were only used on the output of the NPTI with Meso-Eta inputs, since this was the main experiment in this research and are calculated to have a reference for future work on this subject. Finally, the Brier Score (Eq. 17) is a way of calculating the ability of the NPTI to forecast thunderstorm probabilities. This statistic uses the entire probability spectrum in the calculation. By defining an observed thunderstorm to be 95 percent forecast and a day without thunderstorms to have a 5 percent forecast, this method will compare the probabilities forecasted by the NPTI to these limits using the equation

$$BS = \frac{1}{N} \cdot \sum_k (y_k - o_k)^2 \quad (17)$$

where the symbol y_k is the forecast probability and o_k is the observation probability. The Brier Score is negatively oriented with zero being a perfect forecast and anything over zero being the relative imperfection of the algorithm. From the Brier Score we can obtain a ratio skill score (Eq. 18) which is a comparison of the calculated Brier Score to the Brier Score of a reference forecasting technique like persistence or climatology. The ratio skill score can be calculated using the equation

$$RSS = \frac{BS_{ref} - BS}{BS_{ref}} \cdot 100. \quad (18)$$

In order to give these statistics validity, a χ^2 test must be performed to show the dependence of the system. In a dependent system it is logical to investigate the causes of the association (Everitt, 1992). Without proving dependence, the results would be regarded as statistically insignificant. The test used was the Pearson's Chi Squared Test (Eq. 20). In order to calculate the chi squared, the expected value (Eq. 19) for each contingency must first be determined (Everitt 1992). The equation for finding the expected value is given by

$$E_{ij} = \frac{n_i \cdot n_j}{N} \quad (19)$$

where E_{ij} represents the expected value of the i,j block of the contingency table, n_i is the marginal sum of the i^{th} row, n_j is the marginal sum of the j^{th} column, and N is the total sum (Everitt 1992). The expected value can then be used to calculate the chi squared value as follows

$$\chi^2 = \sum_{i=1}^2 \sum_{j=1}^2 \frac{(n_{ij} - E_{ij})^2}{E_{ij}} \quad (20)$$

where n_{ij} is the value in the i,j block of the contingency table. The chi squared value can now be compared with the chi squared distribution to find a p-value for this distribution with one degree of freedom at a 0.05 significance level. The hypothesis is that there is no association, so a high chi squared indicates a failure. If the chi squared value is not less than the p-value given by the significance level then there is an association between the forecasts and observations. A chi squared greater than the p-value is the result desired by

this research because of the need for dependence. The issue of having too small of a sample size has been discussed by many mathematicians over the years and the greater than five expected value rule has been found to be more of a tradition than mathematical truth. Statisticians have shown that the χ^2 distribution is still valid for contingency tables when the cell expectation value in the smallest cell greater than 0.5. Thus the χ^2 test for independence may be used under these circumstances (Everitt, 1992). Because of this mathematical insight, it follows that this research has a basis in statistical theory and is valid to some extent as a result for the method being tested. However, a larger sample size will produce better results merely because it would be able to test an entire season or multiple warm seasons.

According to numerical weather prediction theory, in order to believe the statistics presented on the output from the NPTI algorithm, the "perfect prog" assumption had to be used. This assumption states that the output from a numerical model is a perfect forecast for the dynamic weather variables (Wilks 1995). This allows for the assumption that the variables being extracted for the model output have the value that they would have if measured during the morning sounding. Therefore, they can be used as a comparison to actual events.

These equations were shown in full detail, so that the results of this research can be fully understood and used as needed by weather forecasters at CCAS. These statistics will also be used to compare the performance of the NPTI on a climatological data set against persistence over that period. This is being done to investigate whether the NPTI has any trends, biases, or faults that can be used when interpreting the NPTI results with

numerical model input. When taken together these statistics will illustrate the value of the NPTI used with the Meso-Eta output. This is also useful for interpreting the same-day NPTI, so it will be of use even if the Meso-Eta NPTI does not have positive results.

III. Methodology

3.1 Overview

Research to improve the day two thunderstorm prediction involved the collection and use of Meso-Eta numerical model output and archived observations to compare the results of the NPTI algorithm's forecasting ability to that of persistence. The data used in this research was obtained through several different means. It was then converted into an array for each of the variables that were input into the NPTI algorithm. The NPTI was calculated on the array and transformed into a binary, 'yes' or 'no', forecast for CCAS. These results were then statistically compared to persistence. A case study was then conducted that involved the ability of the NPTI to predict thunderstorms over the entire 20 years of past data and an investigation of missed forecasts for a possible reasons for the poor performance.

3.2 Data Acquisition

There were two main sources for the data used in this research. The first was NCEP which uses its World Wide Web site for distributing model data. The second was the Air Force Combat Climatology Center (AFCCC) which has the responsibility of archiving all weather observations made at Air Force facilities. These two data sources were the only locations found during this research which were able to provide the necessary data to run the NPTI calculations.

The Meso-Eta data was retrieved directly from the NCEP data source on the World Wide Web. It was essential to archive it daily since no other major resource does so for the Meso-Eta. At approximately 1800 UTC daily the AWIPS version of the 24 hour forecast of the 1500 UTC model output was downloaded off of the web page in GRIB format and archived. This process began in early August and continued through September. Some data was lost during this time due to network errors, inconsistent updating of NCEP's web page, and local hard drive errors. This resulted in a limited number of useable days. The total data set consisted of 32 days with 13 in August and 19 in September. It is important to note that NCEP provides a warning stating that the web page is not to be used operationally to retrieve model output.

AFCCC was able to provide the observations from KTTS, which is the station identifier for CCAS, from an archive of station data. A thorough screening was done on the data to identify all days with reported thunderstorms and thunderstorms in the vicinity. This method was chosen as the comparison tool for the NPTI forecast because the use of ground observation is similar to the original method used by Neumann. This data was then examined for thunderstorm occurrence between 1000 UTC and 2200 UTC each day. The days with thunderstorms during this period for August and September, 1997, were marked as thunderstorm days, the others were not. This was the data used for comparison and creation of the persistence forecast. AFCCC also provided observations from approximately 20 years of archived data from the Cape Canaveral station. This was used to test the ability of the NPTI to forecast thunderstorms over a large time frame and in the case study conducted after the results were compiled.

3.3 Meso-Eta Processing and NPTI Calculation

The process of applying the Meso-Eta output to the NPTI algorithm was a major stepping stone in this research. The first goal was to extract the NPTI input variables from the Meso-Eta data. Then the ten by ten matrix of data points from around the station had to be partitioned from the entire map grid. The winds at these points were then rotated from map relative coordinates to Earth relative coordinates before they could be used in the calculations. The first calculation was finding the Showalter Stability Index from the model output. Then the mean layer relative humidity had to be calculated. Finally, the climatology was input as the date. This completed the set of input data needed for the NPTI. Forecast probabilities were calculated for each of the variables and the total thunderstorm probability at all the grid points in the matrix. Finally, the four nearest grid points were averaged to calculate the probability at CCAS. This was the resulting NPTI forecasted probability of thunderstorms.

3.3.1 Meso-Eta Processing. The Meso-Eta output was a single 30 MB file that included the entire 24 hour forecast with every level and all variables. This data had to be degribbed using a program called `unpkgrb1.x` designed by NCEP and downloaded from their server. The program could be manipulated using a hexadecimal control card method, which was described on a basic level in the code comments, to degrib specific variables and levels. This enabled the input variables of the NPTI to be extracted directly from the GRIB file. The variables included the 500-mb temperature, the 850-mb temperature, and the 850-mb dew point temperature which had to be used to calculate the Showalter Stability Index. The other variables extracted were the 600-mb through 800-

mb relative humidity, the 500-mb u and v components of the winds, and the 850-mb wind components. A total of 16 Meso-Eta output variables represented on the entire map projection were saved as the input file to the FORTRAN code which used them to calculate the five NPTI input variables. The code then calculate the complete NPTI forecast.

3.3.2 NPTI Calculations. The code written for this research had to take the 185 by 129 grib point on a tangential Lambert conformal map and reduce it down to a reasonable ten by ten grid around central Florida in order to save computation time. It was also required to run all calculations necessary to get a thunderstorm probability forecast for CCAS using the NPTI algorithm. The code was named eta_a.f and was programmed to run on a 'SPARK 20' SUN workstation. The NPTI algorithm was adapted to accept the entire ten by ten grid and was translated directly from the appendix of the original paper written by Neumann in 1971. This adapted code was included as the main subroutine in the eta_a.f program. The other subroutines involved constructing the ten by ten matrix, calculating the Showalter Stability Index , calculating the 800-mb to 600-mb layer mean relative humidity, and rotating the u and v wind components.

The construction of the ten by ten matrix involved examining the latitude and longitude of each grid point from a chart constructed at NCEP to find a reasonable array of points that would include the entire Cape as well as some inland and Atlantic Ocean area. The ten by ten grid had its corners at the points (136,37), (136,28), (145, 28), (145,37) starting with the upper left hand corner and moving counter clockwise around the square. This was done to lessen the number of calculations and the time needed to

run the program as well as keep a fairly large grid which may enable forecasters to get an idea of nearby thunderstorm probabilities. The problem with this method is that the regression of the variables in the NPTI was done exclusively at Cape Canaveral to assist in space launch forecasting and was not designed for use in the surrounding locations. However, it does give an idea as to the probability of thunderstorms in the area. The inputs to the NPTI do not identify any specific mesoscale features, so it is reasonable to extend the NPTI algorithm to the immediate area. Only synoptic scale thunderstorm generation factors are taken into account in the NPTI algorithm.

The Showalter Stability Index calculations were based on numerical calculations instead of the traditional graphical method. This code used the 850-mb temperature and dew point temperature to find a Lifted Condensation Level (LCL) where the potential temperature could be calculated. The potential temperature indicates the moist adiabat that was followed up to the 500-mb level to obtain the parcels 500-mb temperature. The parcel temperature was then subtracted from the environmental temperature to calculate the Showalter Stability Index. A negative number for the Showalter Stability Index is considered unstable whereas a more positive number is more stable. In order to find the parcels temperature at 500 mb, an iterative numerical method scheme was used which stepped through the calculations until it found a temperature which had a matching potential temperature to the one calculated at the LCL. This method was taken from the Air Weather Service (AWS) standard programming guide, AWS/TR-83/001, Equations and Algorithms For Meteorological Applications in Air Weather Service (Duffield and

Nastrom 1983). The numerically derived temperature was then used in the calculation of the Showalter Stability Index by subtracting it from the actual temperature at 500 mb.

A rotation of the u and v components of the wind at both 500 mb and 850 mb had to be accomplished in order to move from a map relative coordinate system to an Earth relative system. This was done using the inverse of the equations used by NCEP to move to map relative coordinates which was found on NCEP's web page. The Lambert comformal map projection is a conic section that projects the Earth on a secant cone. The projection used by the Meso-Eta moves the projection from a secant cone to a tangential cone. This means that the cone only touches the Earth along a single line instead of entering and exiting the surface of the Earth. See Figure 4 for an geometric illustration of the tangential map projection (Montz and Sloane 1943).

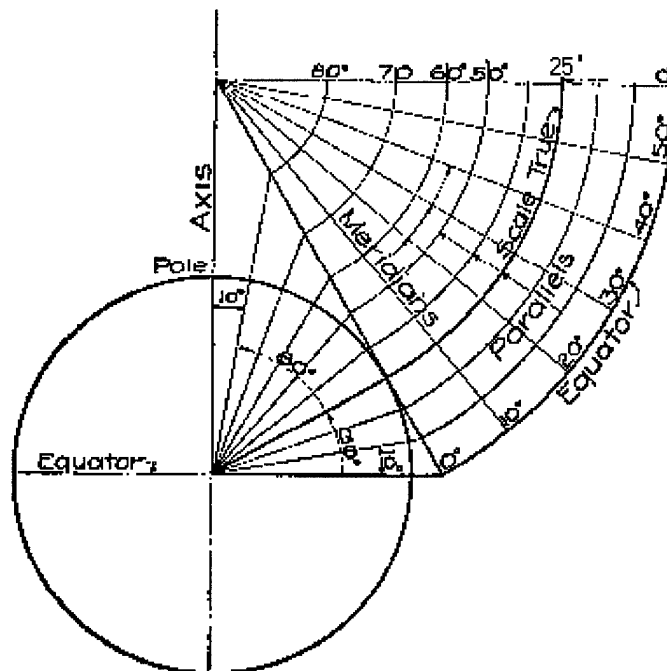


Figure 4. Tangential Lambert Comformal Mapping adapted from *Elements of Topographic Drawing* by Montz and Sloane.

The final subroutine was one designed to calculate the layer mean relative humidity in the 800-mb to 600-mb layer. This was done using a log pressure weighted averaging scheme. The value of the higher pressure levels were weighted more heavily in the average than the lower pressure levels since pressure levels are logarithmically separated. This technique was taken from the AWS/TR-83/001 standard programming guide (Duffield and Nastrom 1983). Finally, because of the location of CCAS, the four points, (140,33), (140,32), (141,32), (141,33), are averaged to find the thunderstorm probability.

The data extracted from the Meso-Eta model and the calculations all had to be check for quality to ensure that the proper numbers were being input into the NPTI code. To check the quality of the Meso-Eta model, the data extracted was put into graphical form in GrADS and visually check to see if the data had reasonable values and synoptic structure. The Showalter Stability Index results were compared using the SHARP sounding generating program. This was done using both real-time data and data extracted from the Meso-Eta model output being run through SHARP and the code used in this research. The layer averaging and rotation matrix codes were check through manual calculations which resulted in very similar answers. Quality control was very necessary in the initial programming phase.

The ultimate outcome of the code was to develop a way to find the thunderstorm probability calculated for the weather station at CCAS. The methods described above were the building blocks to the NPTI code. They were necessary in order to have the

correct inputs to Neumann's algorithm. Once the data processing was complete, the NPTI probabilities were output to set of files that were used as the input to the statistical calculations.

3.4 Statistical Calculations

The process of evaluating the results of the experiment involved an extensive set of statistical calculations. A perfect prog assumption, which states that the output from the numerical model is a perfect forecast for the variables being used in the NPTI code, was required to believe the results from the NPTI forecast (Wilks 1995). This implies that the value output by the model is the same as the value if it were measured during the morning sounding. Therefore, the accuracy and bias statistics show how well those "perfect" variable's forecast. A two-by-two contingency square was used as the basis of the statistics to evaluate the NPTI's worth with model data inputs. A FORTRAN code was used to compare the NPTI forecast percentages to the two months of observation data. This code built the contingency tables and calculated the accuracy and bias statistics as well as the skill score which were described in chapter two. A threshold percentage had to be found in order to compare the binary results in the contingency square. The threshold percentage was judged to be best if set at 30 percent. The two most common methods of setting threshold percentages are to choose the percentage that generate an unbiased forecast or the percentage which has the maximum threat score (Wilks 1995). The maximum threat score method was chosen even though it underforecasts. The justification for using a percentage below 50 was given by the

statistical method and the AMU's review of the performance of the Meso-Eta over CCAS. They found that the Meso-Eta was consistently drier and more stable than the actual atmosphere. For this reason the 30 percent threshold percentage was used. To calculate the remaining statistics, Statistix 1.0 was used. It calculated the Pearson χ^2 and its associated p-value to check the dependence of the observations to the forecast. The same accuracy, bias, and skill score statistics were also run for persistence as a comparison for the NPTI results. Persistence was forecasted using each days weather from the observations as the forecast for 24 hours later. If the NPTI algorithm were not able to outperform persistence, then it would be logical to assume that the Meso-Eta output used in the NPTI is not a useful forecasting tool. The final results of the statistics prompted further study into why four days were underforecast and one day was overforecast.

3.5 Case Study Procedures

Case study was used to look for trends that might describe the reasoning behind the forecast errors. The first part of the study centered around using the NPTI on the 20 years of data to see if the NPTI had a regime where it did not perform well. The other part of the case study examined the model, observations, and satellite data to see if there was a trend that could account for the missed forecasts in three of the overforecast days.

The NPTI algorithm was used in the first part of the case study to look for general trends in its effectiveness during days with different wind directions. As discussed by Bauman, Cape Canaveral forecasters have a difficult time predicting thunderstorms under easterly flow regimes (1997). To investigate the ability of the NPTI during different flow

regimes the 20 years of data was separated by the direction of the 850-mb winds in four categories. These four regimes were the northeast (1-90 degrees), northwest (271-360 degrees), southeast (91-180 degrees), and southwest (181-270 degrees). These different regimes as well as the entire 20 years were then run through a simplified NPTI code, the statistics were generated, and the results were compared to persistence for that time period. These 20 years were the results of rigorous matching of the radiosonde and observation data from almost 50 years of archived data. This showed some general trend of the NPTI's ability to forecast thunderstorms and particularly its poor performance during northeasterly wind flow.

The other part of the case study was conducted using the GrADS program. This program shows meteorological data in a simple and logical map layout. Using NCEP's wgrib and grib2grads programs the raw Meso-Eta model output was converted into GrADS format. This enabled research to be conducted on the meteorological phenomenon present in the model on the days when the forecasts were incorrect. Charts were constructed that showed the 1000-mb winds, relative humidity, temperature, dewpoint, the 850-mb and 700-mb winds, relative humidity, and temperature, and the 500mb winds, geopotential height, temperature, Q-vectors, and Q-vector convergence over Florida. The case study focused on the 24 hour forecasts for September 22, 23, and 24, which were all underforecast. The meteorological charts developed were to show the general trends of the atmosphere on the those days to see if the NPTI algorithm was missing an important event that either caused or stifled thunderstorm occurrence. These charts were compared to the actual ground observations for those days and the 1200 UTC

satellite pictures. This was an attempt to check if the model poorly initialized on these days, thereby, resulting in incorrect inputs to the NPTI algorithm which would trigger a missed forecast. The analysis field for the Meso-Eta model was not downloaded when the 24 hour forecast field was downloaded; however, the models performance can be judged using the observations and satellite images. All of this further research was investigating possible ways to increase the performance of forecasters utilizing the forecast of the Meso-Eta output NPTI algorithm to predict thunderstorms.

IV. Results and Analysis

4.1 Overview

This research began as an attempt use the NPTI algorithm with input data from the Meso-Eta numerical model to produce useful day two thunderstorm forecasts. The research expanded to include an attempt to improve that process and investigate the overall forecasting ability of the NPTI. The data obtained from this research will be presented for the scrutiny of the reader in order to prove that this method is a viable forecasting method for the time frame indicated. The results also present an examination of the forecasts missed by the NPTI algorithm, which includes a climatological NPTI study and a case study of the days with, missed forecasts.

4.2 NPTI with Meso-Eta Results

The NPTI algorithm was designed to predict thunderstorm forecasts using daily soundings. Now the Meso-Eta output has been applied to the NPTI algorithm for prediction of thunderstorms one day in advance. To illustrate the value of this method, a statistical analysis was conducted which utilized a two-by-two contingency matrix method. This allowed for calculation of the accuracy and bias of the method. The accuracy measure result were then compared versus persistence in order to obtain the skill scores. This enabled some conclusions to be drawn on the ability of the NPTI code to predict thunderstorms using the Meso-Eta 24 hour forecast as input. The following tables briefly explain the results of the statistics and the NPTI's general forecasting ability.

Table 2. NPTI Two-By-Two Contingency Table Results.
A, B, C, D, and N are the values for the corresponding blocks
in the contingency table. Percent is the threshold percentage
used in the calculations.

	A	B	C	D	N	Percent
Total NPTI	19	1	4	8	32	30
Persistence	40	6	5	10	61	N/A
August	9	0	2	2	13	40
September	8	0	4	7	19	30

The contingency table produced by the NPTI results showed that the NPTI had a fair handle on the general condition of the atmosphere during the test period. Table 2 shows that, of the 32 days in the sample, it only incorrectly forecast 5 days. In Table 2, the letters designate the corresponding block in the contingency table illustrated in Figure 3. The last column in the chart is the threshold percentage used to convert the probability forecast into a binary forecast that could be used in the contingency table. The NPTI statistics were subsequently split into separate months to investigate the performance by month. The sample size of the monthly separations is statistically insignificant; there were not enough days in the sample to find independence. However, the results of the monthly data were quite interesting, so they have been presented in the following discussion. In the averaging process, standard deviations were calculated, but there was no significant correlation between the value of the standard deviation and the forecast ability of the NPTI. The results are reviewed in Appendix C.

Table 3. Accuracy Measures, Bias, and χ^2 Test Results

	HR (%)	TS (%)	TSN (%)	POD (%)	PODN (%)	FAR (%)	FARN (%)	Bias	χ^2	P- Score
NPTI	84.38	79.17	61.54	82.61	88.89	5.00	33.33	0.8696	14.11	0.0002
Persist	81.97	78.43	47.62	88.89	75.86	13.04	39.82	1.0222	16.81	0.0000
Aug	84.62	81.82	50.00	81.82	100	0.00	50	0.8182	N/A	N/A
Sep	78.95	66.67	63.64	66.67	100	0.00	36.36	0.6667	N/A	N/A

The accuracy measures, bias, and χ^2 test results are presented in Table 3. The χ^2 clearly shows that the sample size is adequate for a preliminary study on the ability of the NPTI to predict day-two thunderstorms. Both the NPTI results and the persistence results were found to have dependence between the forecasts and the observations. The accuracy percentages show that the NPTI was able to outperform persistence over the test period. The only statistic that is not better than persistence is the probability of detection. The 45th Weather Squadron indicated that the most important indicator of success, because of its overall statistical nature, was the threat score (TS), or critical success index. The threat score shows a 3.43 percent increase in forecasting ability over persistence, shown by the skill score (TS SS) in Table 4. This is evidence that there is some value in this procedure, but further study into improving the method is necessary if it is to become an operational technique.

From the skill score results we can see some trends of the NPTI algorithm. In general, the NPTI is able to outperform persistence. This is particularly true for days without thunderstorms. The high skill score of the inverse threat score (TSN SS) and the

Table 4. Skill Score Results

	HR SS (%)	TS SS (%)	TSN SS (%)	POD SS (%)	PODN SS (%)	FAR SS (%)	FARN SS (%)
Total NPTI	13.37	3.43	26.58	-56.53	53.98	61.66	12.22
August	14.70	15.72	4.54	-63.64	100	100	-25.57
September	-16.75	-54.52	30.58	-200	100	100	8.69

inverse probability of detection (PODN SS), which is similar to a hit rate for non-thunderstorm days, coupled with the low skill score for the probability of detection (POD SS), which is how well it found thunderstorms, indicates that the NPTI has much less trouble forecasting for days without thunderstorms than persistence. The incredibly high skill score for the false-alarm rate (FAR SS) is another indicator of this fact because the FAR is a measure of how many times it overforecast. That is why the inverse false-alarm rate (FARN) is so much higher than the FAR. The four days that the algorithm underforecast are much more noticeable in the statistics. Therefore, it is fairly safe to conclude that the NPTI algorithm is able to predict non-thunderstorm days fairly accurately. However, it must be remarked that not all of the days where a thunderstorm is not forecast are going to be clear, as seen by the comparatively low probability of detection. This is more critical for mission success because an incorrect "no" forecast could cause the loss of millions of dollars and possibly endanger crews, whereas, an incorrect "yes" forecast is just a missed opportunity. This would indicate that improving this method should result in an increased inverse false-alarm rate skill score (FARN SS), an increased POD SS, an increased hit rate skill score (HR SS), and the most important

measure to increase is the TS SS. Overall, the method has a sound statistical basis and can slightly outperform persistence for forecasting either weather phenomena as seen by the HR SS.

It is interesting to note that the NPTI was much better at forecasting thunderstorms during the August time frame in this study. First, it generates significantly higher forecast percentage probabilities during the month of August. Second, it produced better statistics in every category except probability of detection than those produced by the entire test period combined. This may be a factor of climatology, since August is the month with the greatest number of thunderstorms in eastern Florida. It could also be a bias of the NPTI code, which may be able to better predict thunderstorms in August because of the variables used in the probability calculation. A point that may be considered in future research is to check if different threshold probabilities should be used for each month instead of one percentage over the entire time. This may produce better results from the NPTI code. The climatology study investigates this question for the extended time frame.

The Heidke Skill Score, Kuipers Skill Score, and Brier Score all indicate the general performance of the forecasting method. The Heidke Skill Score (HSS) uses the hit rate as its accuracy measure with a reference of a random forecast with the same marginal distributions as the actual observational data. This shows us that the NPTI method is able to well outperform a random method with the thunderstorms on 62 percent of the days. The Kuiper Skill Score (KSS) method is very similar except it uses an unbiased reference forecast. Our forecast method was highly biased to underforecasting,

but it was able to outperform this method even better than it did for the HSS. The Brier Score covers the ability of the method over the entire range of the probability forecasts. It shows just how far off the NPTI method was from a perfect forecast. A score of zero would be perfection with everything over zero being the difference in the forecasting method from the perfect forecast. With a Brier Score of 0.2402, it can be said that the NPTI method is not nearly perfect. This means that it has a relative error of about 24 percent away from a perfect forecasting ability. The ratio skill score versus persistence (RSS(P)) also shows this general trend of not being a perfect technique for forecasting the day-two thunderstorm probability.

Table 5. Skill Scores Involving Other Reference Techniques.

	HSS (%)	KSS (%)	BS	RSS(P) (%)
Total NPTI	64.91	71.5	0.2402	-9.9

4.3 NPTI Over Extended Period Results

A climatological data set of approximately 20 years was used to test the ability of the NPTI algorithm over an extended period. The data set was tested both as a whole and as subsets that divided the data by its low level flow regime into four major groups. This division would give general ideas about the NPTI's overall ability and any particular problems that it may have due to the difficulty in forecasting thunderstorms in easterly flow regimes.

The accuracy statistics, shown in Table 7, for the climatological study show some very interesting results about the forecast ability of the NPTI. The same method was used to calculate the accuracy and bias measures over the entire time frame, so that it could be directly compared to the tests conducted on the research with model input. Table 7 only shows the statistics for the 50 percent threshold level. Refer to Appendix D to see a range of levels from 40 percent to 55 percent or Appendix E for the entire range. This threshold percentage was shown because it is nearly the same as the unbiased threshold of 47 percent. The maximum skill score threshold for this data is low-38 percent, seen in Table 6. It is clear from these statistics that the NPTI does have a bias toward underforecasting. This bias agrees with the results found from the model input NPTI calculations. It is also fairly obvious that the NPTI has a split forecasting ability. During easterly flow regimes, especially from the north east, the NPTI will almost always forecast no thunderstorms because that is the dominant weather pattern, thus the high hit rate (HR). Conversely, the NPTI will forecast thunderstorms for most days when the winds are out of the southwest. This is shown by the low inverse threat score, and the high probability of detection. The excellent distribution of this climatological data resulted in definite dependence for the entire period, with a χ^2 of 427.49 and a p-score of 0.00

Table 6. Accuracy Measures and Bias for the 38 Percentile Threshold Level

	HR (%)	TS (%)	TSN (%)	POD (%)	PODN (%)	FAR (%)	FARN (%)	Bias
Persistence	69.38	47.65	57.55	64.63	75.86	35.53	24.05	1.0024
Climo. NPTI	70.1	52.5	55.35	81.88	62.13	40.6	16.48	1.3784

Table 7. Accuracy Measures and Bias for the 50 Percentile Threshold Level.
NC means not calculated.

	HR (%)	TS (%)	TSN (%)	POD (%)	PODN (%)	FAR (%)	FARN (%)	Bias
Persistence	69.38	47.65	57.55	64.63	75.86	35.53	24.05	1.0024
Climo. NPTI	70.56	44.54	61.44	58.59	78.65	35.00	26.27	0.9014
NE NPTI	83.83	14.97	83.36	18.33	NC	55.10	NC	0.4083
NW NPTI	67.69	30.46	62.36	39.47	NC	42.86	NC	0.6908
SE NPTI	71.00	29.25	67.05	41.75	NC	50.57	NC	0.8447
SW NPTI	62.18	51.06	37.52	70.89	NC	35.38	NC	1.0971

The skill scores for these variables, as shown in Table 8, indicate that the overall ability of the NPTI is very similar with that of persistence over a large time frame. However, if used properly the NPTI could be a useful tool for forecasters and enable them to outperform the persistence technique. Realizing the algorithm's strengths and weaknesses will enable the forecaster to estimate the reliability of the NPTI forecast. It is obvious that the NPTI is more believable when it forecasts no thunderstorms and the winds are out of the northeast or forecasts thunderstorm occurrence when the winds are from the southwest. This can be seen in the statistics because of the huge differences in the POD SS and TS SS, which are the main indicators of a successful thunderstorm forecast. This is most likely true because no convergence zone is created when the sea breeze and synoptic flow are both in the same general direction. The high temperature,

humidity, and convergent direction of winds from the southwest are the main reasons that most thunderstorms occur under those conditions.

If the desired outcome of the NPTI is to have fewer days underforecast, then it may be better to use the 38 percent threshold of the maximum threat score. This would noticeably decrease the inverse false-alarm rate, and increase the probability of detection and the threat score, illustrated in Table 8. All of these conditions were the recommendations given earlier to improve the forecast ability of the NPTI in an attempt to lower the number of days falsely forecast as being clear. This was preferred forecast because of the relative impact that these incorrect forecasts have on the mission.

Table 8. Skill Score for the 50 and 38 Percentile Threshold Level Statistics

	HR SS (%)	TS SS (%)	TSN SS (%)	POD SS (%)	PODN SS (%)	FAR SS (%)	FARN SS (%)
Climo. NPTI (50%)	3.85	-5.94	9.16	-17.08	11.56	1.49	-9.23
Climo. NPTI Skill Score	2.35	9.26	-5.18	48.77	-56.88	-14.27	31.48
NE NPTI	47.19	-62.43	60.8	-130.9	NC	-55.08	NC
NW NPTI	-5.52	-32.84	11.33	-71.13	NC	-20.63	NC
SE NPTI	5.29	-35.15	22.38	-64.69	NC	-42.33	NC
SW NPTI	-21.49	6.51	-47.18	17.7	NC	0.42	NC

It is also interesting to investigate the forecast ability of the NPTI for the different months of the warm season. To best accomplish this task, multiple charts have been made which show the accuracy measures and bias versus the threshold percentage. This will show how the different thresholds affect the outcome of the total forecast. The

general rule applied in most studies that use contingency tables is to choose either the unbiased threshold percentage or the percentage which corresponds to the maximum threat score value. In the case of the NPTI, it is logical to choose either threshold. These graphs will let the 45th Weather Squadron determine which threshold is the best for their applications. The ultimate goal is still to improve the forecasting ability of the NPTI algorithm.

The graphs shown in Figures 5 through 16 show the reliance of the different accuracy and bias measures on the choice of the threshold percentage. It is interesting to note the different thresholds where the forecast is unbiased. The months with more active thunderstorm generation have much higher unbiased threshold percentages, whereas, the less active months, like September and May, have much lower unbiased thresholds. Over the entire warm season these discrepancies are averaged out. It is also interesting to note the location of the maximum in threat score and the maximum in hit rate. Either of these thresholds could also be used to calculate the binary forecast, remembering that the maximum in threat score was able to provide the decrease in underforecast days by providing an overforecasting bias. This presentation shows that there is some possibility for different threshold percentages for different months during the warm season.

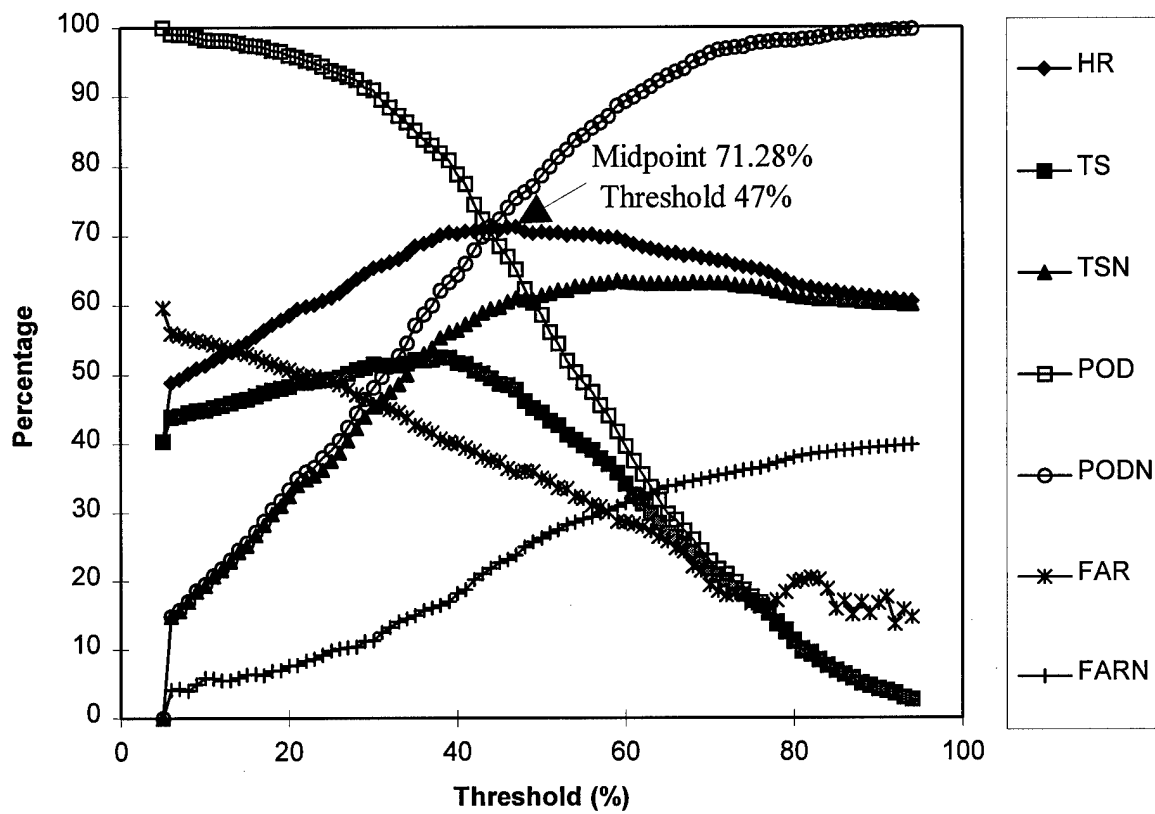


Figure 5. Graph of Accuracy Measures versus the Threshold Percentage.

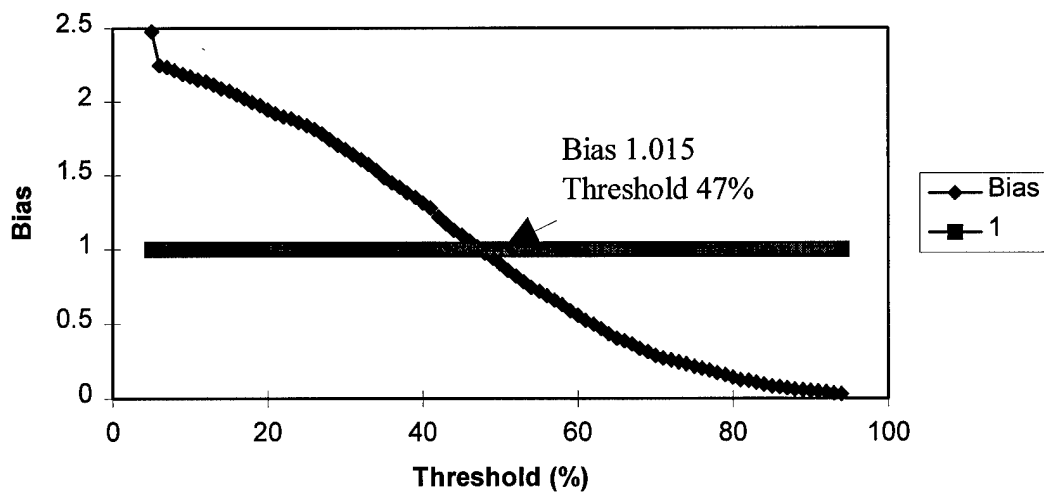


Figure 6. Graph of Bias versus Threshold Percentage.

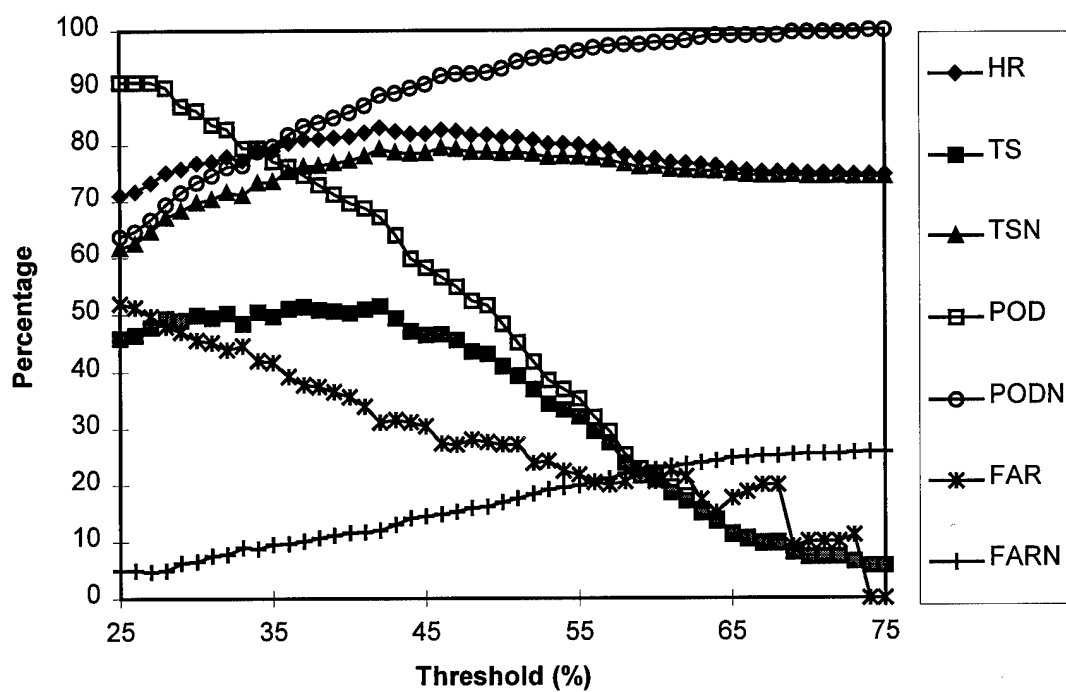


Figure 7. Graph of Accuracy Measures versus the Threshold Percentage: May.

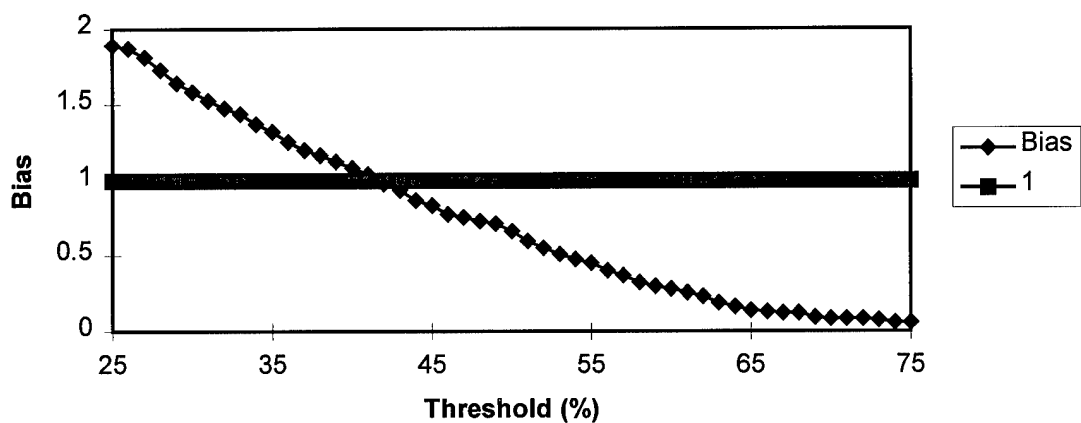


Figure 8. Graph of Bias versus Threshold Percentage: May.

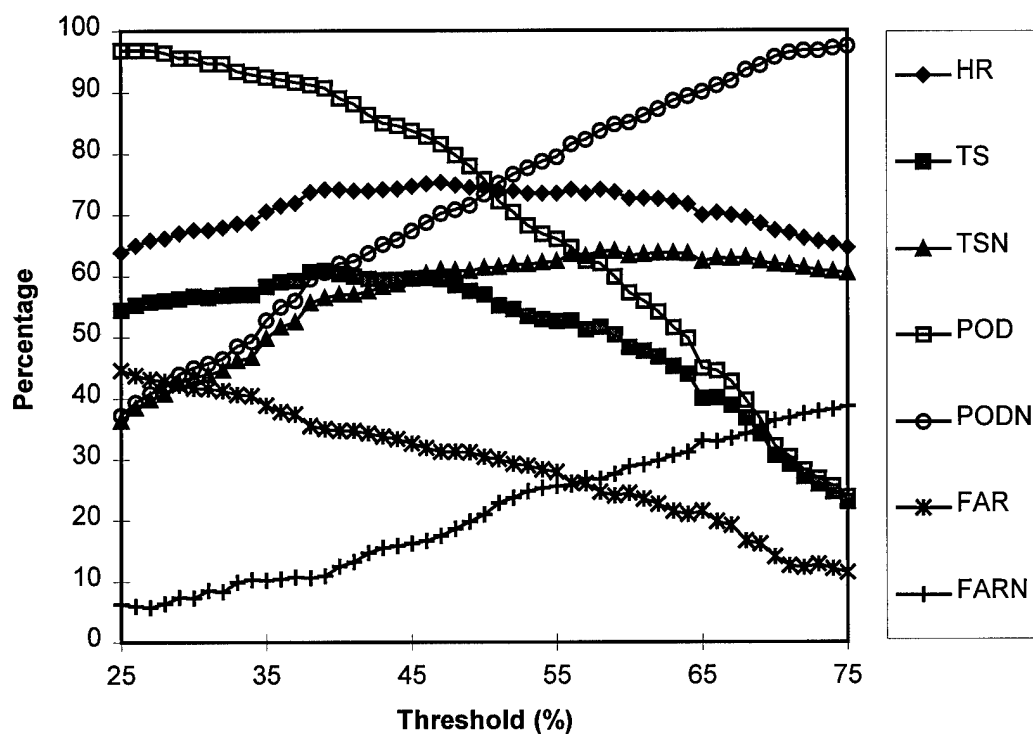


Figure 9. Graph of Accuracy Measures versus the Threshold Percentage: June.

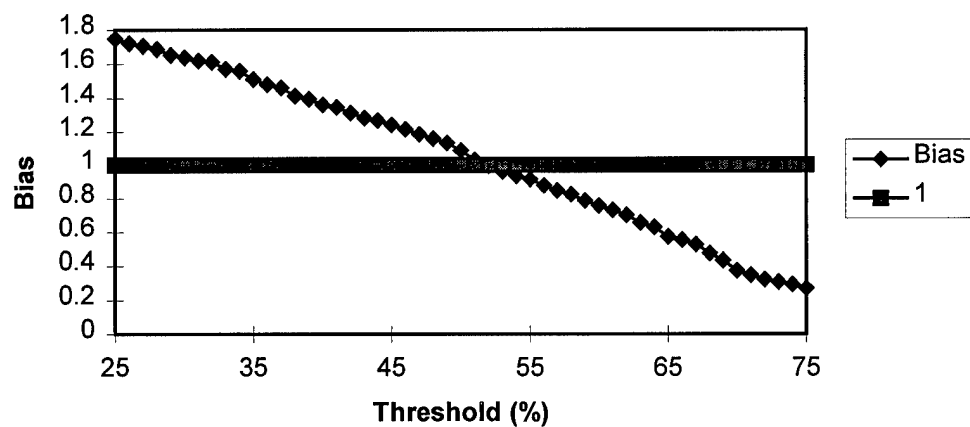


Figure 10. Graph of Bias versus Threshold Percentage: June.

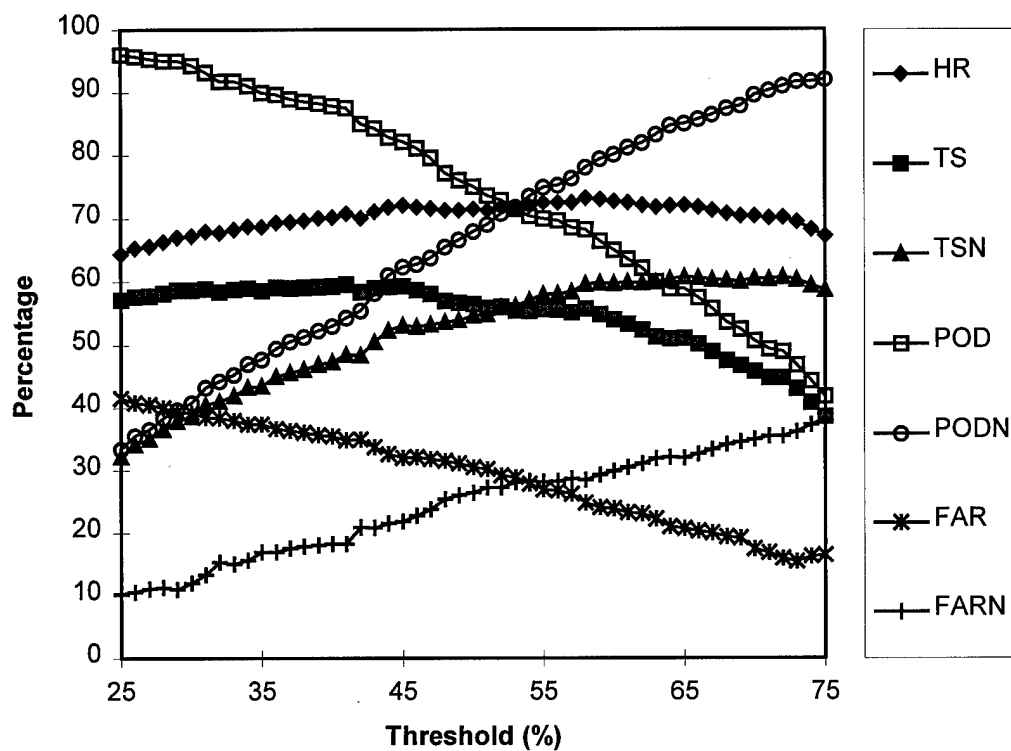


Figure 11. Graph of Accuracy Measures versus the Threshold Percentage: July.

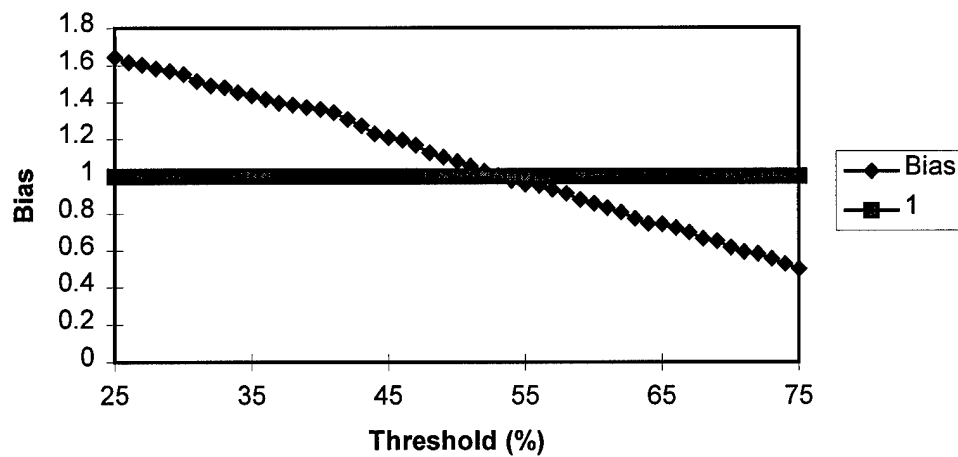


Figure 12. Graph of Bias versus Threshold Percentage: July.

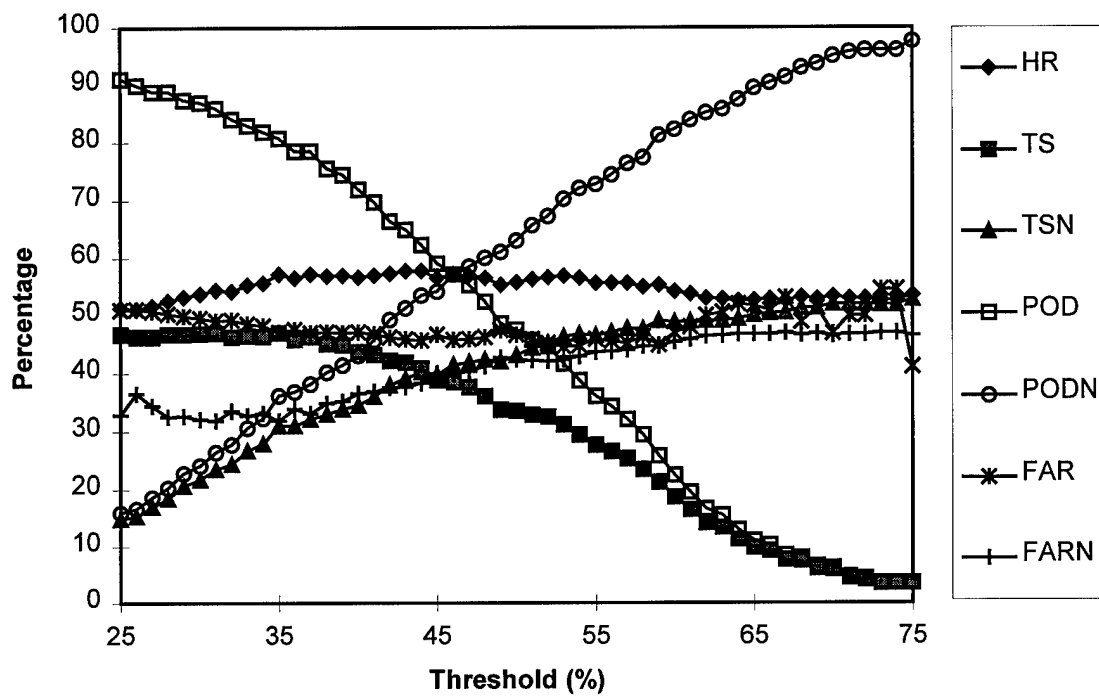


Figure 13. Graph of Accuracy Measures versus the Threshold Percentage: August.

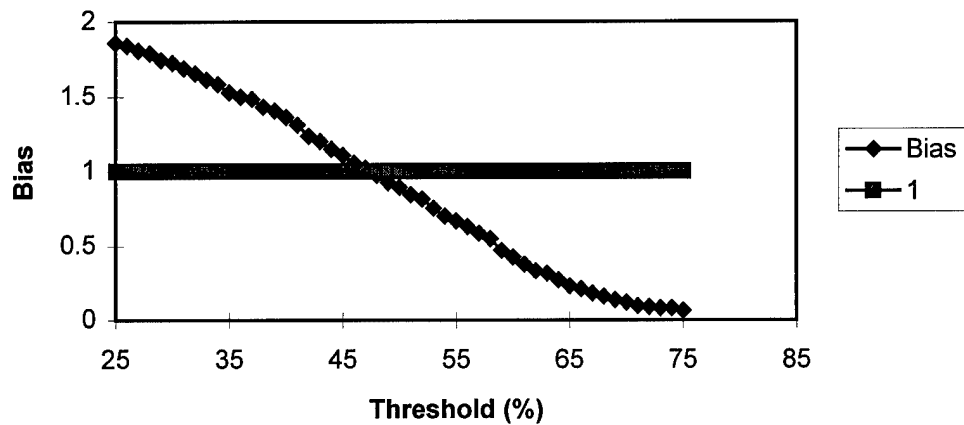


Figure 14. Graph of Bias versus Threshold Percentage: August.

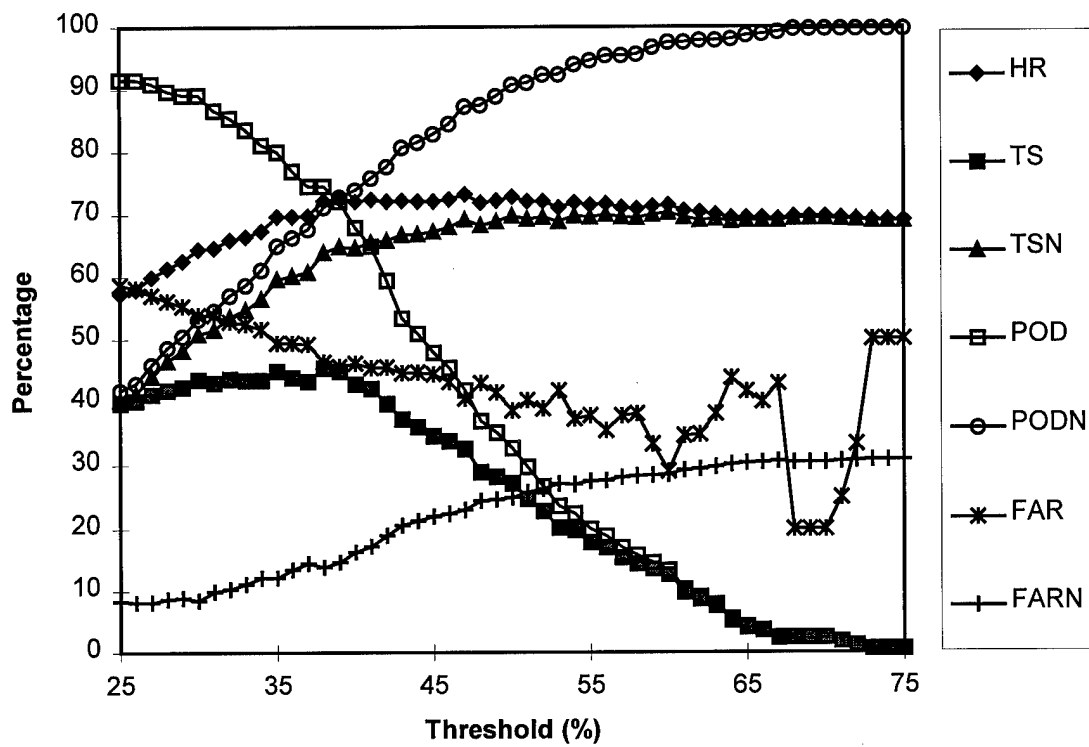


Figure 15. Graph of Accuracy Measures versus the Threshold Percentage: September.

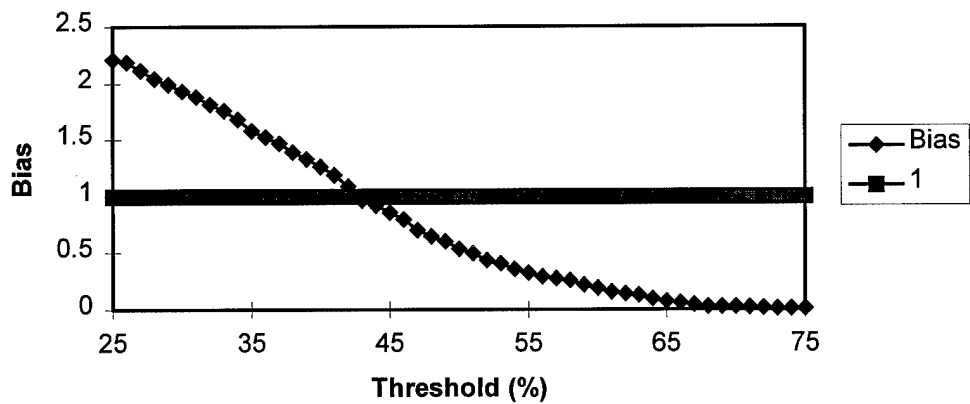


Figure 16. Graph of Bias versus Threshold Percentage: September.

The statistical tests run for the ability of the NPTI using a climatological data base also included the Brier Score (BS) and the ratio skill score versus both persistence (RSS(P)) and climatology (RSS(C)). These statistics judge the ability of the NPTI's probability forecasts versus a probability forecast derived for both persistence and climatology. The Brier Score calculated for persistence was 0.3000 and the Brier Score for climatology was 0.2245. These were then used in the ratio skill score to calculate how well the method performed as a probability calculation. The results of those statistics are shown in table 9. The BS and the associated RSS statistics show a view of the NPTI as a reasonable forecasting technique. It definitely has a better RSS(P) than the experimental scheme which was -9.9%. However, it still is not an extremely accurate scheme versus climatology. Another way to examine the probability forecasts of the NPTI is through the use of an attributes diagram. This chart, shown in figure 17, is a visual way of identifying how the method performs versus the perfect forecast. It can be analyzed given the position of a perfect reliability line, a no skill line, a no resolution line, and the skill region, which is defined by the no skill line and the line that vertically crosses at the junction point of the no resolution and perfect reliability line. The forecast probability points are group in five percent increments from five to ninety five. This data

Table 9. Brier Score and the Ratio Skill Score versus persistence RSS(P) and climatology RSS(C).

	BS	RSS(P) (%)	RSS(C) (%)
Climo. NPTI	0.1850	38.3	17.6

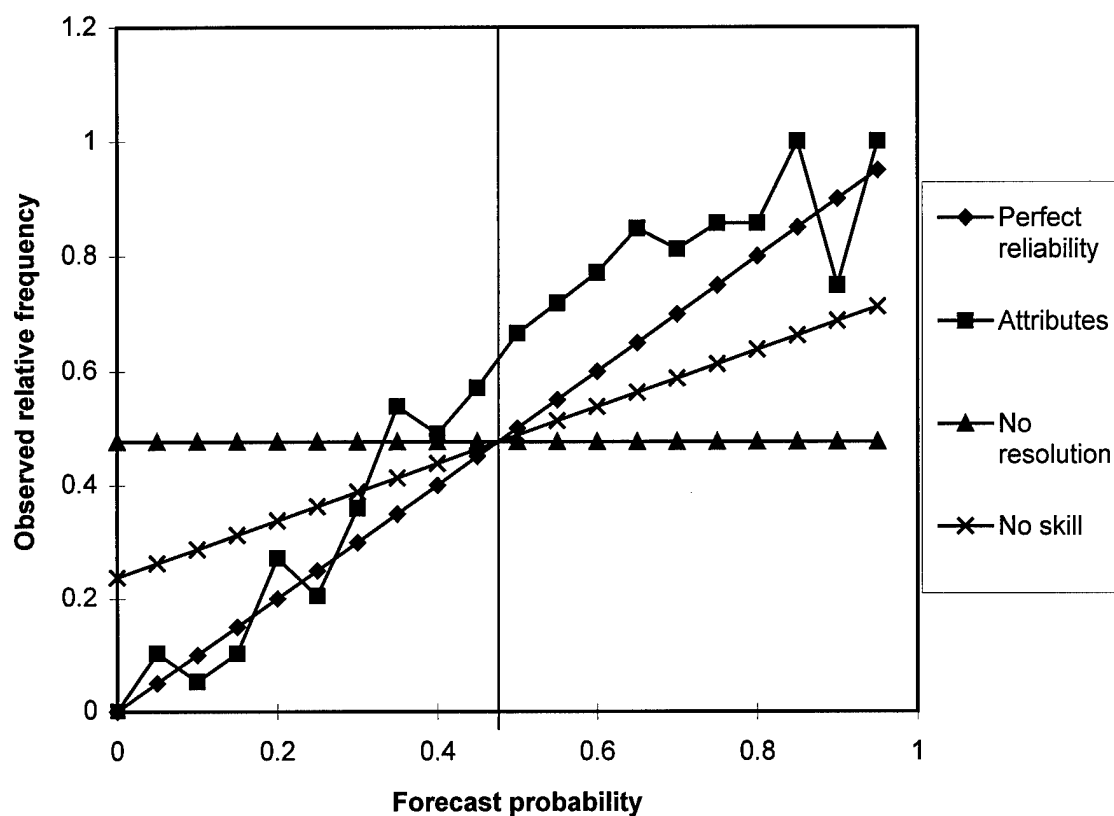


Figure 17. Attributes diagram for the four independent years.

Table 10a. Observed relative frequency per forecast probability group.

Forecast probability	0.05	0.10	0.15	0.20	0.25	0.30	0.35	0.40	0.45
Observed rel. freq.	0.103	0.053	0.103	0.273	0.205	0.360	0.539	0.490	0.571

Table 10b. Observed relative frequencies for 50 through 95 percent.

P(For.)	0.50	0.55	0.60	0.65	0.70	0.75	0.80	0.85	0.90	0.95
Obs. rel. freq.	0.667	0.719	0.771	0.849	0.813	0.857	0.857	1.00	0.75	1.00

is detailed in table 10a and 10b. The data used was from the years 1983, 1985, 1986, and 1988 because they were independent from the data used by Neumann in the NPTI regression equations. The attributes diagram also shows the NPTI as a forecasting scheme with some skill. The diagram does, however, shows a definite bias toward underforecasting since the attribute line is consistently above the perfect reliability line, which corresponds with the earlier analysis of the two-by-two contingency tables. The diagram also shows that the NPTI is a method, which has fairly good resolution at the expense of good reliability. The NPTI is a forecasting method that has some ability to accurately forecast thunderstorms, but a more reliable technique would be much more useful for the operational forecasters.

After reviewing the forecasting ability of the NPTI over the climatological data set it is important to note the results of the NPTI with Meso-Eta inputs. The NPTI calculated with the Meso-Eta inputs did have problems with days when the winds were out of the northeast. This may be caused by the lack of data points to the east of Cape Canaveral. This is always a problem for models because they are unable to produce as accurate a forecast in data sparse regions. It may also be a factor of the NPTI algorithm. The case study covers those days with missed forecasts in more depth and shows the meteorological backing to these results.

4.4 Case Study Results

The case study was conducted in order to provide a better idea for why the forecasts were incorrect. The model output was the source of the graphical data used in the case study. The observational data, satellite imagery, and a surface chart for each day were also used as comparison tools. A meteorological study was conducted on three of the four underforecast days. This is because these three days are consecutive and it should be easier to find any commonalities. The one overforecast day was not reviewed because no general conclusion can be drawn from a single missed forecast, and the result may be due to the threshold level chosen for making the forecast binary.

This case study involves three consecutive days in which the NPTI did not predict a thunderstorm, but one was observed. On 22 September 1997, the forecasted probability was 5 percent but a thunderstorm occurred that day. The other days were almost as bad with 21.75 percent on the 23rd and 19 percent on the 24th. This study will try to answer the question of why the NPTI forecasted so poorly. In order to investigate for any meteorological significance to this occurrence, this case study will focus primarily on the similarities between the days, but will also try to determine if there is any factors which may have generated the thunderstorms present in the model which was not picked up by the NPTI.

The significant levels for this study are 500 mb, 700 mb, 850 mb, and 1000 mb. There are 39 charts in this case study with thirteen for each day of the study. The first day is 22 September 1997, with Figures 18 through 34, Figures 35 through 51 cover 23 September, and 24 September is presented on Figures 52 through 68. These figures

follow the same order for each day, with 500-mb geopotential height first, followed by the winds at all the levels, then the 500-mb Q-vectors and Q-vector convergence, the temperature at all levels with the dew point at 1000 mb, the relative humidity at the three lower levels, followed at the end by the surface chart and the GOES East infrared satellite image for that day. This will provide an organized method for locating a chart being discussed.

The 500-mb geopotential heights for the three days in question (Figures 18, 35, and 52) show the presence of a gradually weakening high pressure over the southeast, but Cape Canaveral is under the same pressure system during the entire case study. The flow regime appears to be a potential forecasting problem. On the 22nd (Figures 19, 20, 21, and 22), the flow is directed from the northeast because of the high pressure system to the north and the lower pressure moving in from the west. As the high pressure moves eastward on the 23rd (Figures 36, 37, 38, and 39), the winds switch from a northeast to a southeasterly flow. With the edge of the high pressure system sitting over Florida on the 24th (Figures 53, 54, 55, and 56), the wind has become almost parallel to the shape of the Cape. They arrive from the southeast and head out over Cape Canaveral. The winds at the low levels are also fairly weak winds with speeds only around 5 to 10 knots. The temperature fields for all of the days appear to be fairly constant, with temperatures around 30 degrees Celsius, as would be expected under a high pressure system. These factors do not indicate the presence of a great amount of instability, but with the large gradient of the dew point temperature (Figures 29, 46, and 63) around the coast there may be some instability generated. The relative humidity charts for 700 mb (Figures 30, 47,

and 64) show a clear lack of mid-level moisture. However, the low level moisture is present as seen on the 850-mb and 1000-mb charts (Figures 31, 32, 48, 49, 65, and 66). The observations for the three days all indicated thunderstorms over the stations. The 22nd and the 24th had late morning/afternoon thunderstorms that weren't too heavy according to the remarks. The 23rd had thunderstorms all day that traveled from the southeast to the northwest. The winds recorded for the 22nd were from the northeast with the winds moving to the east and southeast on the 23rd. The 24th had winds which ranged from 180 to 140 meaning that they were mainly out of the south by southeast. These wind directions tends to support the model products for the low level winds. The temperatures were missing for the most of the observations, but those recorded were around 17 to 24 degrees Celsius which are close to those seen on the 1000-mb temperature charts. The surface plots, seen in Figures 33, 50, and 67, show the same wind directions as the model, and a fairly stable stationary front to the north of Florida which is very common during the summer months. The 23 September surface plot shows moisture from the radar overlay over the east coast of Florida. This is supported by the IR satellite image which clearly shows some development. Thunderstorm development is not evident on the 22nd or the 24th, but both of those days had later thunderstorms than on the 23rd. All three of the satellite images (Figures 34, 51, and 68) show a branch of the subtropical jet moving across Florida during the forecast period. However, no clear sign of jet streaks or their associated secondary circulations were noticeable on the satellite images. Another prevalent large scale weather forcing factor seen on all of the satellite images is the huge cyclone off the Pacific Coast of Central America. The 500-

mb Q-vectors (Figures 23, 40, and 57), and especially their convergence (Figures 24, 41, and 58), indicate the presence of vertical motion in the atmosphere. The convergence of the Q-vector is proportional to upward vertical motion. It is interesting to see that all three days had convergent Q-vectors over Cape Canaveral. They were especially strong on the 23rd, which happens to be the day with the strongest thunderstorms.

The evidence of thunderstorm-generating features is clearly visible. There is the combination of vertical motion, moisture, and heating. The only thing that is not present is a sea breeze front or other significant forcing mechanism. However, the forcing mechanism may be present in an unseen source of significant upward vertical motion. The one factor that seems to severely detract from that hypothesis is the direction of the synoptic scale winds. The winds are all out of an easterly direction, which is not good for sea breeze fronts. The difficulty in predicting thunderstorms during easterly flow regimes tends to support the findings of Bauman in his study of thunderstorms over Cape Canaveral. Since this is such a small sample with only three days to investigate, this is clearly not a climatological study. However, even the climatological study partially supports the theory that the NPTI has difficulty forecasting thunderstorms that occur when the synoptic scale wind patterns are from the east. It is possible the forcing mechanism was on a scale that was not perceived by the model; therefore, the NPTI was not able to include it in its probability forecasts. The other possibility is that the NPTI is not able to adequately distinguish certain forcing factors that are not common during the entire warm season. Since the NPTI involves a regression, it catches most of the common features of the thunderstorm-generation process, especially on the synoptic

scale. The calculation may be naturally biased against thunderstorms during easterly flow regimes. These results may not be adequate for the forecasting precision necessary to operate in the environment where near perfect forecasts are the daily requirement because of the expense and danger of space launch and recovery.

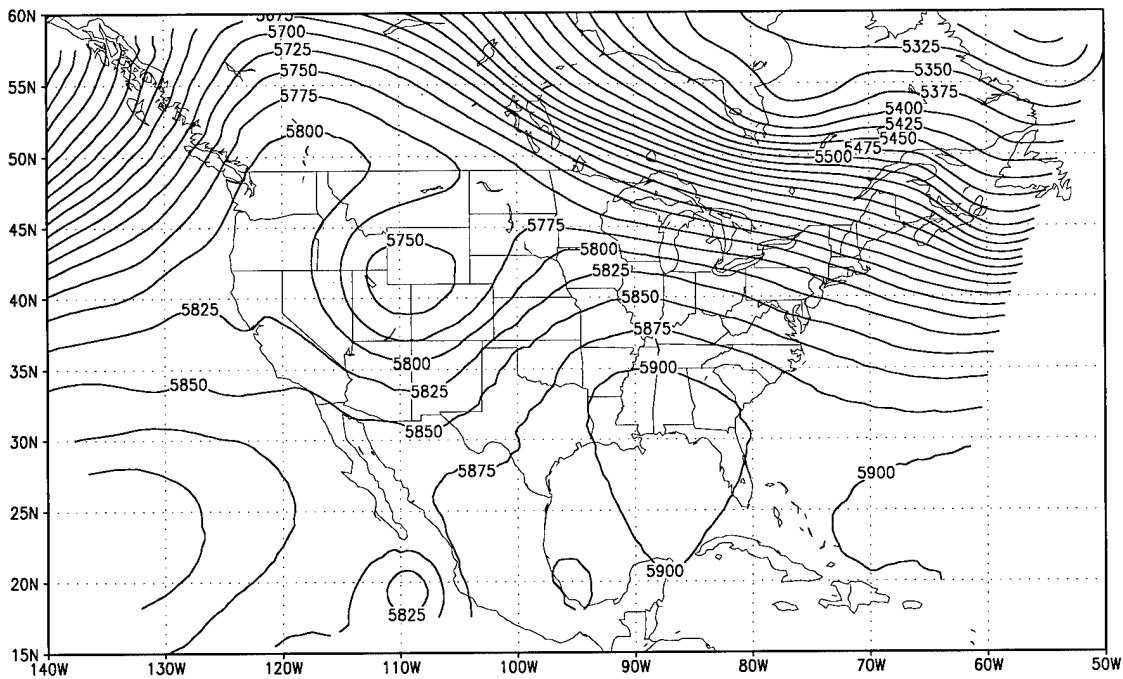


Figure 18. Meso-Eta 500-mb Geopotential Height for 1500 UTC, 22 September 1997.

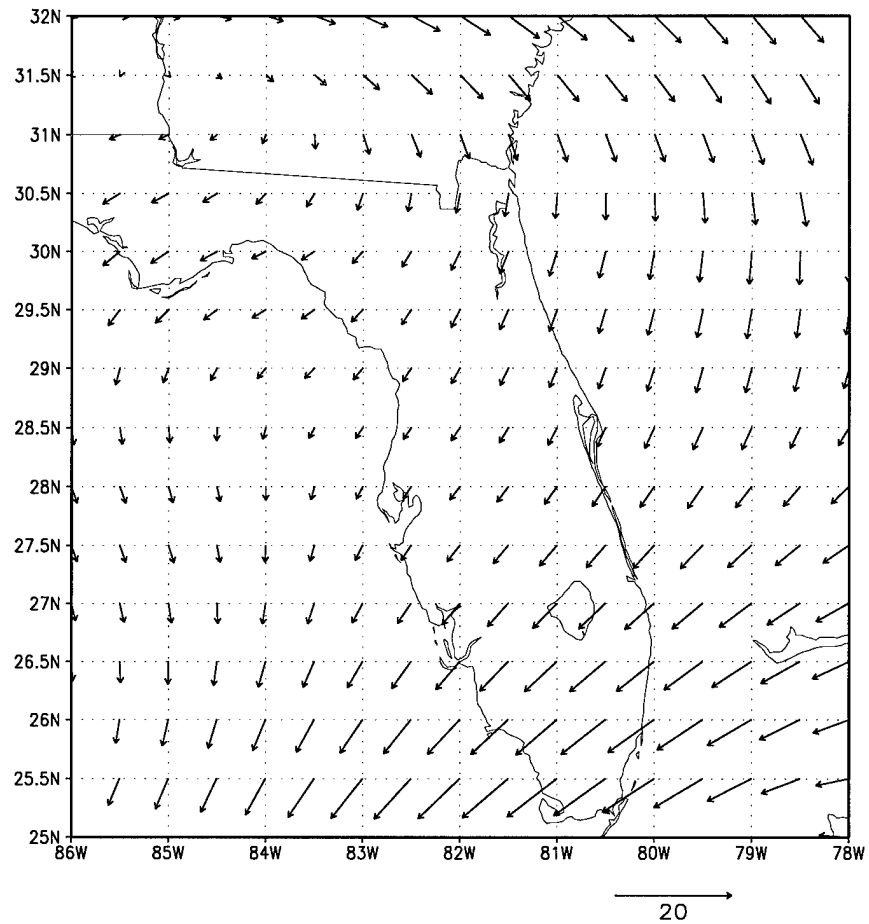


Figure 19. Meso-Eta 500-mb Winds Over Florida for 1500 UTC, 22 September 1997.

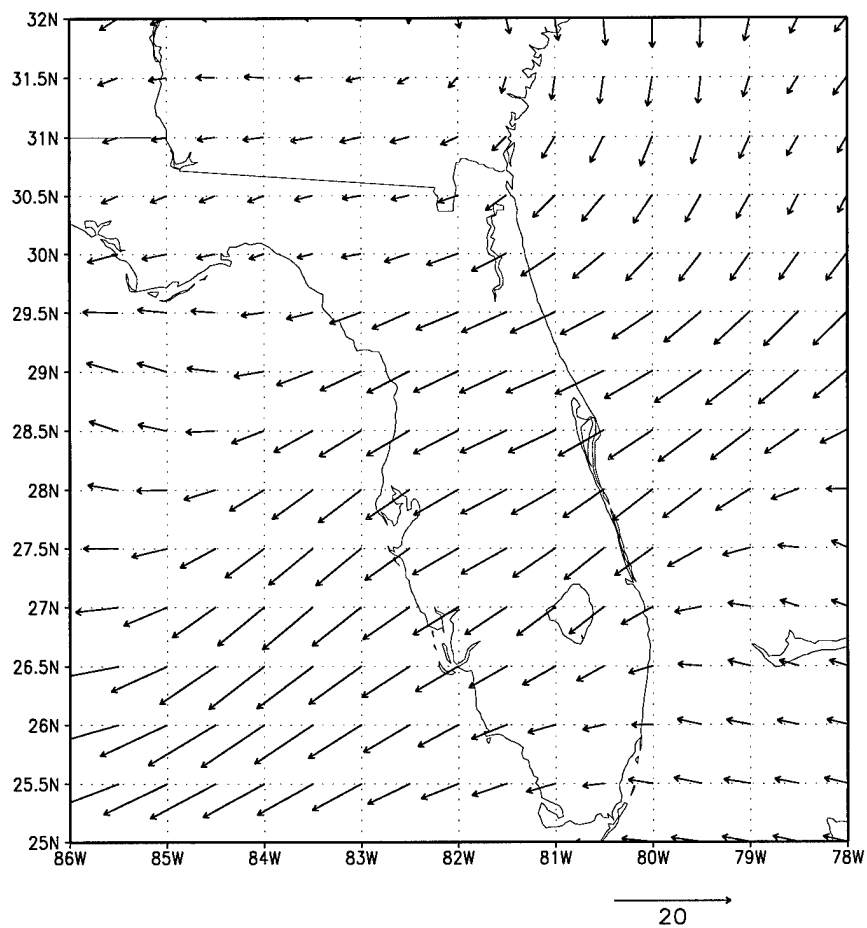


Figure 20. Meso-Eta 700-mb Winds Over Florida for 1500 UTC, 22 September 1997.

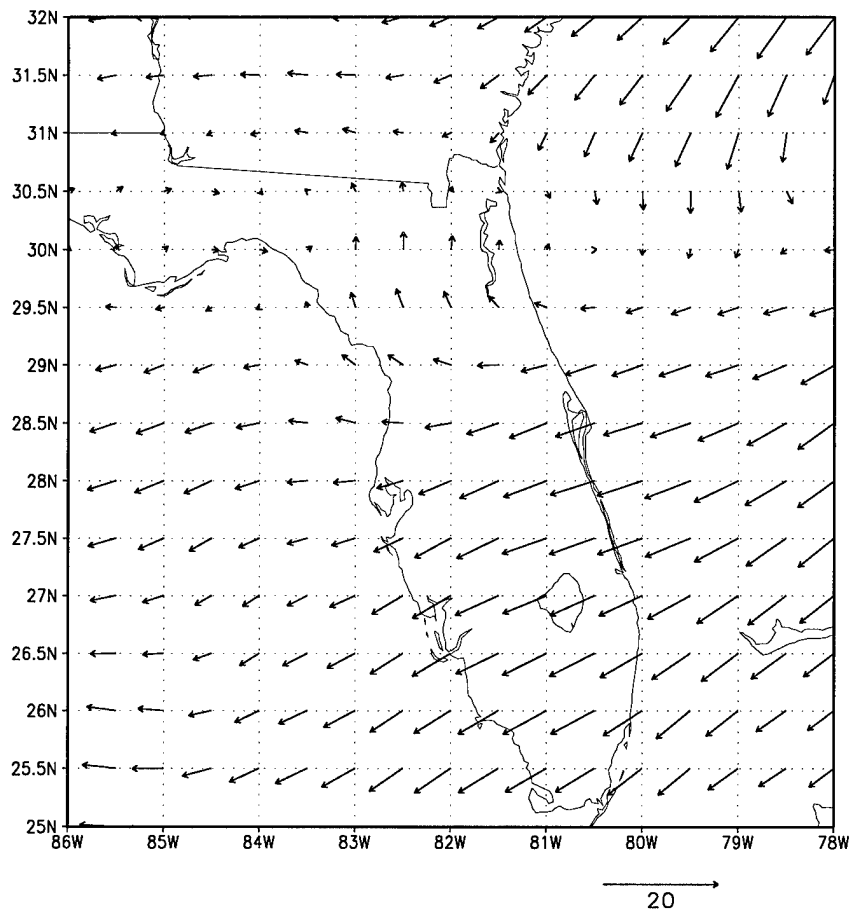


Figure 21. Meso-Eta 850-mb Winds Over Florida for 1500 UTC, 22 September 1997.

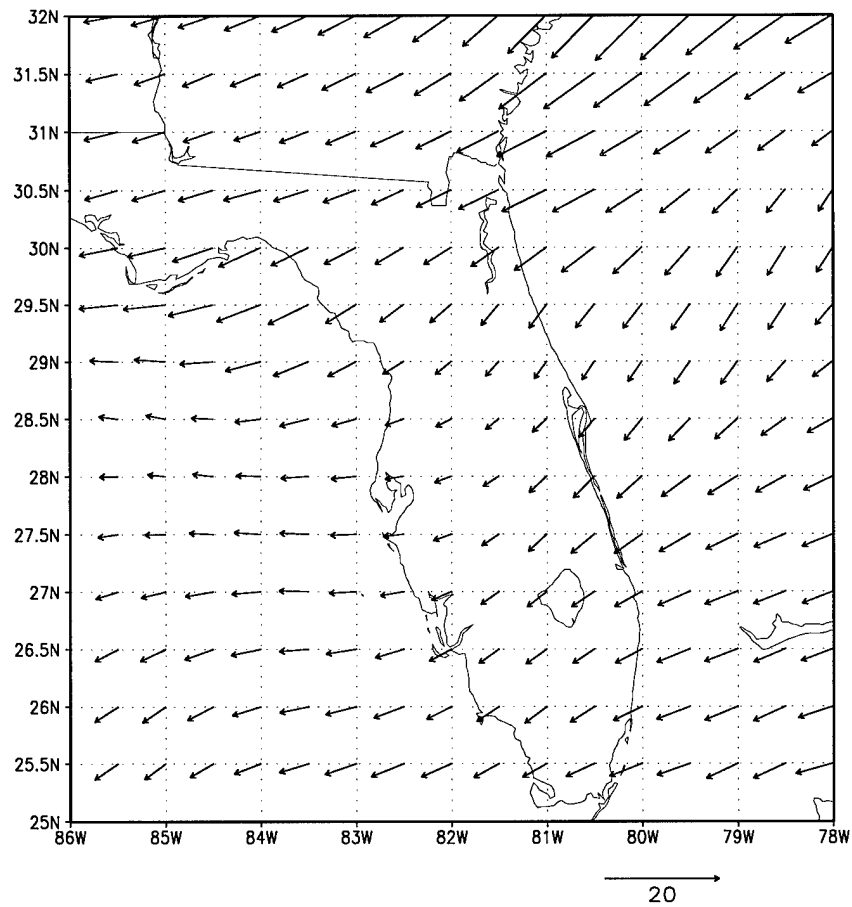


Figure 22. Meso-Eta 1000-mb Winds Over Florida for 1500 UTC, 22 September 1997.

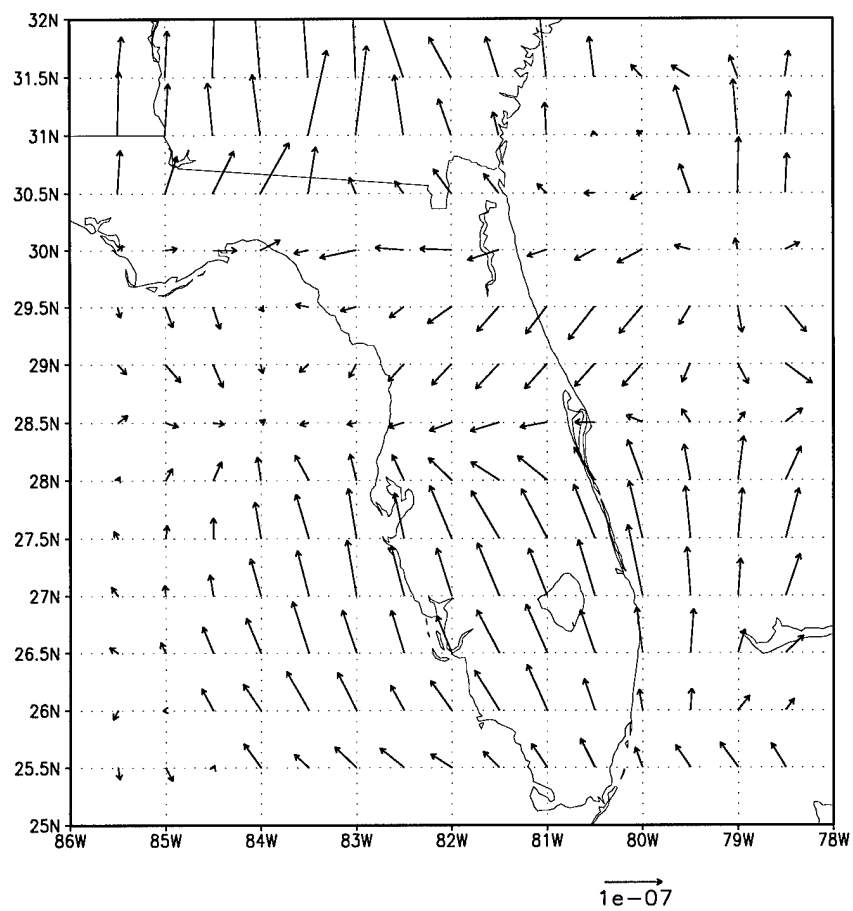


Figure 23. Meso-Eta 500-mb Q-vectors Over Florida for 1500 UTC, 22 September 1997.

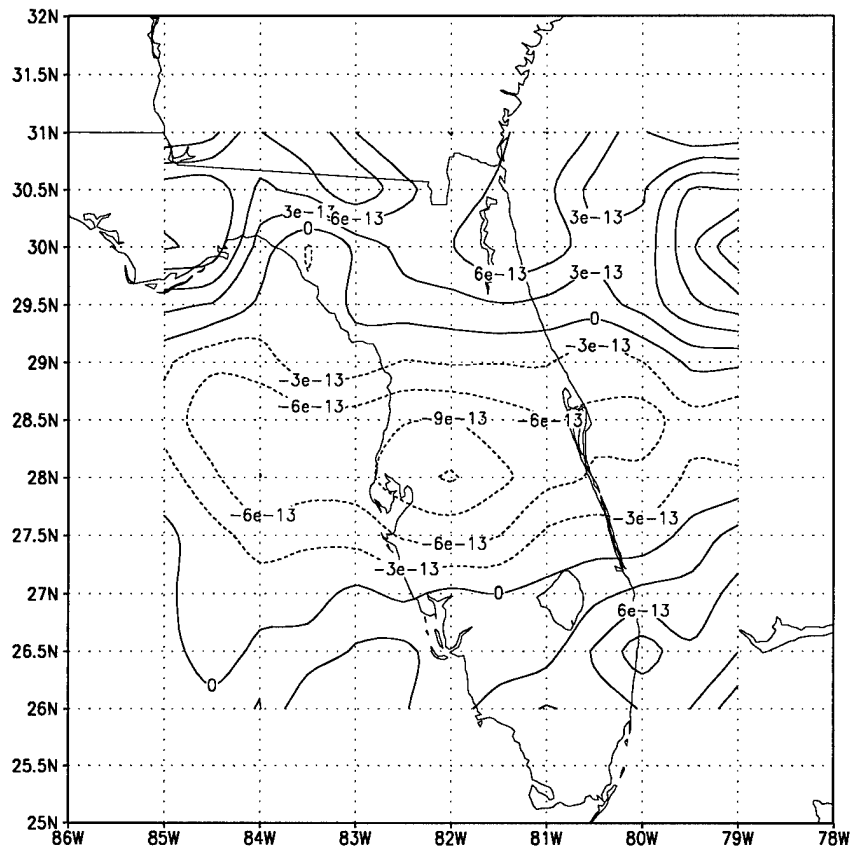


Figure 24. Meso-Eta 500-mb Q-vector Divergence Over Florida for 1500 UTC, 22 September 1997.

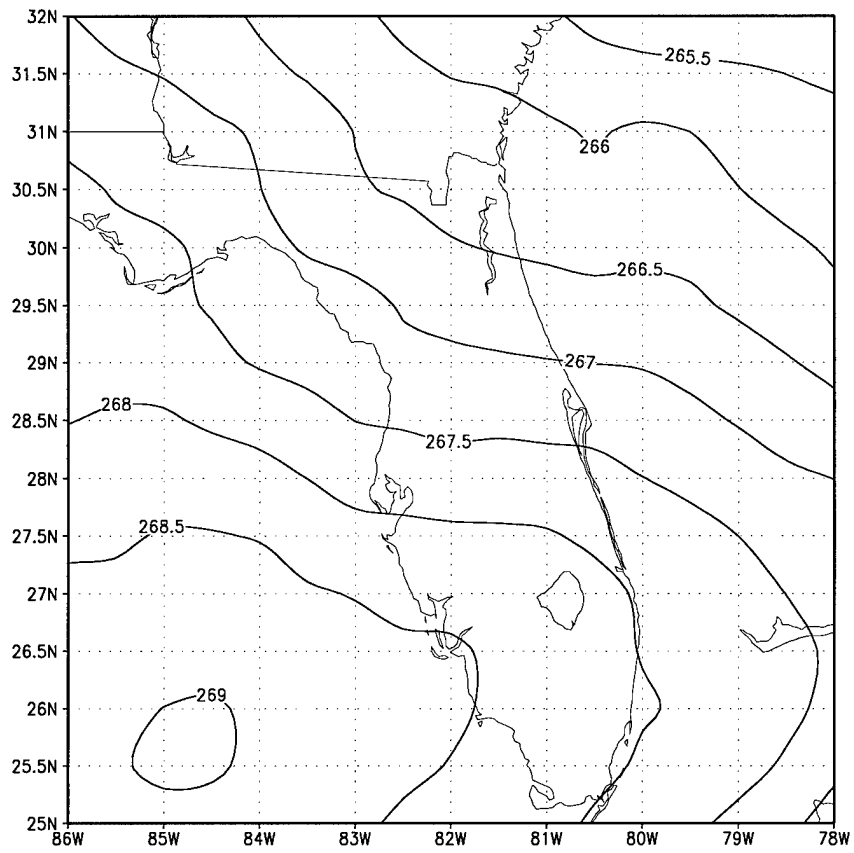


Figure 25. Meso-Eta 500-mb Temperatures Over Florida for 1500 UTC, 22 September 1997.

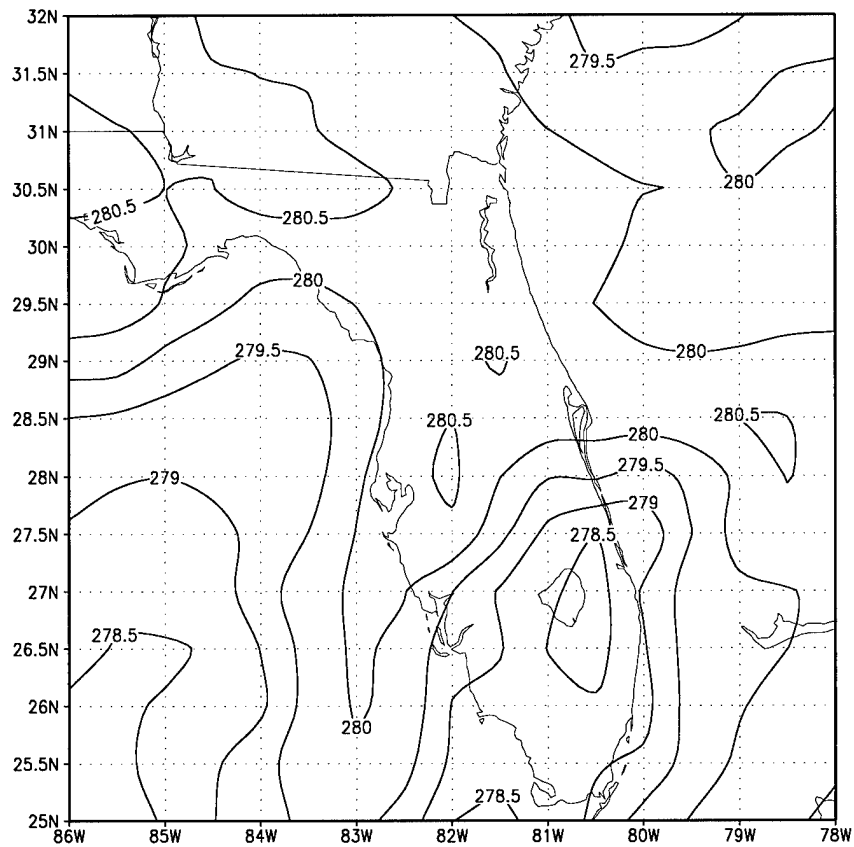


Figure 26. Meso-Eta 700-mb Temperatures Over Florida for 1500 UTC, 22 September 1997.

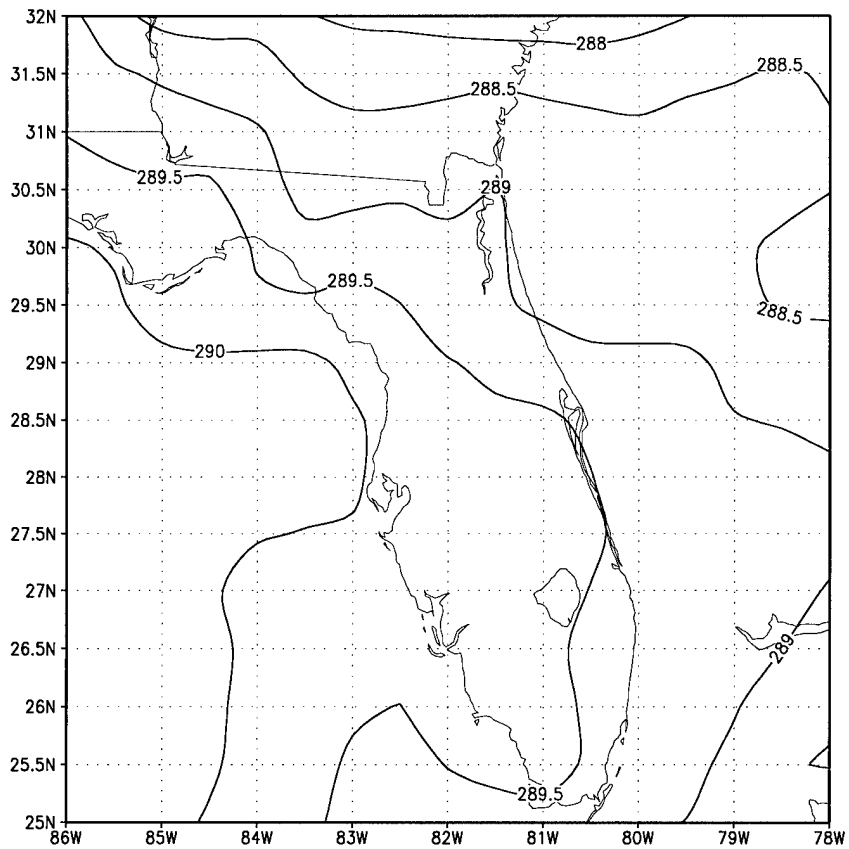


Figure 27. Meso-Eta 850-mb Temperatures Over Florida for 1500 UTC, 22 September 1997.

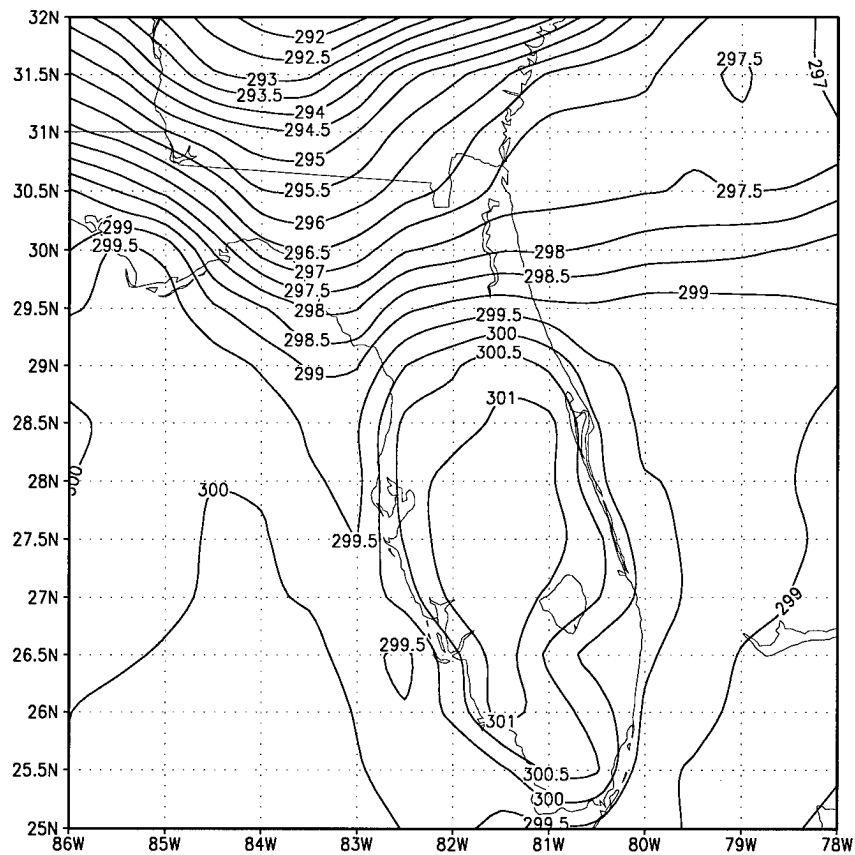


Figure 28. Meso-Eta 1000-mb Temperatures Over Florida for 1500UTC, 22 September 1997.

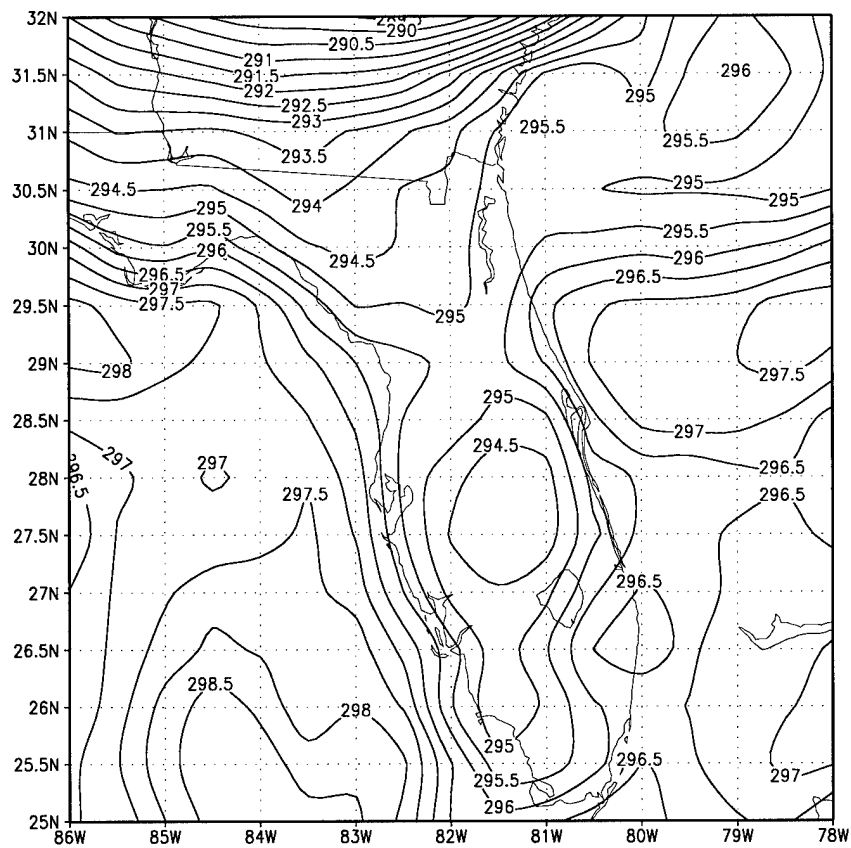


Figure 29. Meso-Eta 1000-mb Dew Point Temperatures Over Florida for 1500 UTC, 22 September 1997.

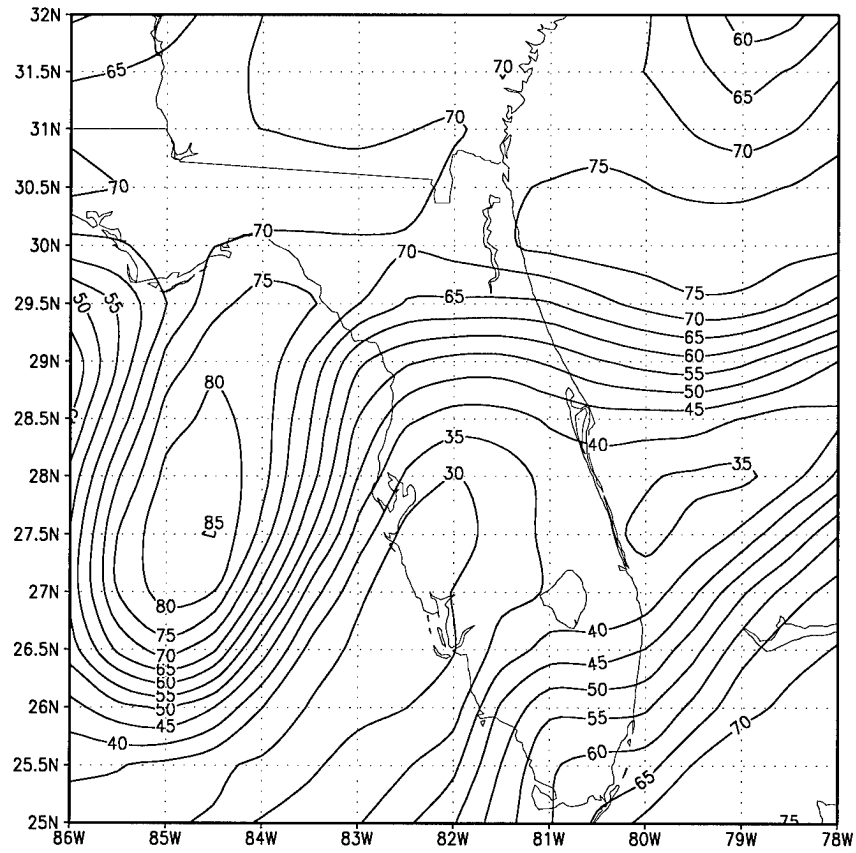


Figure 30. Meso-Eta 700-mb Relative Humidity Over Florida for 1500 UTC, 22 September 1997.

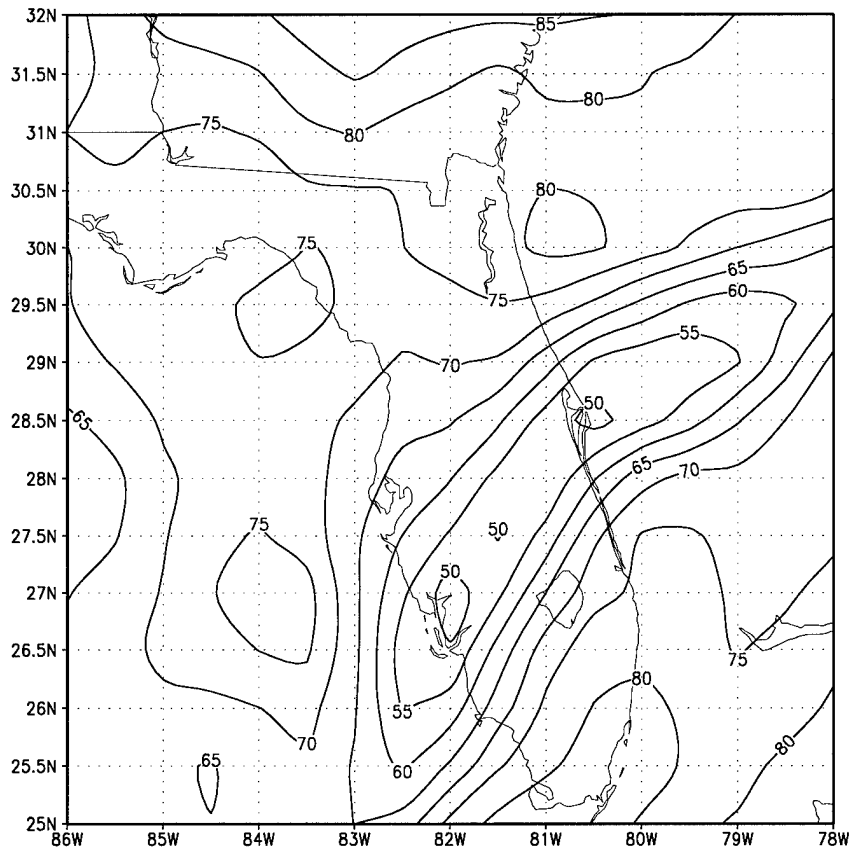


Figure 31. Meso-Eta 850-mb Relative Humidity Over Florida for 1500 UTC, 22 September 1997.

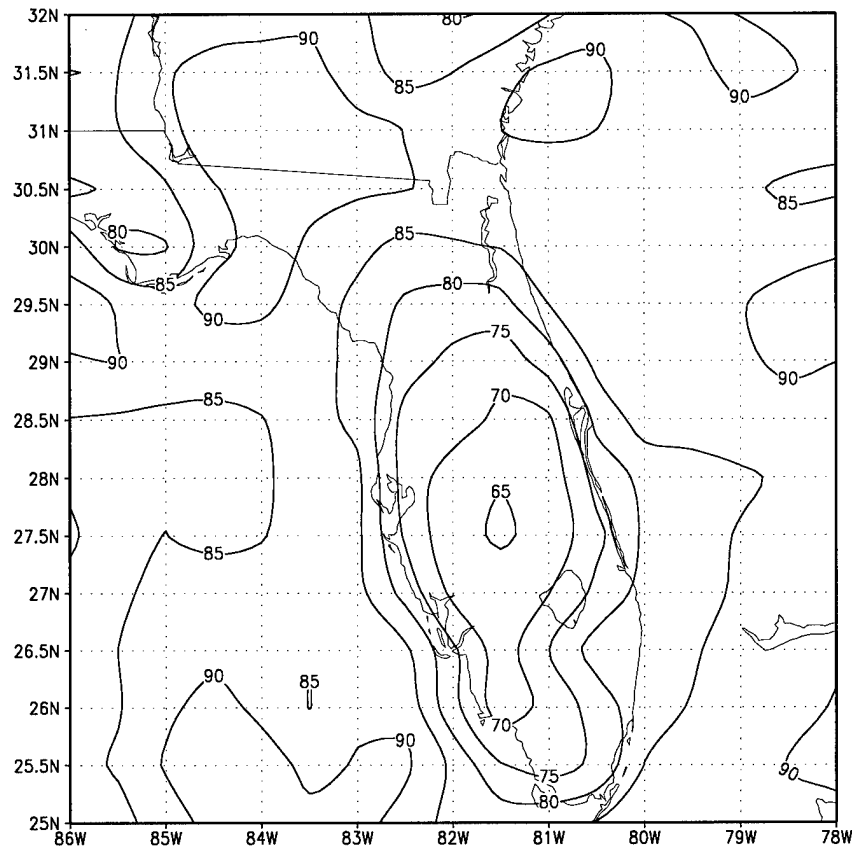


Figure 32. Meso-Eta 1000-mb Relative Humidity Over Florida for 1500 UTC, 22 September 1997.

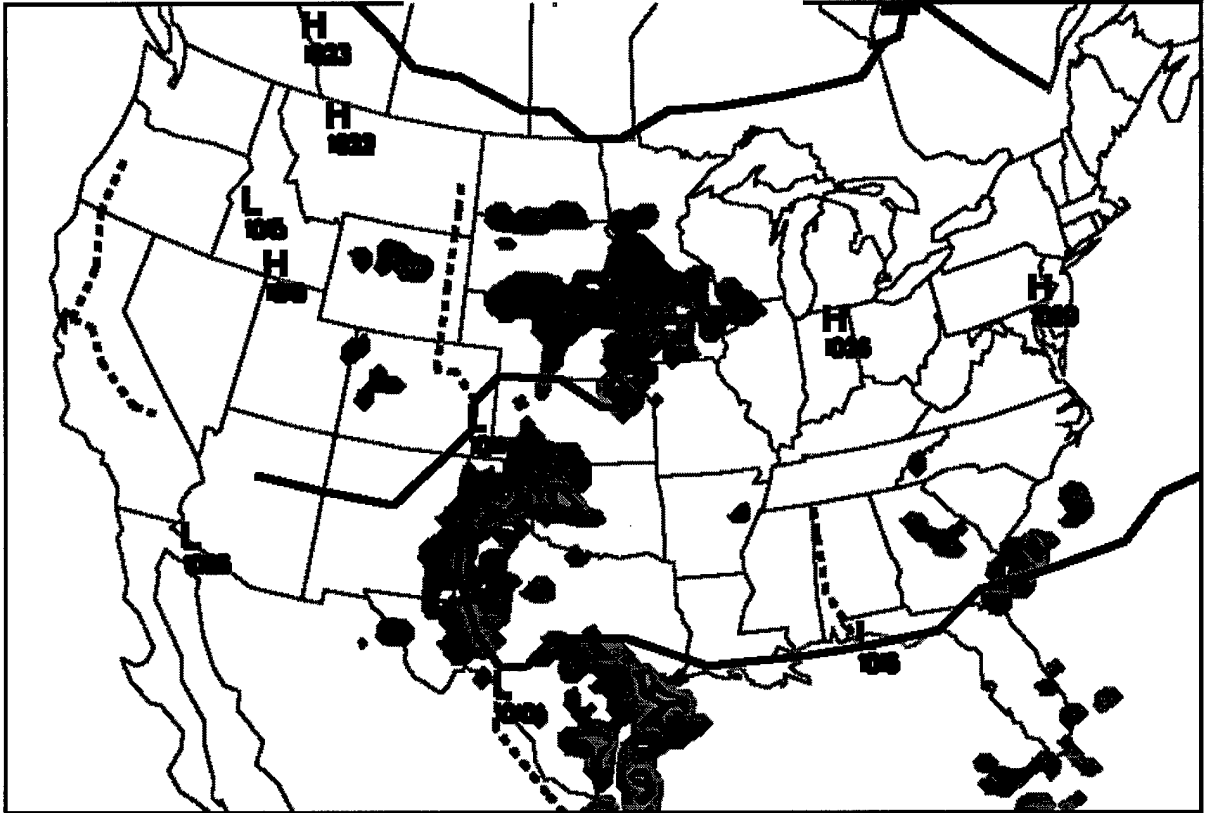


Figure 33. Surface Map with Radar Overlay for 1200 UTC, 22 September 1997.

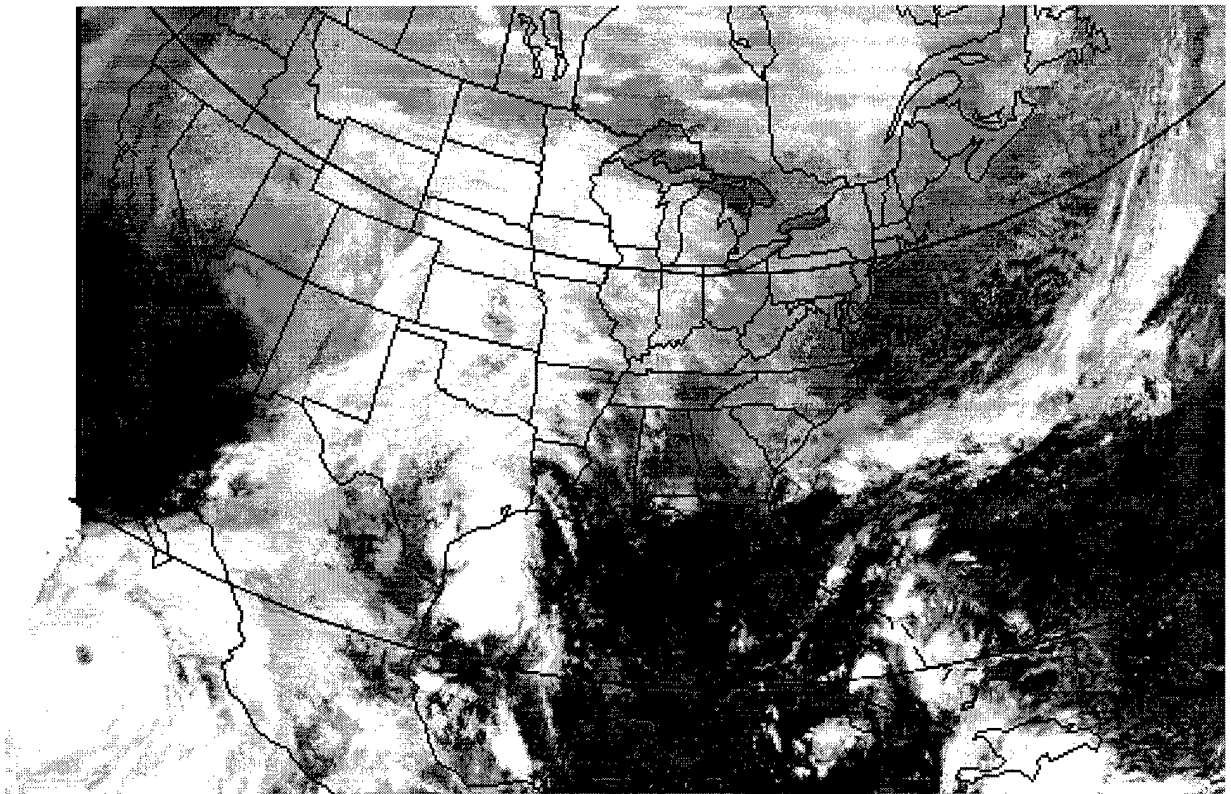


Figure 34. GOES East IR Satellite Image for 1215 UTC, 22 September 1997.

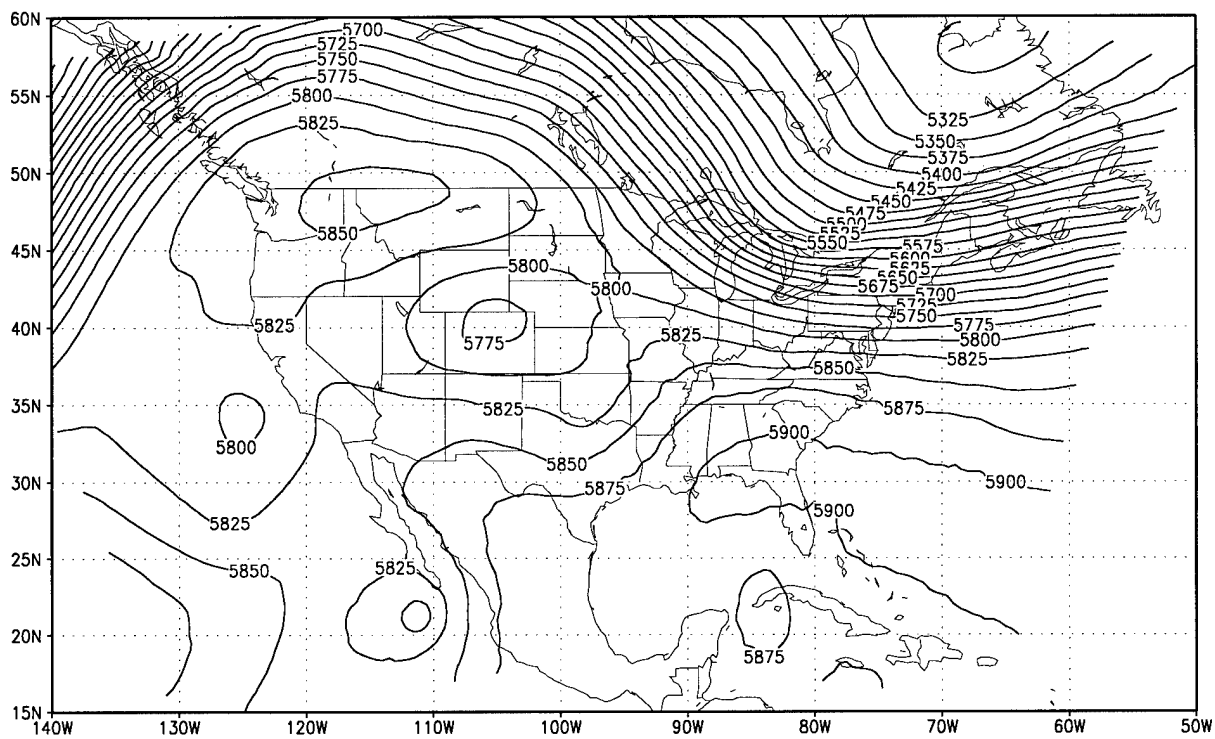


Figure 35. Meso-Eta 500-mb Geopotential Height for 1500 UTC, 23 September 1997.

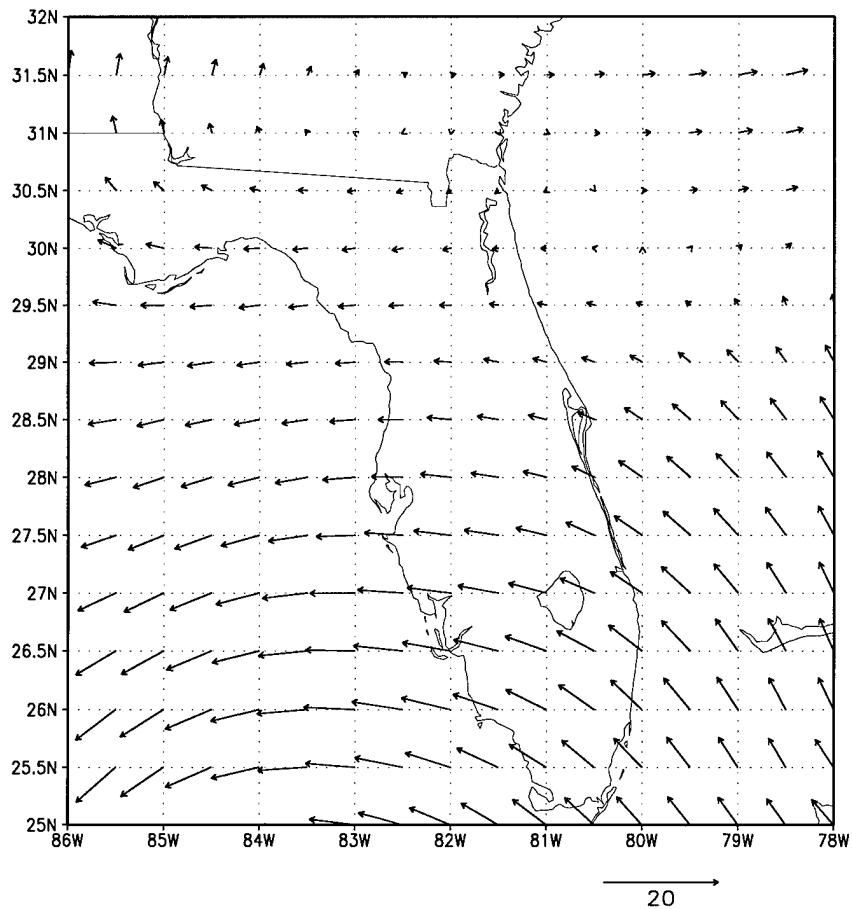


Figure 36. Meso-Eta 500-mb Winds Over Florida for 1500 UTC, 23 September 1997.

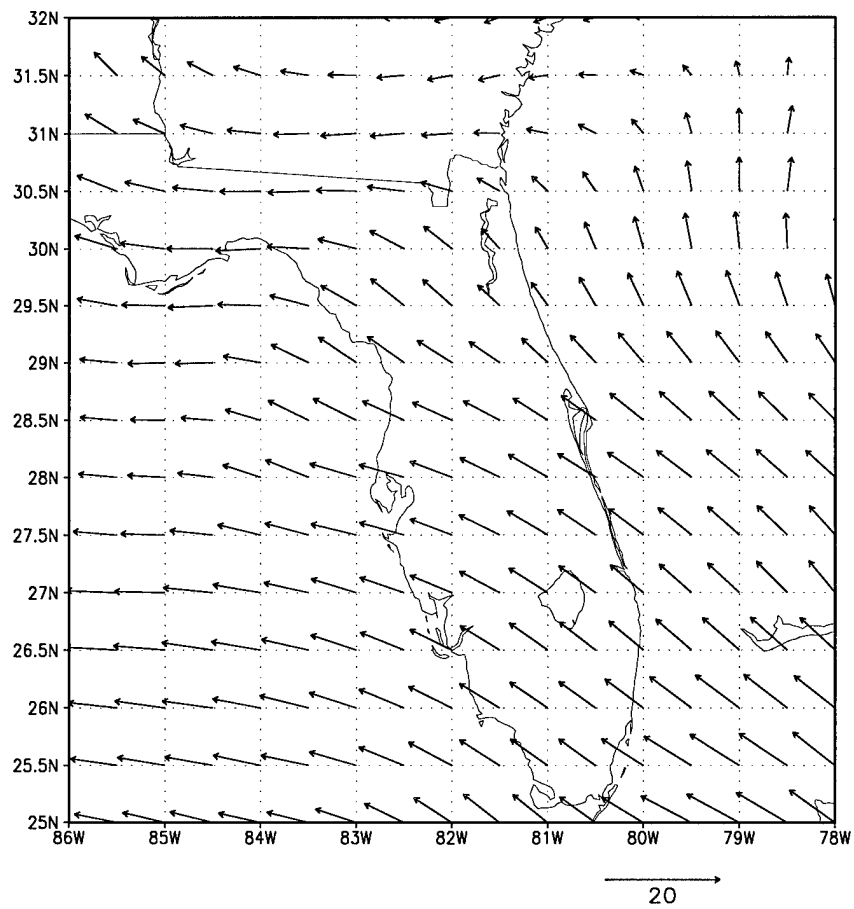


Figure 37. Meso-Eta 700-mb Winds Over Florida for 1500UTC, 23 September 1997.

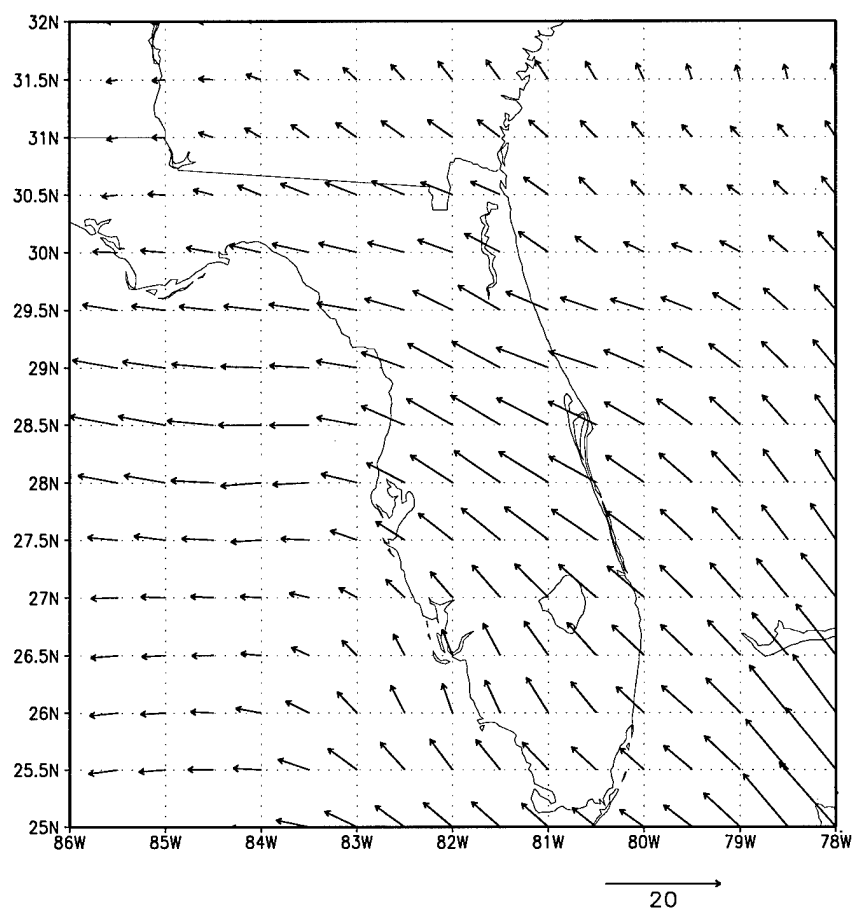


Figure 38. Meso-Eta 850-mb Winds Over Florida for 1500 UTC, 23 September 1997.

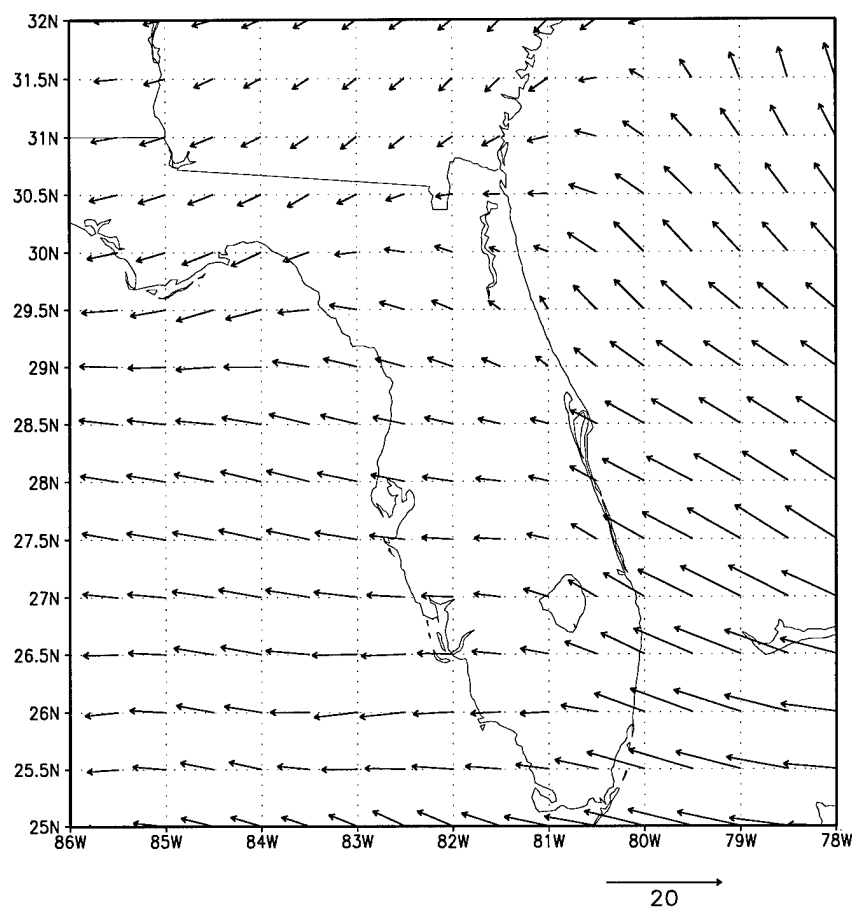


Figure 39. Meso- Eta 1000-mb Winds Over Florida for 1500 UTC, 23 September 1997.

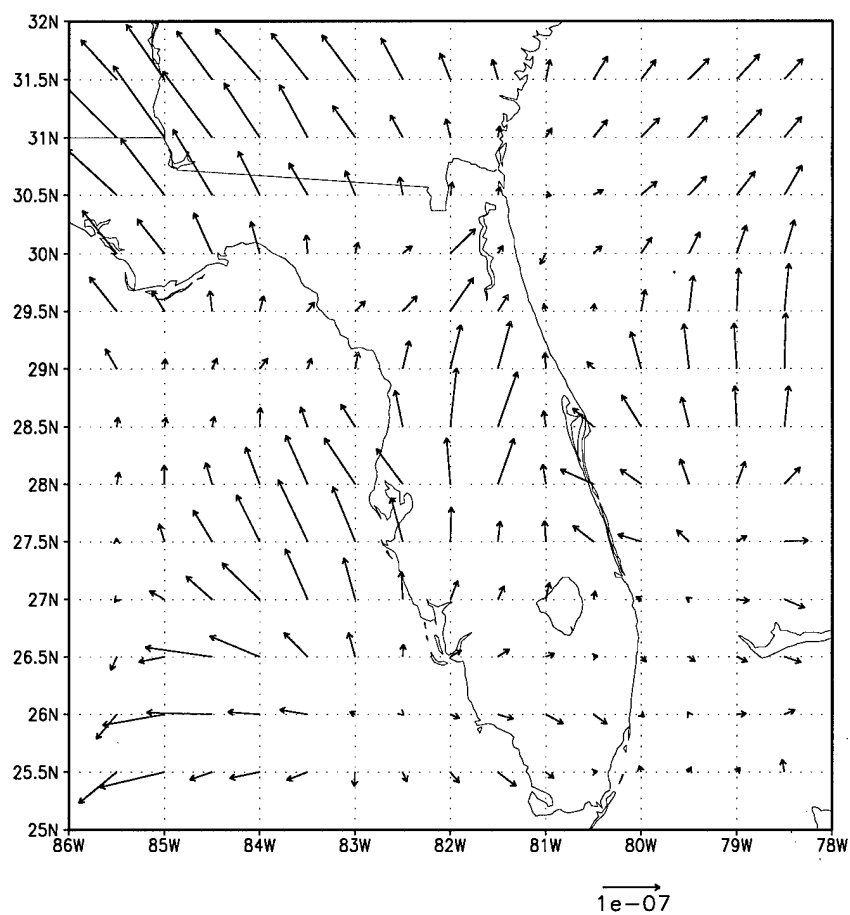


Figure 40. Meso-Eta 500-mb Q-vectors Over Florida for 1500 UTC, 23 September 1997.

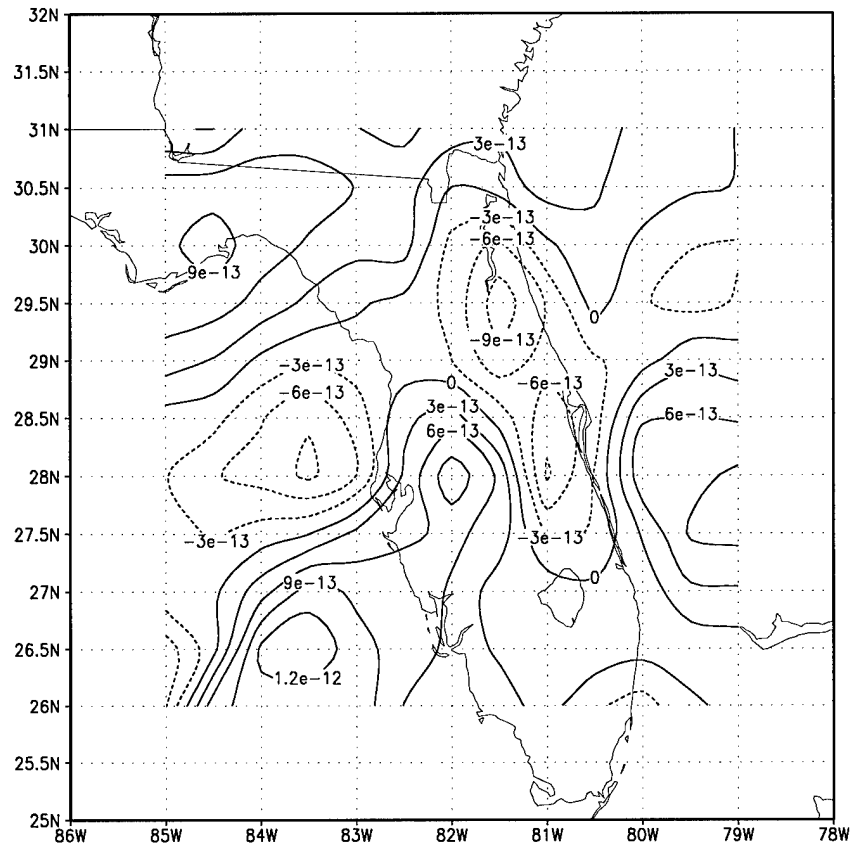


Figure 41. Meso-Eta 500-mb Q-vector Divergence Over Florida for 1500 UTC, 23 September 1997.

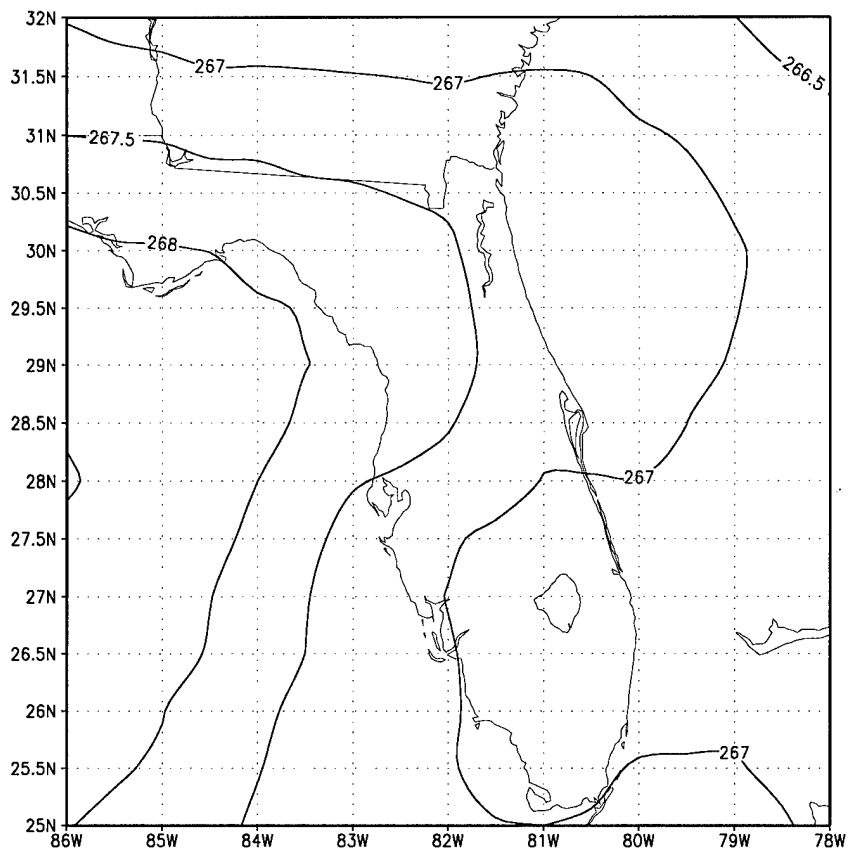


Figure 42. Meso-Eta 500-mb Temperatures Over Florida for 1500 UTC, 23 September 1997.

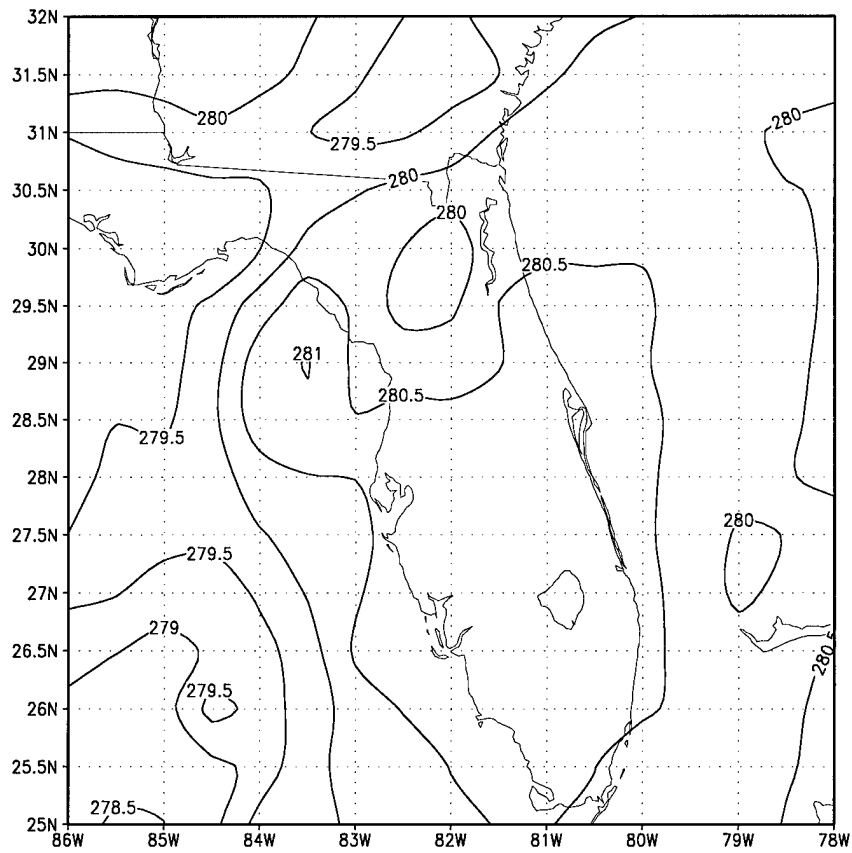


Figure 43. Meso-Eta 700-mb Temperatures Over Florida for 1500 UTC, 23 September 1997.

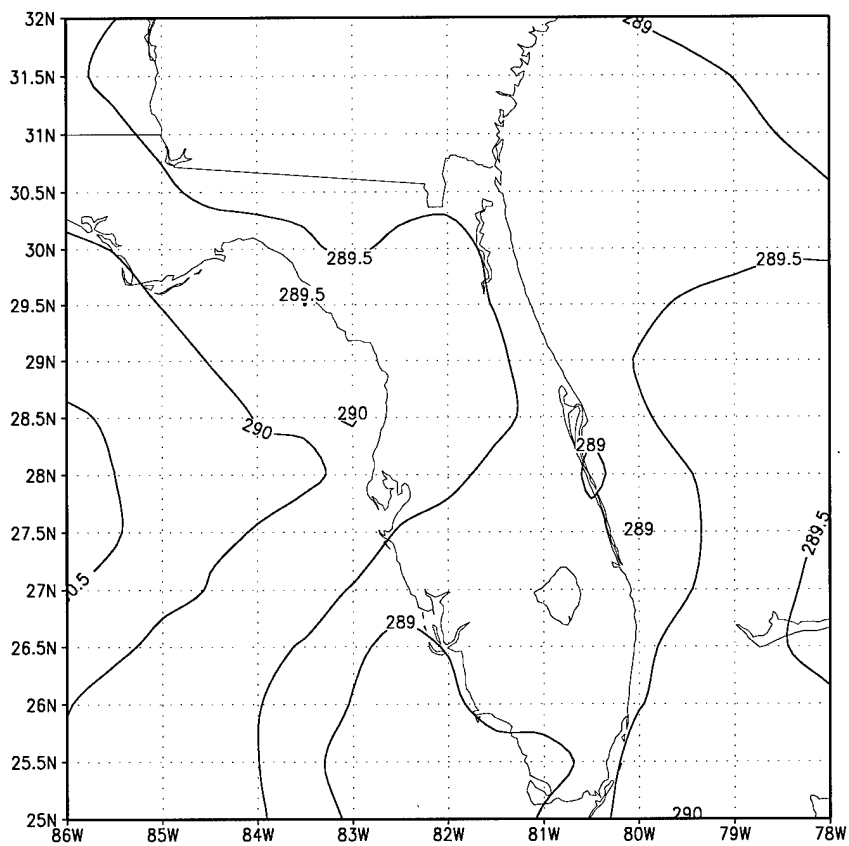


Figure 44. Meso-Eta 850-mb Temperatures Over Florida for 1500 UTC, 23 September 1997.

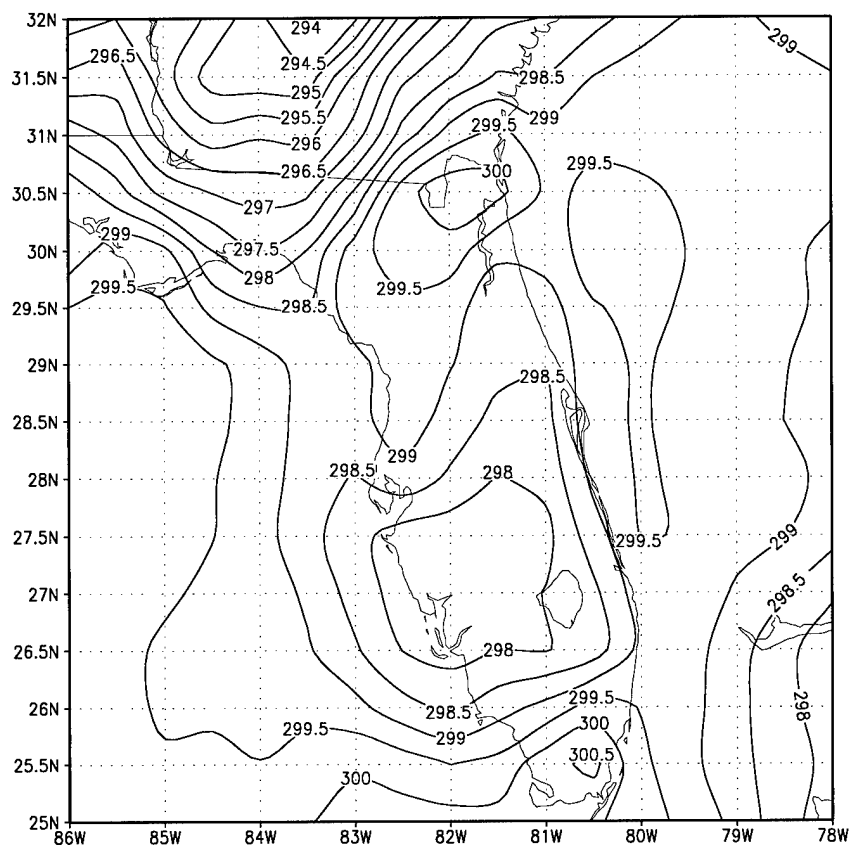


Figure 45. Meso-Eta 1000-mb Temperatures Over Florida for 1500 UTC, 23 September 1997.

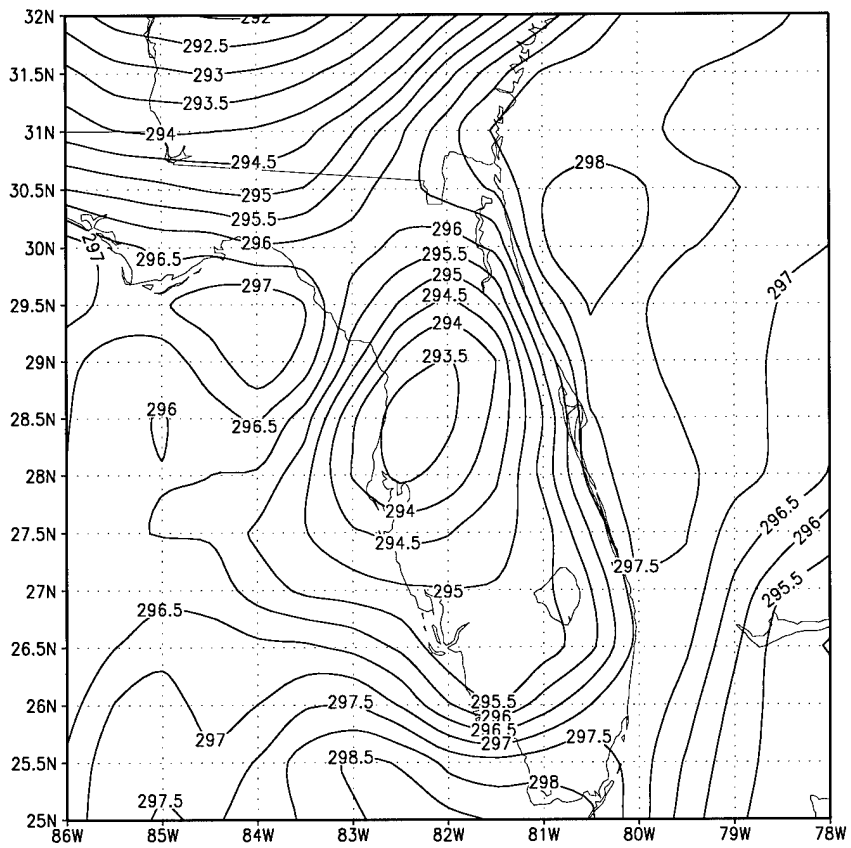


Figure 46. Meso-Eta 1000-mb Dew Point Temperature Over Florida for 1500 UTC, 23 September 1997.

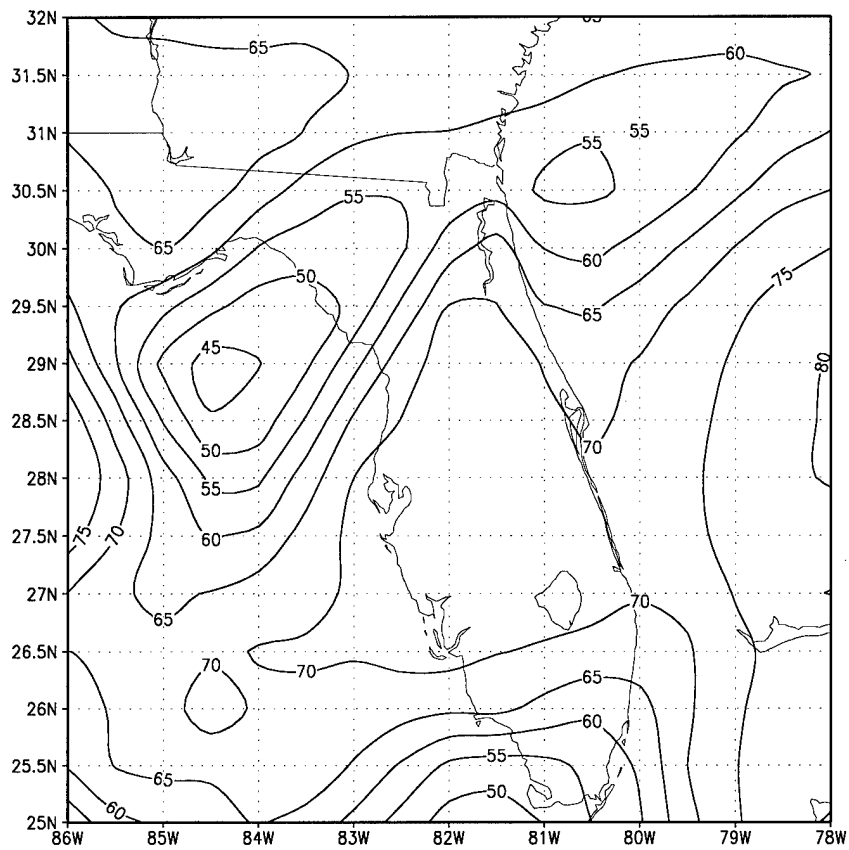


Figure 47. Meso-Eta 700-mb Relative Humidity Over Florida for 1500 UTC, 23 September 1997.

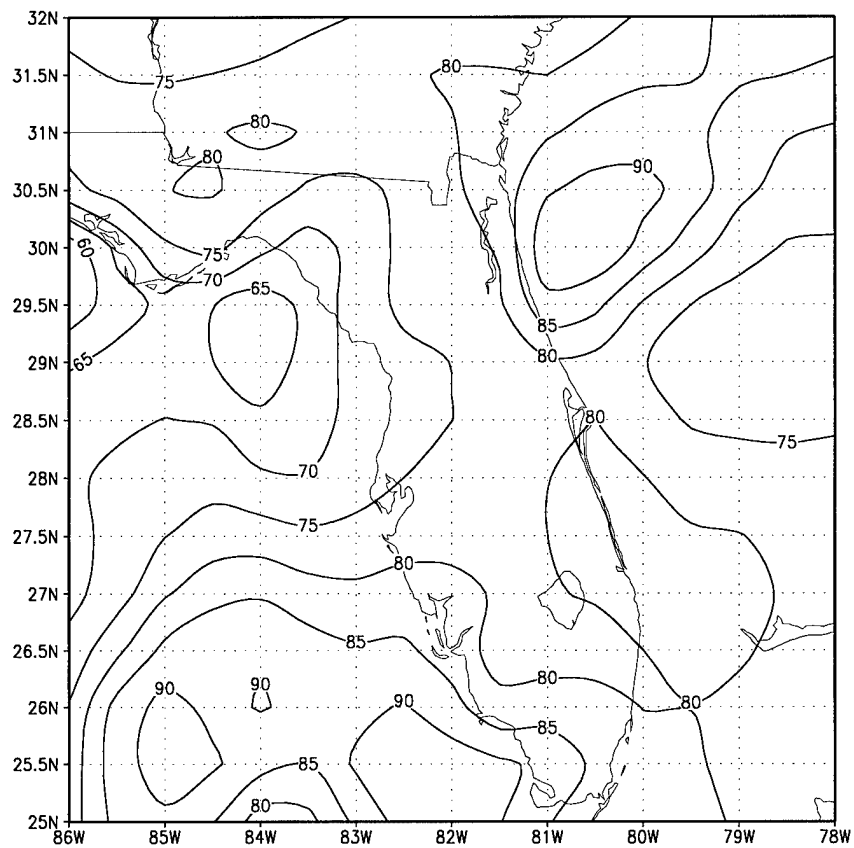


Figure 48. Meso-Eta 850-mb Relative Humidity Over Florida for 1500 UTC, 23 September 1997.

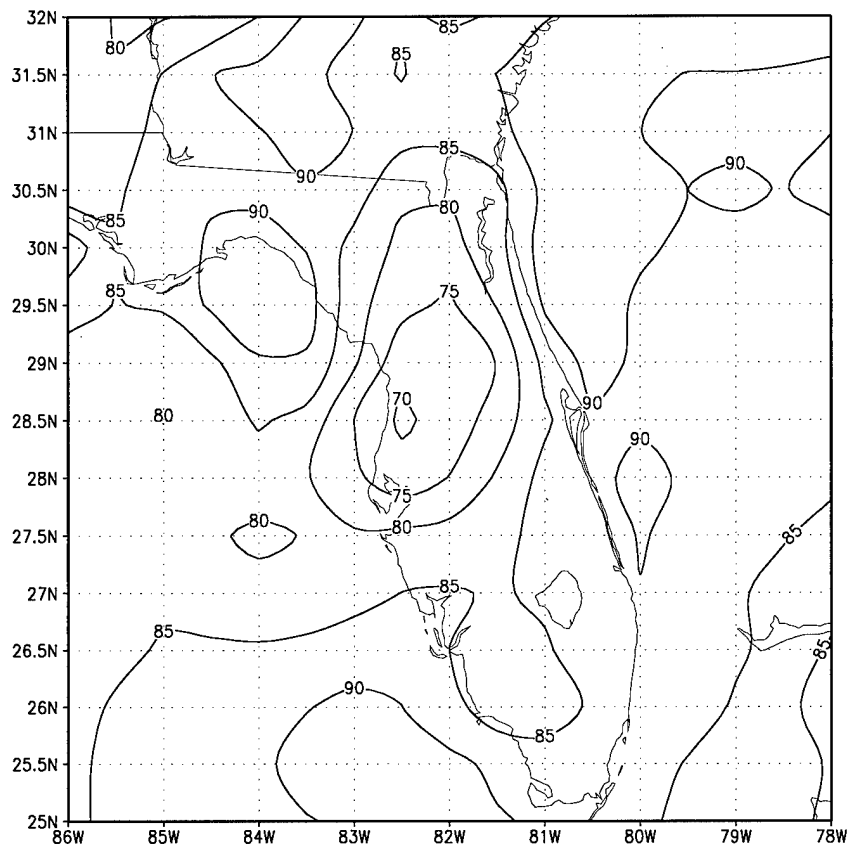


Figure 49. Meso-Eta 1000-mb Relative Humidity Over Florida for 1500 UTC, 23 September 1997.

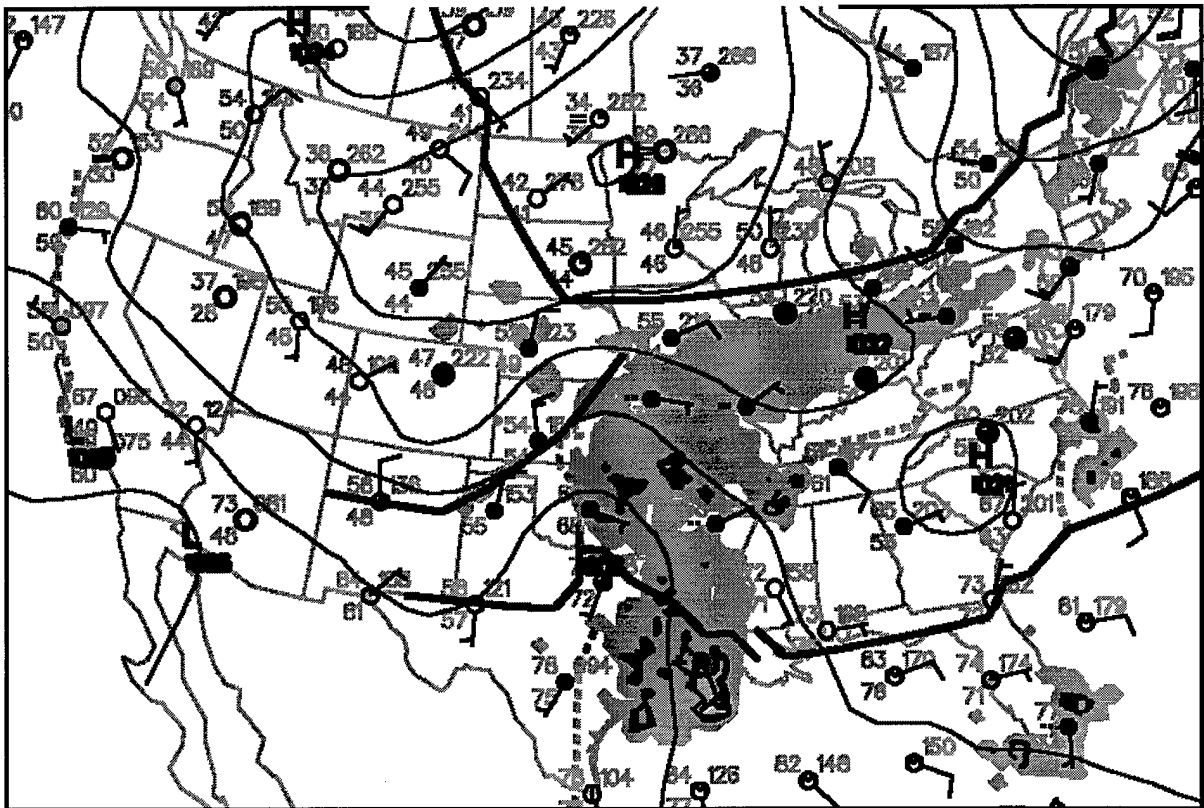


Figure 50. Surface Map with Radar Overlays for 1200 UTC, 23 September 1997.

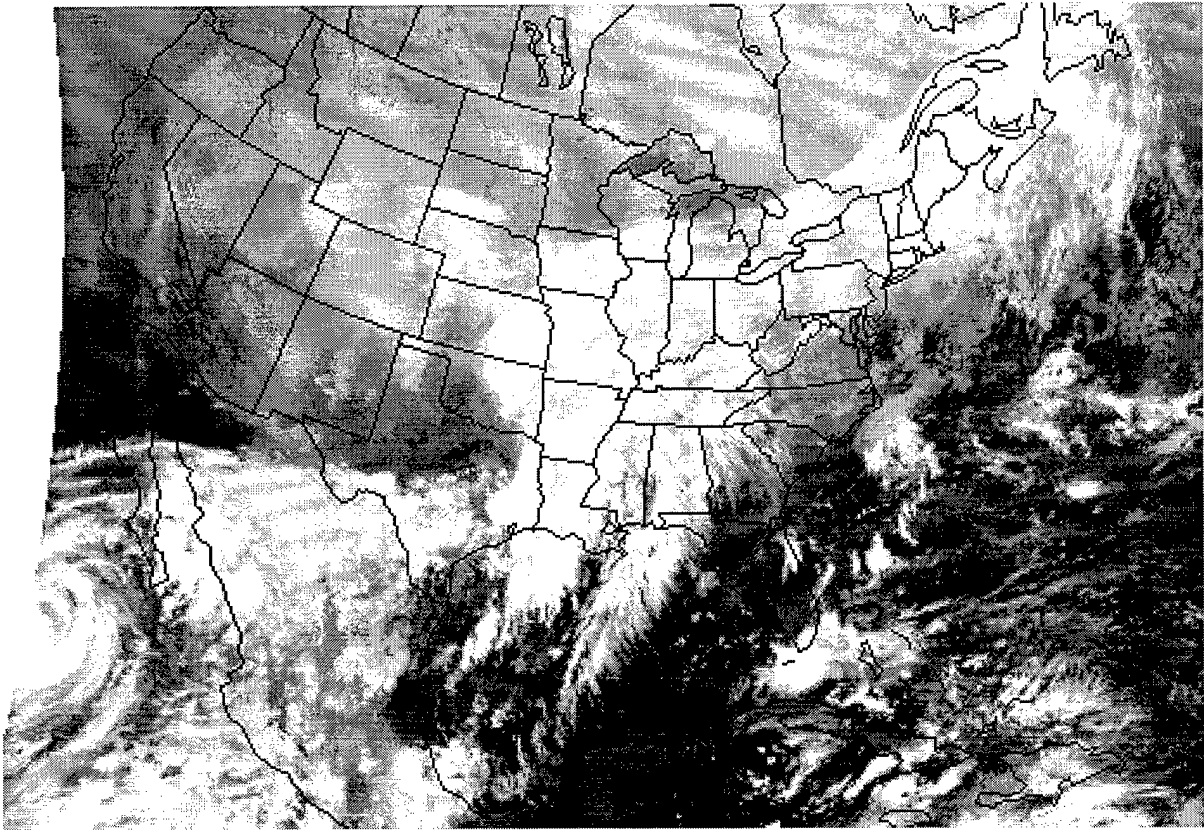


Figure 51. GOES East IR Satellite Image for 1215 UTC, 23 September 1997.

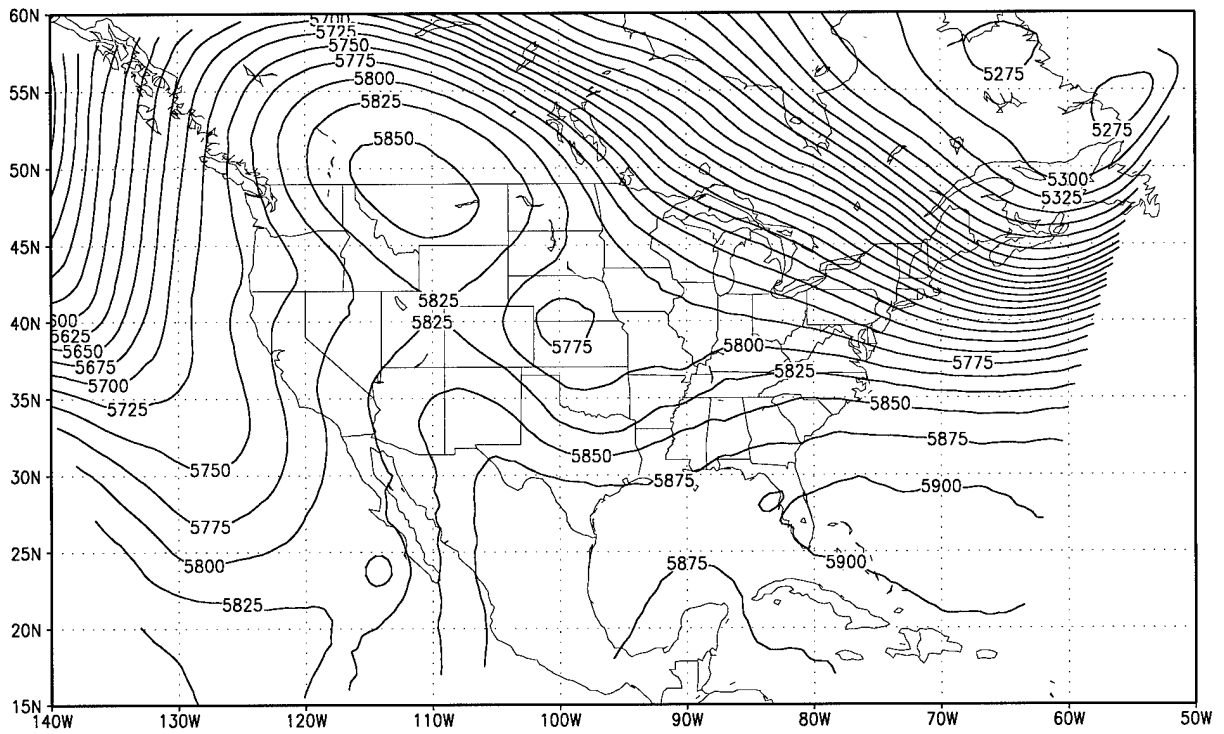


Figure 52. Meso-Eta 500-mb Geopotential Height for 1500 UTC, 24 September 1997.

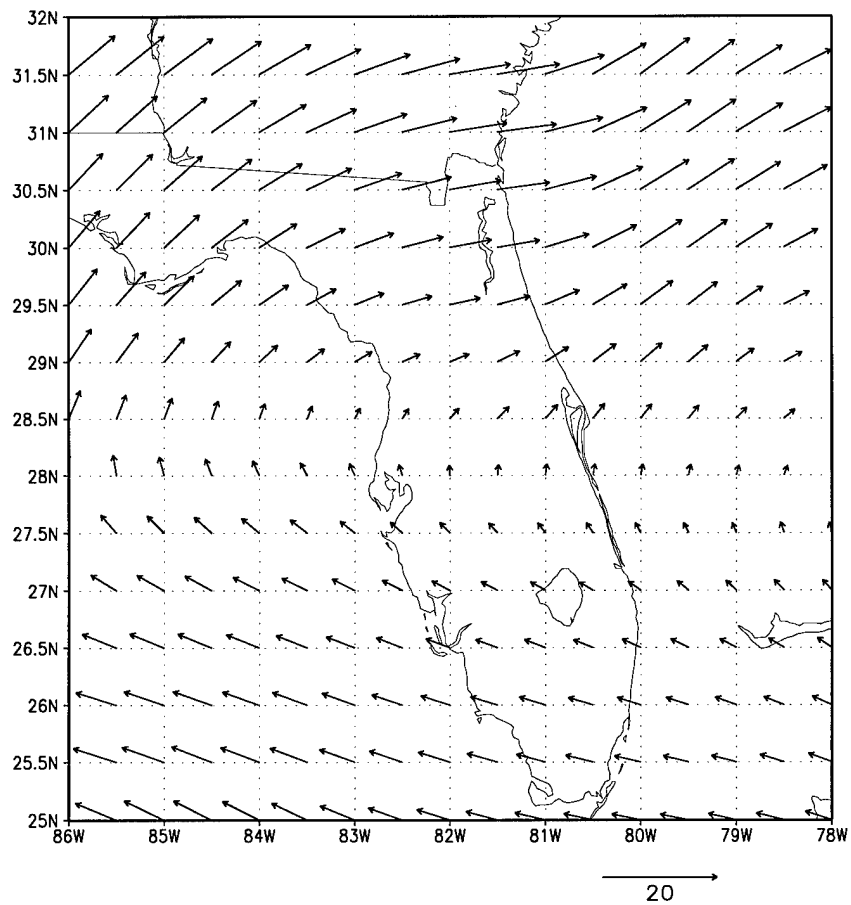


Figure 53. Meso-Eta 500-mb Winds Over Florida for 1500 UTC, 24 September 1997.

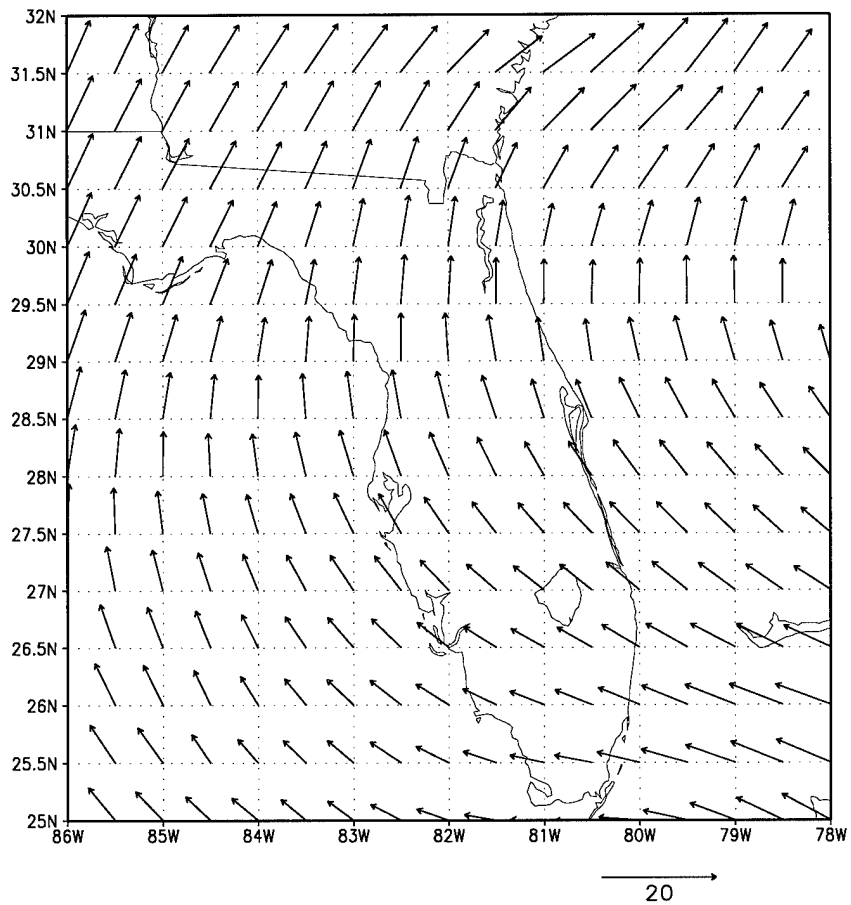


Figure 54. Meso-Eta 700-mb Winds Over Florida for 1500 UTC, 24 September 1997.

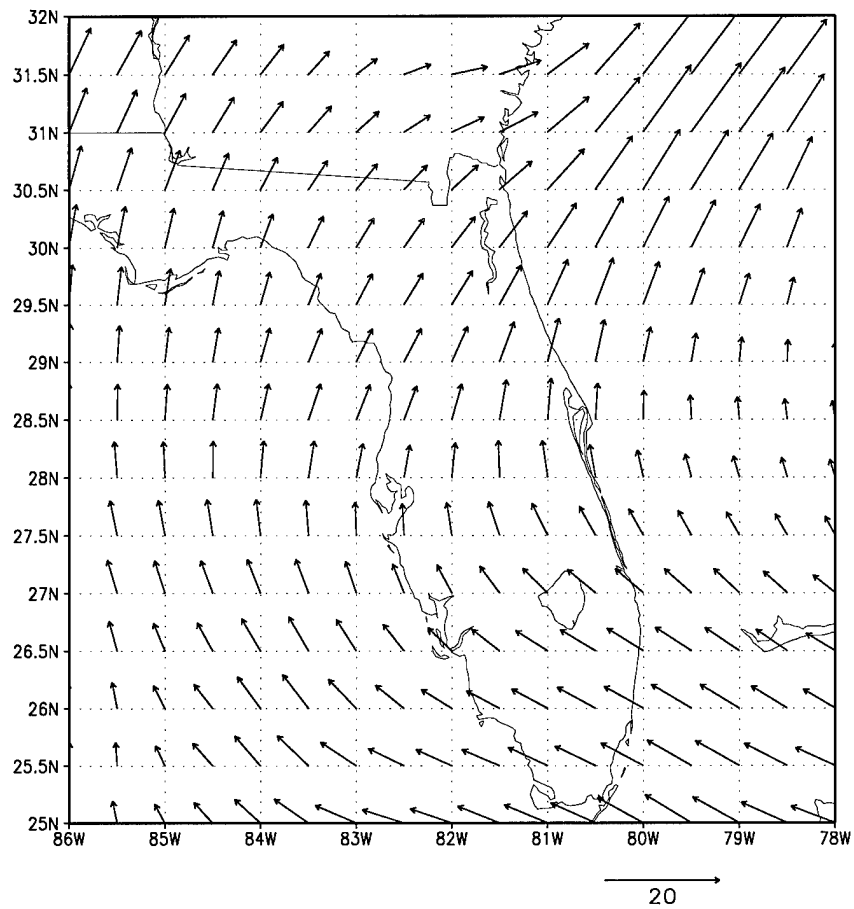


Figure 55. Meso-Eta 850-mb Winds Over Florida for 1500 UTC, 24 September 1997.

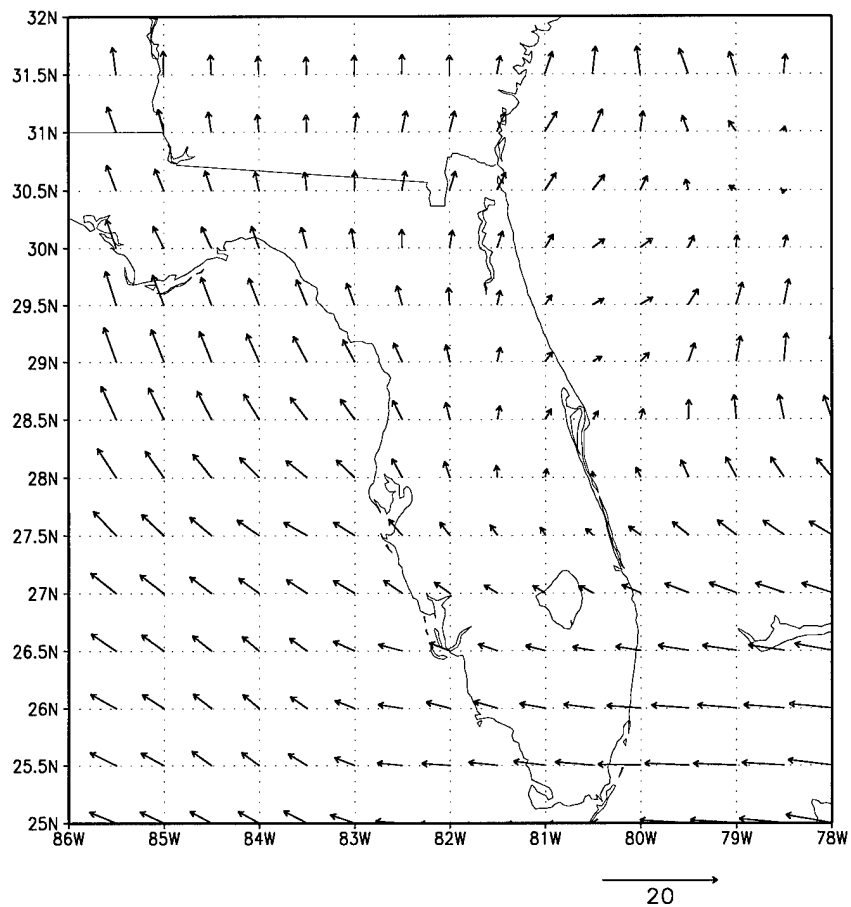


Figure 56. Meso-Eta 1000-mb Winds Over Florida for 1500 UTC, 24 September 1997.

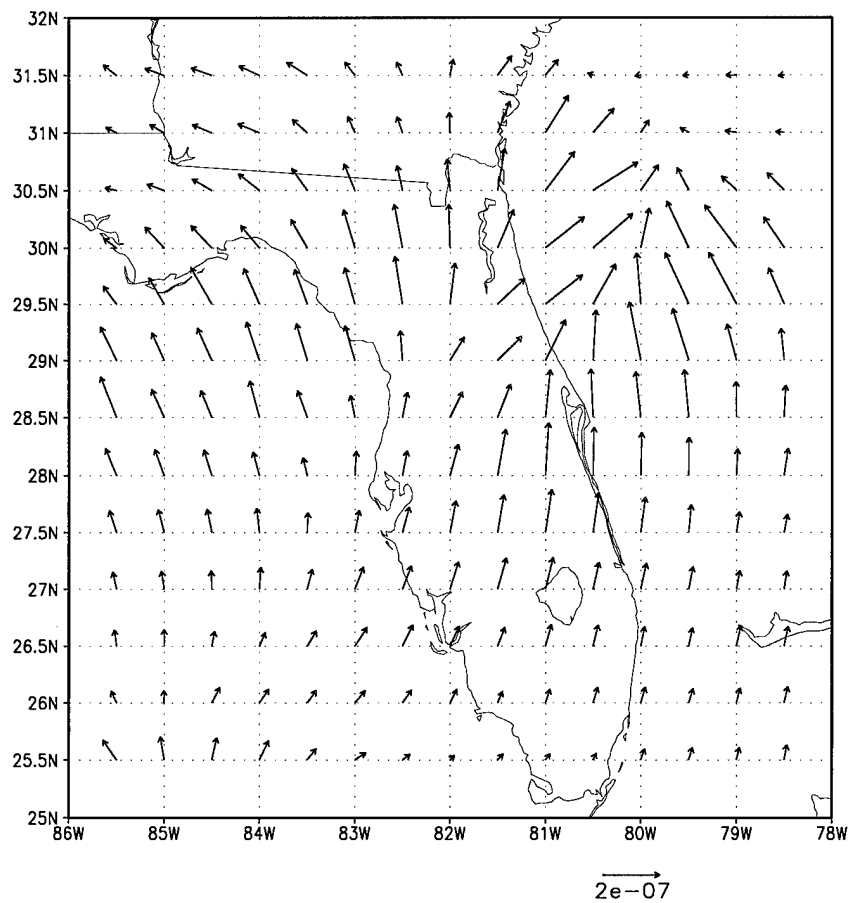


Figure 57. Meso-Eta 500-mb Q-vectors Over Florida for 1500 UTC, 24 September 1997.

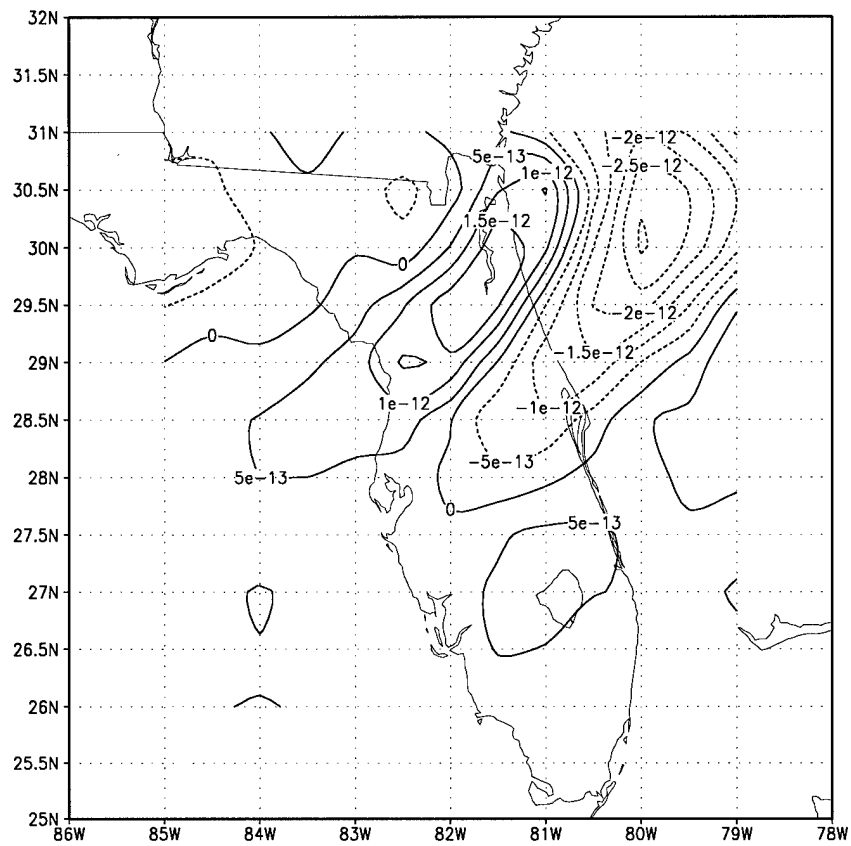


Figure 58. Meso-Eta 500-mb Q-vector Divergence Over Florida for 1500 UTC, 24 September 1997.

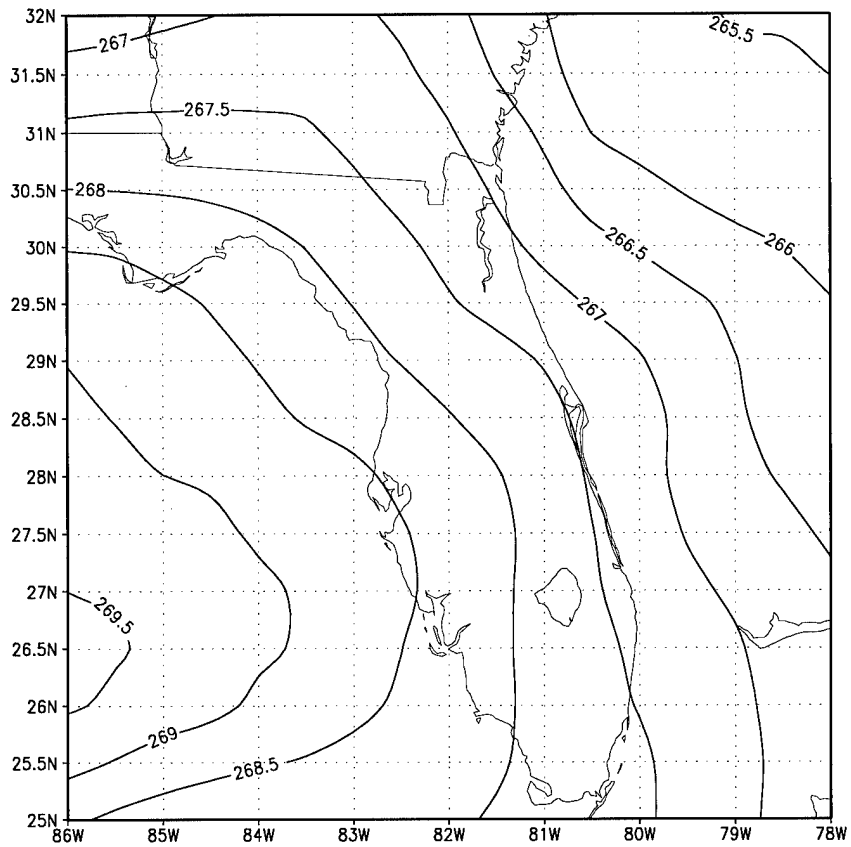


Figure 59. Meso-Eta 500-mb Temperatures Over Florida for 1500 UTC, 24 September 1997.

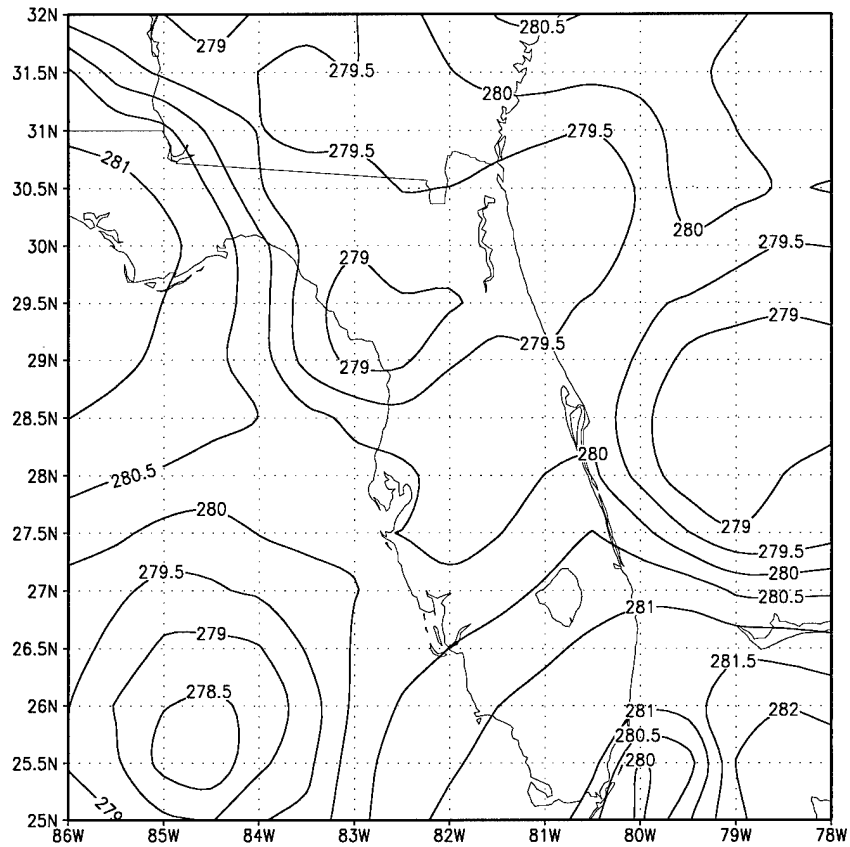


Figure 60. Meso-Eta 700-mb Temperatures Over Florida for 1500 UTC, 24 September 1997.

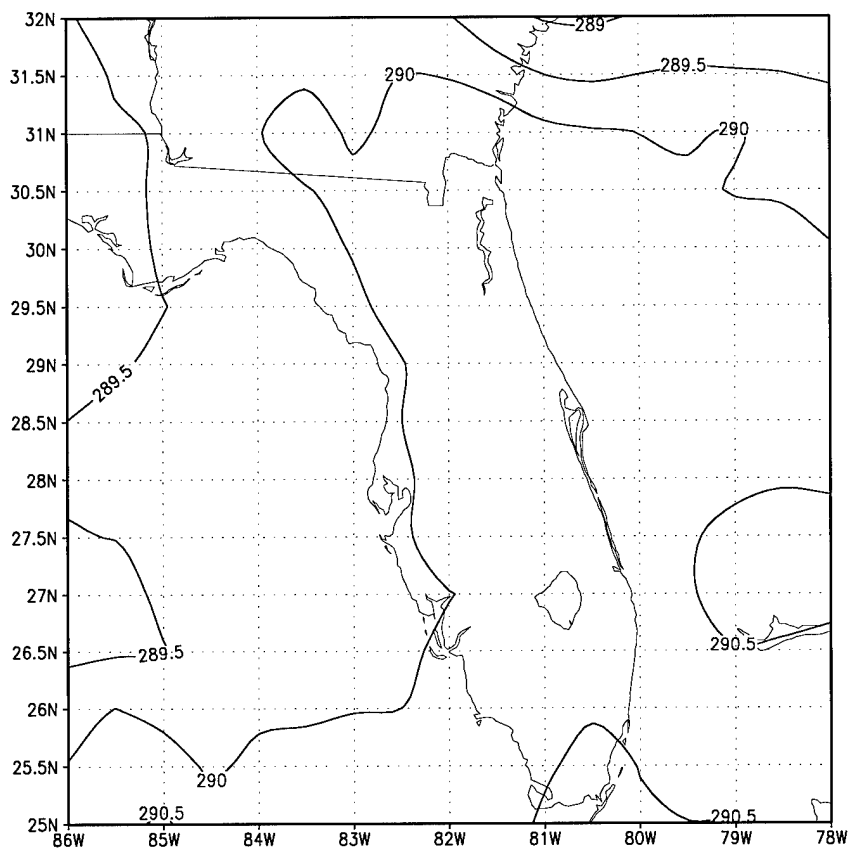


Figure 61. Meso-Eta 850-mb Temperatures Over Florida for 1500 UTC, 24 September 1997.

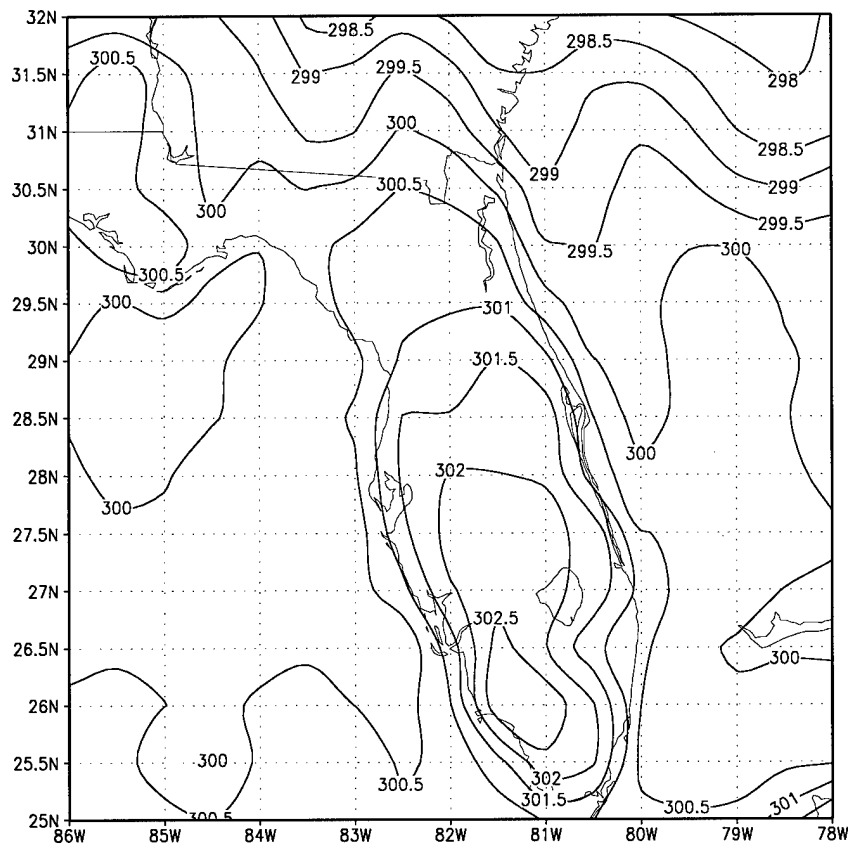


Figure 62. Meso-Eta 1000-mb Temperatures Over Florida for 1500 UTC, 24 September 1997.

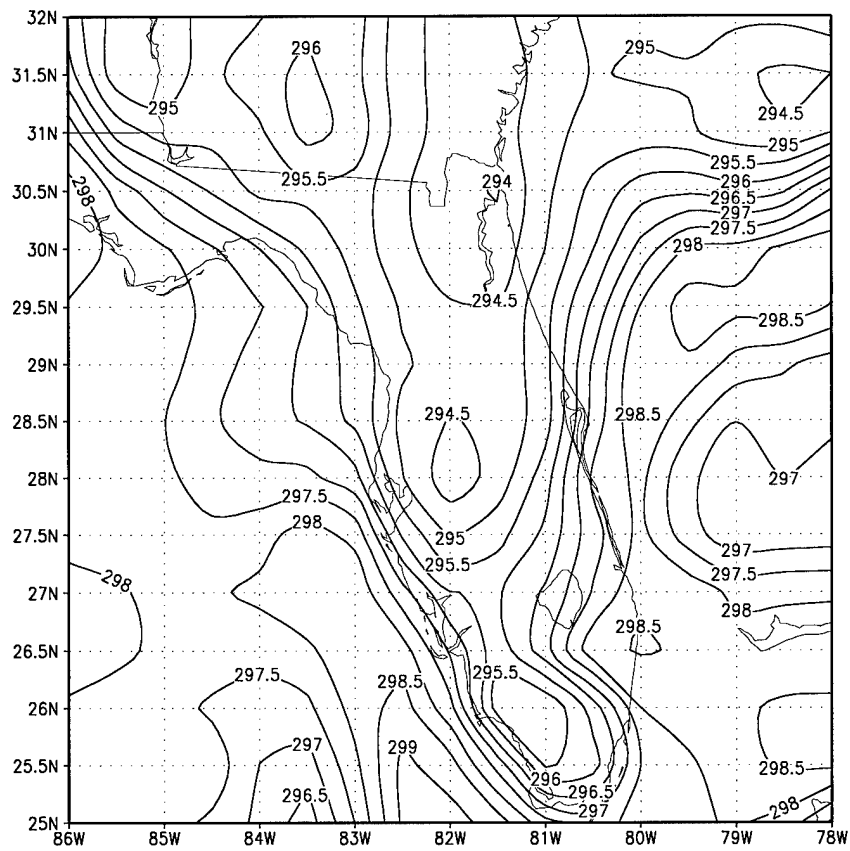


Figure 63. Meso-Eta 1000-mb Dew Point Temperatures Over Florida for 1500 UTC, 24 September 1997.

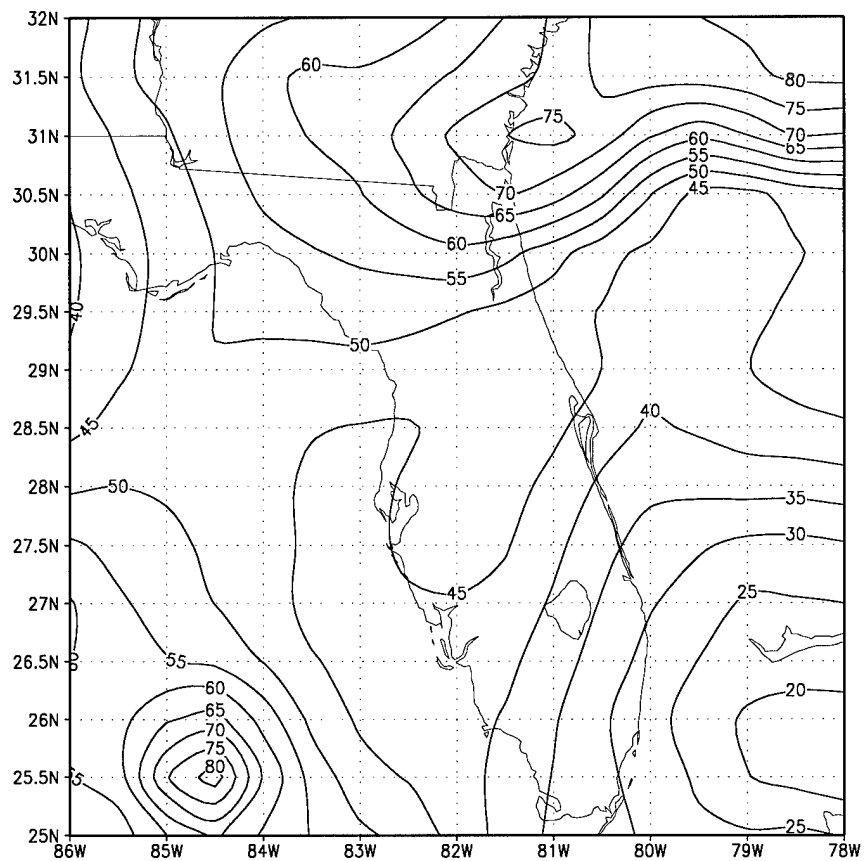


Figure 64. Meso-Eta 700-mb Relative Humidity Over Florida for 1500 UTC, 24 September 1997.

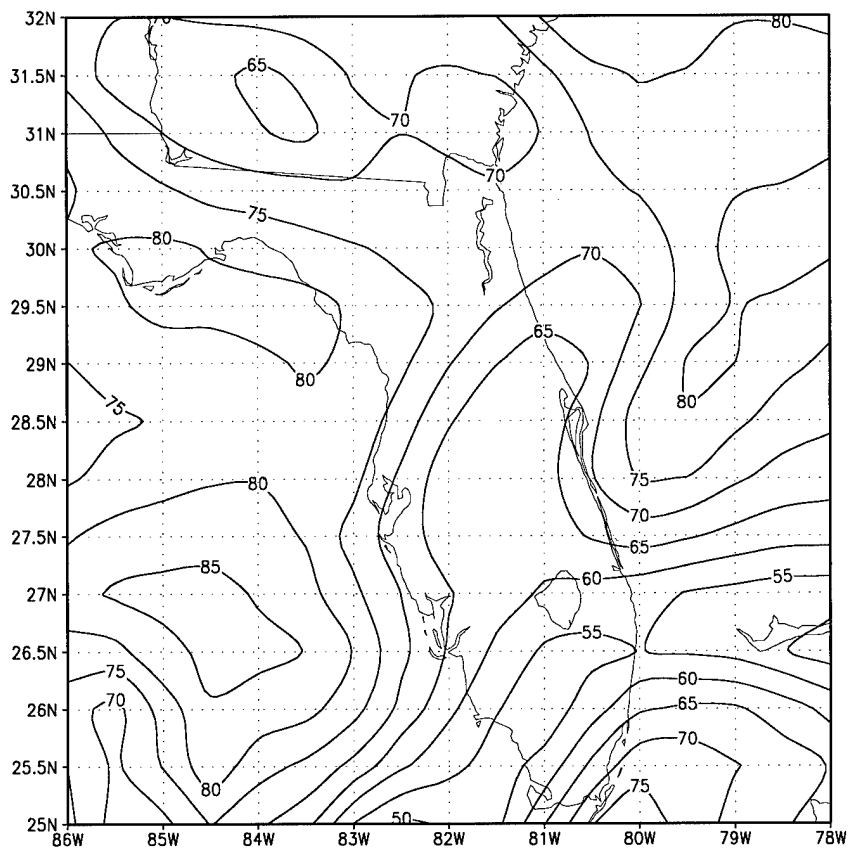


Figure 65. Meso-Eta 850-mb Relative Humidity Over Florida for 1500 UTC, 24 September 1997.

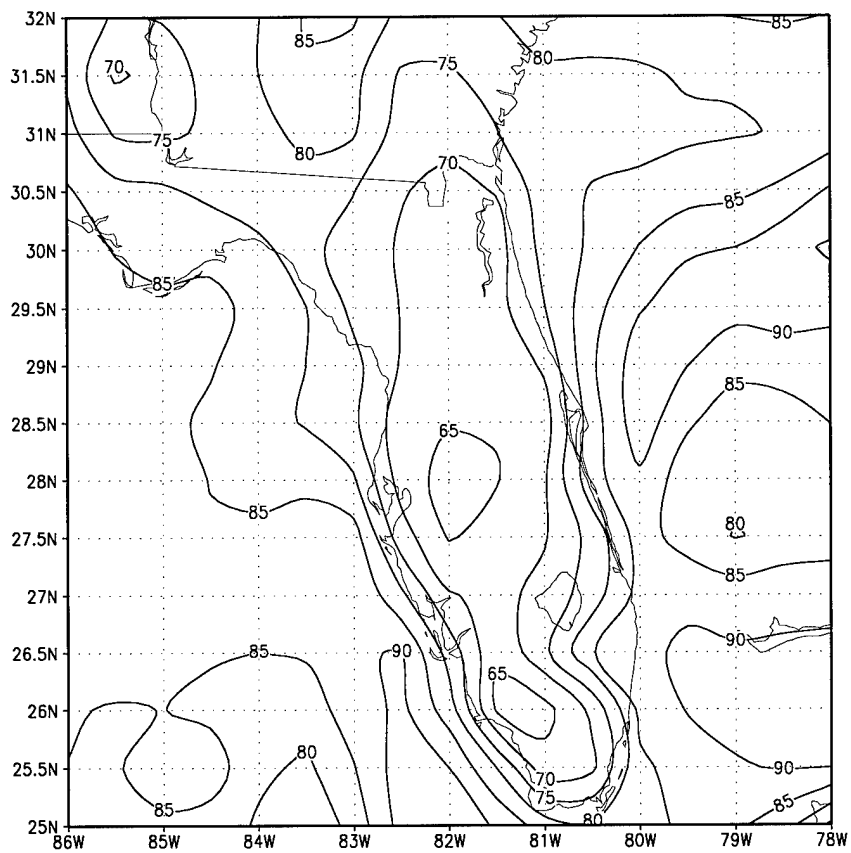


Figure 66. Meso-Eta 1000-mb Relative Humidity Over Florida for 1500 UTC, 24 September 1997.

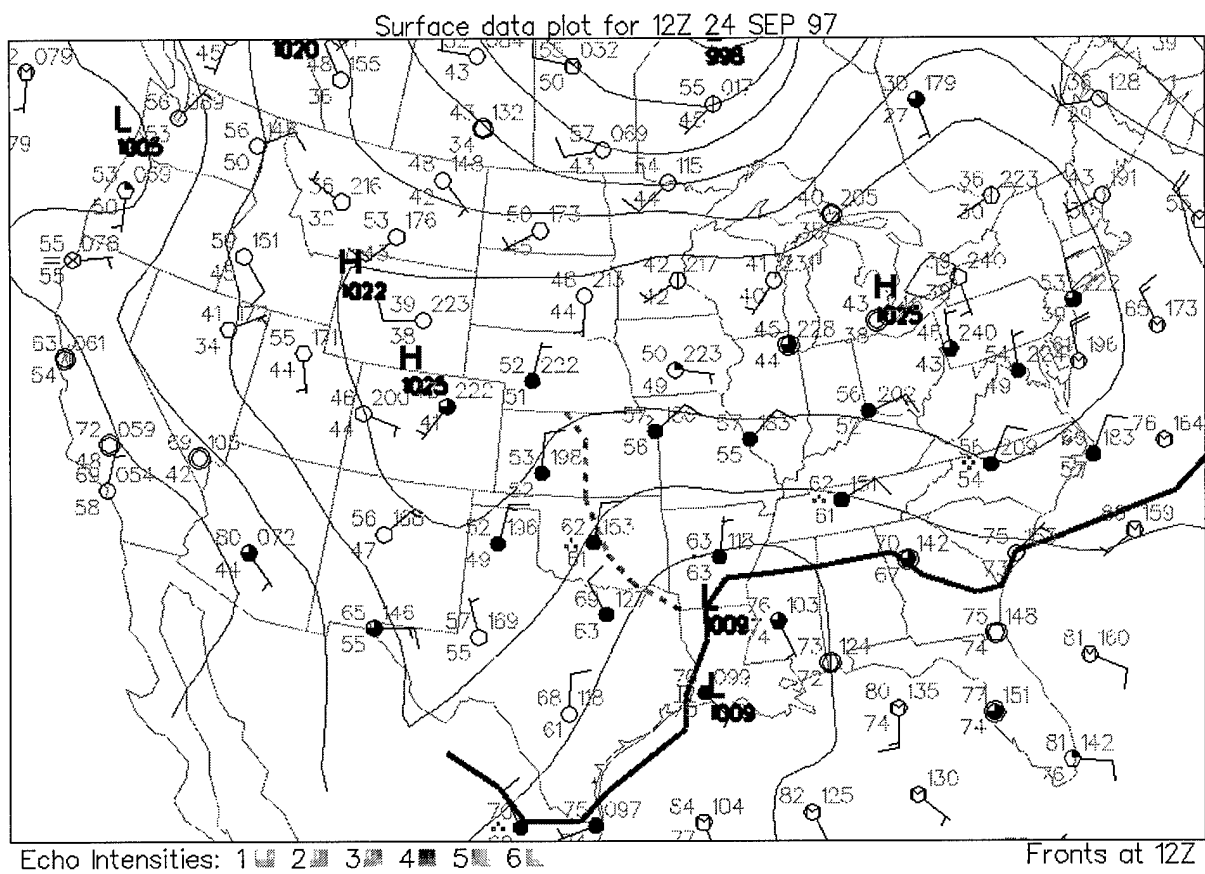


Figure 67. Surface Map with Radar Overlays for 1200 UTC, 24 September 1997.

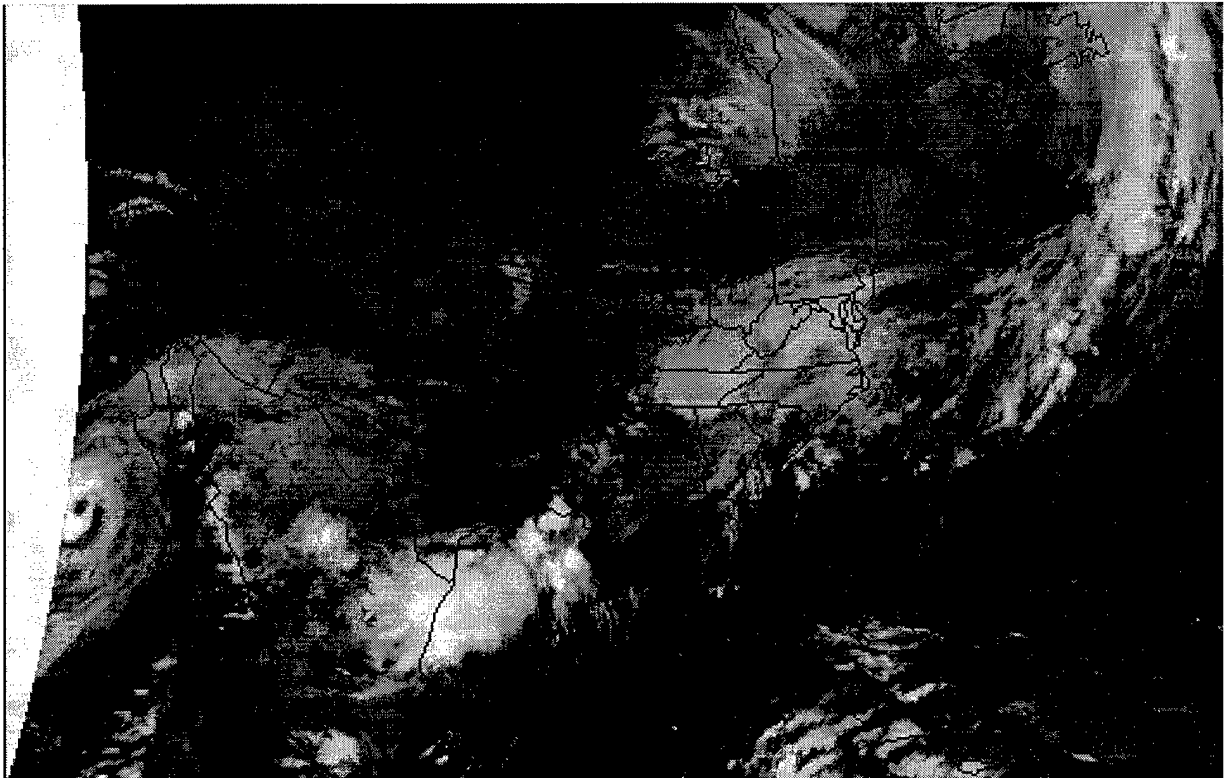


Figure 68. GOES East IR Satellite Image for 1215 UTC, 24 September 1997.

V. Conclusions and Recommendations

5.1 Overview

As an initial exploration into the use of the Meso-Eta numerical model with the NPTI algorithm, this research indicated that it may have potential as a forecasting technique. Although use of this combination may provide a viable option for forecasting thunderstorms over CCAS and KCS, there is still a significant amount of research that can be done to test and improve the method. Mesoscale modeling and the use of statistics to help automate forecasts will continue to be a vital area of study for many years as the modeling, computers, and data sources continue to expand and increase our knowledge of the environmental system.

5.2 Conclusions

The hypothesis that the NPTI algorithm with Meso-Eta inputs could produce a forecast which could outperform persistence was tested. This method does perform slightly better than persistence on the limited time frame of this study according to the statistical analysis. The small sample size does not make this a definitive study on the subject, but it does provide an initial investigation into the value of this forecasting method for use by the 45th Weather Squadron. The operational value of this technique is very limited, but future research may provide a valuable forecasting aid. With continued research and improvements in technology over the next few years, this research may lead to an automated forecasting method that can be used by the forecasters to improve the

seven day planning forecast. The Applied Meteorology Unit, which resides with the 45th Weather Squadron at CCAS, is a valuable source of information and insight into the use of new technology and how to deliver that to the forecaster. With their aid, this could become a useful tool for the forecasters who support the space launch and recovery program.

5.3 Recommendations

The research completed was an initial study into the use of numerical model output as input to a local thunderstorm index. Many other approaches can be taken to improve this method of forecasting. We have seen that this small sample size was able to create somewhat skillful forecasts. Continued research should attempt to utilize a much larger sample size with at least a whole warm season and preferably multiple warm seasons. A problem with future research is that the Meso-Eta is being continually improved by NCEP. The model used in this research is scheduled to be updated sometime in the next year with future versions already being anticipated. Another direction that can be taken with future research is to use the actual model output to develop a multiple regression based thunderstorm probability algorithm instead of the NPTI, which was created for use with the daily radiosonde sounding. It is possible that other variables produced by the model will provide better input into probability calculation for thunderstorm occurrence. Other models may also provide some useful information for thunderstorm forecasting. This method could be tested on different models which have different dynamic calculation methods, different resolutions, and

different forecast lengths. The forecast period of the model is important because the 45th Weather Squadron is required to produce a seven day planning forecast. This research only concentrated on day-two of the planning forecast. Another idea is to include radar, satellite, and the extensive lightning detection network at Cape Canaveral to confirm thunderstorms on site. Because of the huge savings possible by providing improved support to the space launch program, continuation of similar research is highly encouraged.

Appendix A. Code for NPTI Algorithm with Meso-Eta Inputs

```

*****
*
* This program is designed to take eta model output and use it to
* calculate the Neumann-Pfeffer Thunderstorm Index. This code was
* written for thesis work by 2LT Christian Wohlwend, AFIT/ENP.
*
* Last Modified: 20 NOV 97
*****
*
PROGRAM ETA_A
PARAMETER(IE=10,JE=10)
PARAMETER(MAXREC=16)
REAL      D(73,73), DD(5329)
REAL      C(260000)
REAL      ROW(IE,JE)
REAL      T500(IE,JE)
REAL      U500(IE,JE)
REAL      V500(IE,JE)
REAL      RH600(IE,JE)
REAL      RH625(IE,JE)
REAL      RH650(IE,JE)
REAL      RH675(IE,JE)
REAL      RH700(IE,JE)
REAL      RH725(IE,JE)
REAL      RH750(IE,JE)
REAL      RH775(IE,JE)
REAL      RH800(IE,JE)
REAL      T850(IE,JE)
REAL      TD850(IE,JE)
REAL      U850(IE,JE)
REAL      V850(IE,JE)
REAL      RH_AVE(IE,JE)
REAL      SSI(IE,JE)
REAL      SPD8(IE,JE)
REAL      SPD5(IE,JE)
REAL      DIR8(IE,JE)
REAL      DIR5(IE,JE)
REAL      COF
REAL      TTS
INTEGER    KGDS(200)
INTEGER    N1(IE,JE)

```

INTEGER	N2(IE,JE)
INTEGER	N3(IE,JE)
INTEGER	N4(IE,JE)
INTEGER	N5(IE,JE)
INTEGER	N6(IE,JE)
INTEGER	NPTI(IE,JE)
* INTEGER	KTIME(IE,JE)
INTEGER	KERR
INTEGER	I
INTEGER	J
INTEGER	L
INTEGER	V
INTEGER	IREC
INTEGER	LENPDS
INTEGER	LENKGDS
INTEGER	NWORDS
INTEGER	DAY
INTEGER	MO
INTEGER	YR
INTEGER	HR
INTEGER	P
INTEGER	Q
INTEGER	YEARC(92)
INTEGER	MONTHC(92)
INTEGER	DAYC(92)
INTEGER	TSTC(92)
INTEGER	YEART(92)
INTEGER	MONTHT(92)
INTEGER	DAYT(92)
INTEGER	TSTT(92)
INTEGER	PREC
INTEGER	PRET
INTEGER	JSPD8(IE,JE)
INTEGER	JSPD5(IE,JE)
INTEGER	JDIR8(IE,JE)
INTEGER	JDIR5(IE,JE)
INTEGER	KCOF
INTEGER	KTTS
CHARACTER*1	PDS(100)
CHARACTER*2	Y
CHARACTER*2	M
CHARACTER*2	DA
CHARACTER*2	H

```

    CHARACTER*8 OUT
    CHARACTER*44 INFILE
    CHARACTER*44 OUTFILE
*
    EQUIVALENCE (D(1,1),DD(1))
*
113  FORMAT (A16)
112  FORMAT (10I4)
111  FORMAT (10F10.5)
114  FORMAT (A8,2X,F5.2)
115  FORMAT (I2,I2,I2,4X,I1)
116  FORMAT (10(I4,1X))
    OPEN(7,FILE='~/Thesis/programs/KCOF.dat',STATUS='OLD')
    OPEN(8,FILE='~/Thesis/programs/KTTS.dat',STATUS='OLD')
    DO 2 Q = 1,92
        READ(7,115) YEARC(Q),MONTHC(Q),DAYC(Q),TSTC(Q)
        READ(8,115) YEART(Q),MONTHT(Q),DAYT(Q),TSTT(Q)
2    CONTINUE
    DO 1000 P=1,69
        OPEN(9,FILE='~/Thesis/programs/input.dat',STATUS='OLD')
        READ(9,113) INFILE
        INFILE = '~/Thesis/output/'//INFILE
*****
*          Enter data here                                     *
*****
        OPEN (UNIT=11,FILE=INFILE,STATUS='OLD',
&    ACCESS='SEQUENTIAL',FORM='UNFORMATTED',IOSTAT=KERR)
*
        IF (KERR.NE.0) THEN
            PRINT 50 , INFILE, KERR
50    FORMAT ( ' ERROR OPENING UNIT=11, FILE NAME = ',A44,
&    ' ', IOSTAT = ',I8)
            STOP 50
        ENDIF
*
        IREC=1
        V=1
*
        DO 100 IREC=1,MAXREC
            READ (11,END=1100) LENPDS, LENKGDS, NWORDS
            PRINT *,LENPDS,LENKGDS,NWORDS = ',LENPDS,LENKGDS,NWORDS
            READ (11,END=1100) (PDS(L),L=1,LENPDS)
            YR = PDS(13)

```

```

MO = PDS(14)
DAY = PDS(15)
HR = PDS(16)
PRINT *, 'YEAR =', YR, ' MONTH =', MO, ' DAY =', DAY, ' HOUR =', HR
IF (LENKGDS.GT.0) THEN
  READ (11,END=1100) (KGDS(L),L=1,LENKGDS)
*   PRINT *, 'KGDS = '
*   PRINT *, (KGDS(L),L=1,LENKGDS)
  END IF
  READ (11,END=1100) (C(L),L=1,NWORDS)
*****
*
* Organize the data into readable form that will incorporate into the
* NPTI code.
*****

  CALL GRID1 (C,NWORDS,ROW)
*
  IF(V.EQ.1)THEN
    DO 14 J=1,JE
      DO 13 I=1,IE
        T500(I,J) = ROW(I,J)
13      CONTINUE
14      CONTINUE
    ENDIF
    IF(V.EQ.2)THEN
      DO 16 J=1,JE
        DO 15 I=1,IE
          U500(I,J) = ROW(I,J)
15      CONTINUE
16      CONTINUE
        ENDIF
        IF(V.EQ.3)THEN
          DO 18 J=1,JE
            DO 17 I=1,IE
              V500(I,J) = ROW(I,J)
17      CONTINUE
18      CONTINUE
            ENDIF
            IF(V.EQ.4)THEN
              DO 20 J=1,JE
                DO 19 I=1,IE
                  RH600(I,J) = ROW(I,J)
19      CONTINUE

```

```

20    CONTINUE
    ENDIF
    IF(V.EQ.5)THEN
        DO 22 J=1,JE
            DO 21 I=1,IE
                RH625(I,J) = ROW(I,J)
21        CONTINUE
22    CONTINUE
    ENDIF
    IF(V.EQ.6)THEN
        DO 24 J=1,JE
            DO 23 I=1,IE
                RH650(I,J) = ROW(I,J)
23        CONTINUE
24    CONTINUE
    ENDIF
    IF(V.EQ.7)THEN
        DO 26 J=1,JE
            DO 25 I=1,IE
                RH675(I,J) = ROW(I,J)
25        CONTINUE
26    CONTINUE
    ENDIF
    IF(V.EQ.8)THEN
        DO 28 J=1,JE
            DO 27 I=1,IE
                RH700(I,J) = ROW(I,J)
27        CONTINUE
28    CONTINUE
    ENDIF
    IF(V.EQ.9)THEN
        DO 30 J=1,JE
            DO 29 I=1,IE
                RH725(I,J) = ROW(I,J)
29        CONTINUE
30    CONTINUE
    ENDIF
    IF(V.EQ.10)THEN
        DO 32 J=1,JE
            DO 31 I=1,IE
                RH750(I,J) = ROW(I,J)
31        CONTINUE
32    CONTINUE

```



```

ENDIF
IF(V.EQ.11)THEN
  DO 34 J=1,JE
    DO 33 I=1,IE
      RH775(I,J) = ROW(I,J)
33    CONTINUE
34  CONTINUE
ENDIF
IF(V.EQ.12)THEN
  DO 36 J=1,JE
    DO 35 I=1,IE
      RH800(I,J) = ROW(I,J)
35    CONTINUE
36  CONTINUE
ENDIF
IF(V.EQ.13)THEN
  DO 38 J=1,JE
    DO 37 I=1,IE
      T850(I,J) = ROW(I,J)
37    CONTINUE
38  CONTINUE
ENDIF
IF(V.EQ.14)THEN
  DO 40 J=1,JE
    DO 39 I=1,IE
      TD850(I,J) = ROW(I,J)
39    CONTINUE
40  CONTINUE
ENDIF
IF(V.EQ.15)THEN
  DO 42 J=1,JE
    DO 41 I=1,IE
      U850(I,J) = ROW(I,J)
41    CONTINUE
42  CONTINUE
ENDIF
IF(V.EQ.16)THEN
  DO 44 J=1,JE
    DO 43 I=1,IE
      V850(I,J) = ROW(I,J)
43    CONTINUE
44  CONTINUE
ENDIF

```

```

      V = V + 1
100  CONTINUE
      DO 102 I = 1,IE
        DO 101 J = 1,JE
          SPD8(I,J) = SQRT(U850(I,J)*U850(I,J)+V850(I,J)*V850(I,J))
          DIR8(I,J) = ATAN(V850(I,J)/U850(I,J))
          SPD5(I,J) = SQRT(U500(I,J)*U500(I,J)+V500(I,J)*V500(I,J))
          DIR5(I,J) = ATAN(V500(I,J)/U500(I,J))
101  CONTINUE
102  CONTINUE

```

```

*****
*
* This section calculates the mean RH, the Showalter Index, unrotates
* the wind coordinates, and finds the NPTI by calling subroutines.
*****

```

```

      CALL RELH (RH600,RH625,RH650,RH675,RH700,RH725,RH750,RH775,
&      RH800,RH_AVE)
      CALL SHOW (T850,TD850,T500,SSI)
      CALL ROT1 (U850,V850,U500,V500)
      CALL NP70 (U850,V850,U500,V500,RH_AVE,SSI,DAY,MO,
&      N1,N2,N3,N4,N5,N6)
      CALL PRCNT (HR,N1,N2,N3,N4,N5,N6,NPTI)
      CALL POINT (N5,COF,TTS,KCOF,KTTS)

```

```

*****
*
* This section writes the output to file.
*****

```

```

      WRITE(Y,'(I2)')YR
      WRITE(M,'(I2)')MO
      WRITE(DA,'(I2)')DAY
      WRITE(H,'(I2)')HR
      M = '0'//M(2:2)
      IF(DAY.LT.10)DA = '0'//DA(2:2)
      IF(HR.LT.10)H = '0'//H(2:2)
      IF(HR.EQ.15)THEN
        OUTFILE = '~/Thesis/f15'//INFILE(17:17)//Y//M//DA//H//
&'NPTI.dat'
      ELSE
        OUTFILE = '~/Thesis/f03'//INFILE(17:17)//Y//M//DA//H//
&'NPTI.dat'
      ENDIF

```

```

OUT = Y//M//DA//H
OPEN(51,FILE=OUTFILE,STATUS='UNKNOWN')
OPEN(61,FILE='~/Thesis/programs/KCOF_OUT',STATUS='UNKNOWN')
OPEN(71,FILE='~/Thesis/programs/KTTS_OUT',STATUS='UNKNOWN')
*
DO 900 Q = 1,92
  IF((YEARC(Q).EQ.YR).AND.(MONTHC(Q).EQ.MO).AND.
& (DAYC(Q).EQ.DAY))THEN
    WRITE(61,114) OUT,COF
    IF(KCOF.EQ.TSTC(Q))PREC=1
  ELSE
    GOTO 900
  ENDIF
  IF((YR.EQ.YEART(Q)).AND.(MO.EQ.MONTHT(Q)).AND.
& (DAY.EQ.DAYT(Q)))THEN
    WRITE(71,114) OUT,TTS
    IF(KTTS.EQ.TSTT(Q))PRET=1
  ELSE
    GOTO 900
  ENDIF
900 CONTINUE
*
WRITE(51,112) ((N1(I,J),I=1,IE),J=1,JE)
WRITE(51,*)
WRITE(51,*)
WRITE(51,112) ((N2(I,J),I=1,IE),J=1,JE)
WRITE(51,*)
WRITE(51,*)
WRITE(51,112) ((N3(I,J),I=1,IE),J=1,JE)
WRITE(51,*)
WRITE(51,*)
WRITE(51,112) ((N4(I,J),I=1,IE),J=1,JE)
WRITE(51,*)
WRITE(51,*)
WRITE(51,112) ((N6(I,J),I=1,IE),J=1,JE)
WRITE(51,*)
WRITE(51,*)
WRITE(51,112) ((N5(I,J),I=1,IE),J=1,JE)
WRITE(51,*)
WRITE(51,*)
WRITE(51,112) ((NPTI(I,J),I=1,IE),J=1,JE)
WRITE(51,*)
* WRITE(51,*)

```

```

*   WRITE(51,116) ((KTIME(I,J),I=1,IE),J=1,JE)
WRITE(*,*) 'Output File = ',OUTFILE
*   WRITE(51,*)
*   WRITE(51,*) 'KCOF PREDICTION =',KCOF,', PREDICTABILITY =',PREC
*   WRITE(51,*) 'KTTS PREDICTION =',KTTS,', PREDICTABILITY =',PRET
DO 903 J = 1,JE
  DO 901 I = 1,IE
    IF(NTEST(U850,V850,1,(MO-4)).GT.0)THEN
      JSPD8(I,J) = INT(SPD8(I,J) + 0.5)
      JDIR8(I,J) = INT(DIR8(I,J) + 0.5)
      WRITE(51,*) 'The 850mb winds of ,JDIR8(I,J),JSPD8(I,J),
&               'at point: I =',I,', J =',J
      WRITE(51,*) 'are beyond the 99% ellipse of the dependant
&               data.'
    ENDIF
    IF(NTEST(U500,V500,2,(MO-4)).GT.0)THEN
      JSPD5(I,J) = INT(SPD5(I,J) + 0.5)
      JDIR5(I,J) = INT(DIR5(I,J) + 0.5)
      WRITE(51,*) 'The 500mb winds of ,JDIR5(I,J),JSPD5(I,J),
&               'at point: I =',I,', J =',J
      WRITE(51,*) 'are beyond the 99% ellipse of the dependant
&               data.'
    ENDIF
901  CONTINUE
903  CONTINUE
    WRITE(51,*) "
    CLOSE(51)
1000 CONTINUE
*
    CLOSE(61)
    CLOSE(71)
1100 END
*
*****
*
* This program is designed to take the 40-km AWIPS eta data and put
* it in the six by six grid that is being used in the calculations
* of the NPTI over Cape Canaveral,FL. This code was written for
* thesis work by 2LT Christian Wohlwend, AFIT/ENP.
*
* Last Modified: 29 OCT 97
*****
*
```

```

SUBROUTINE GRID1 (C,NWORDS,ROW)
  PARAMETER(IM=185,JN=129,IE=10,JE=10)
  REAL      C(NWORDS)
  REAL      GRID(IM,JN)
  REAL      ROW(IE,JE)
  INTEGER    NWORDS
  INTEGER    L
  INTEGER    I
  INTEGER    J
  INTEGER    M
  INTEGER    N
*
  L=1
  DO 200 N=1,JN
    DO 150 M=1,IM
      GRID(M,N)=C(L)
      L=L+1
150  CONTINUE
200  CONTINUE
*
  I = 1
  J = 1
  DO 210 N = 28,37
    DO 205 M = 136,145
      ROW(I,J) = GRID(M,N)
      IF(I.LT.10)THEN
        I = I + 1
      ELSE
        I = 1
        J = J + 1
      ENDIF
205  CONTINUE
210  CONTINUE
*
  RETURN
END
*
```

```

*****
*
* This program is designed to calculate the mean Relative Humidity
* over the 800-mb to 600-mb layer using Meso-Eta, 25 mb spaced surfaces
* The code was written with the aid from AWS/TR-83/001, Equations and
* Algorithms for Meteorological Applications in Air Weather Service
* (1983) for thesis work by 2LT Christian S. Wohlwend, AFIT/ENP.
*
* Last Modified: 29 OCT 97
*
*****
*
SUBROUTINE RELH (RH600,RH625,RH650,RH675,RH700,RH725,RH750,
&      RH775,RH800,RH_AVE)
PARAMETER(IE=10,JE=10,KE=9)
REAL    RH(IE,JE,KE)
REAL    RH_P(IE,JE,KE)
REAL    RH_AVE(IE,JE)
REAL    RH800(IE,JE)
REAL    RH775(IE,JE)
REAL    RH750(IE,JE)
REAL    RH725(IE,JE)
REAL    RH700(IE,JE)
REAL    RH675(IE,JE)
REAL    RH650(IE,JE)
REAL    RH625(IE,JE)
REAL    RH600(IE,JE)
REAL    P(KE)
INTEGER I
INTEGER J
INTEGER K
*
P(1)=800
P(2)=775
P(3)=750
P(4)=725
P(5)=700
P(6)=675
P(7)=650
P(8)=625
P(9)=600
*****
*      Input Data
*
*****

```

```

DO 111 J = 1,JE
DO 110 I = 1,IE
  RH(I,J,1) = RH800(I,J)
110 CONTINUE
111 CONTINUE
DO 113 J = 1,JE
DO 112 I = 1,IE
  RH(I,J,2) = RH775(I,J)
112 CONTINUE
113 CONTINUE
DO 115 J = 1,JE
DO 114 I = 1,IE
  RH(I,J,3) = RH750(I,J)
114 CONTINUE
115 CONTINUE
DO 117 J = 1,JE
DO 116 I = 1,IE
  RH(I,J,4) = RH725(I,J)
116 CONTINUE
117 CONTINUE
DO 119 J = 1,JE
DO 118 I = 1,IE
  RH(I,J,5) = RH700(I,J)
118 CONTINUE
119 CONTINUE
DO 121 J = 1,JE
DO 120 I = 1,IE
  RH(I,J,6) = RH675(I,J)
120 CONTINUE
121 CONTINUE
DO 123 J = 1,JE
DO 122 I = 1,IE
  RH(I,J,7) = RH650(I,J)
122 CONTINUE
123 CONTINUE
DO 125 J = 1,JE
DO 124 I = 1,IE
  RH(I,J,8) = RH625(I,J)
124 CONTINUE
125 CONTINUE
DO 127 J = 1,JE
DO 126 I = 1,IE
  RH(I,J,9) = RH600(I,J)

```

```

126  CONTINUE
127  CONTINUE
*****
*          Calculate Mean RH                      *
*****
      DO 130 K=1,KE-1
        DO 129 J=1,JE
          DO 128 I=1,IE
            RH_P(I,J,K) = (0.5*(RH(I,J,K)+RH(I,J,K+1))*
&              (LOG(P(K))-LOG(P(K+1))))
128    CONTINUE
129    CONTINUE
130    CONTINUE
*
      DO 132 J=1,JE
        DO 131 I=1,IE
          RH_AVE(I,J) = (1/(LOG(P(1))-LOG(P(KE))))*(RH_P(I,J,1)+
&              RH_P(I,J,2)+RH_P(I,J,3)+RH_P(I,J,4)+
&              RH_P(I,J,5)+RH_P(I,J,6)+RH_P(I,J,7)+
&              RH_P(I,J,8))
131    CONTINUE
132    CONTINUE
*
      RETURN
      END
*

*****
*  This Program is designed to calculate the Showalter Stability      *
*  Index for the desired input.  The program is designed to run with  *
*  the only inputs being Temperature at 850 mb and 500 mb and the    *
*  Dew Point at 850 mb.  Temp values are to be input in degrees      *
*  Kelvin.  The output value will be the SSI.  This code was          *
*  written with aid from AWS/TR-83/001, Equations and Algorithms      *
*  for Meteorological Applications in Air Weather Service (1983)      *
*  for thesis work by 2LT Christian S. Wohlwend, AFIT/ENP             *
*                                                                      *
*  Last Modified: 29 OCT 97                                           *
*****
*

```



```

SUBROUTINE SHOW (T850,TD850,T500,SSI)
PARAMETER(IE=10,JE=10)
REAL    T850(IE,JE)  ! Temperature at 850 mb
REAL    TD850(IE,JE) ! Dew Point at 850 mb
REAL    T500(IE,JE)  ! Temperature at 500 mb
REAL    CP            ! Specific Heat of dry air
REAL    C             ! Kelvin conversion
REAL    K             ! RD/CP
REAL    DELTA_T       ! Fraction of temp guess
REAL    EPSILON       ! Allowable error
REAL    ZERO          ! Number zero
REAL    TP500(IE,JE)  ! Calculated Temp of parcel
REAL    TLCL(IE,JE)   ! Temperature of the LCL
REAL    PLCL(IE,JE)   ! Pressure of the LCL
REAL    E(IE,JE)      ! Vapor Pressure at LCL
REAL    EP            ! Saturation Vapor Pressure
REAL    L(IE,JE)      ! Latent Heat of water vapor
REAL    LP            ! Latent heat of parcel
REAL    WLCL(IE,JE)   ! Mixing ratio at 850 mb
REAL    WP            ! Saturation Mixing ratio
REAL    THETA_D(IE,JE) ! Partial Potential Temp
REAL    THETA_SE(IE,JE) ! Pseudo-equiv. Potential Temp
REAL    THETAP        ! Theta D of parcel
REAL    THETA_EP       ! Theta SE of parcel
REAL    SSI(IE,JE)    ! Showalter Stability Index
REAL    ERR           ! Error function
REAL    ERR_P         ! Second Error function
REAL    TP            ! Temp guess
REAL    TP2           ! Second Temp guess
INTEGER I             ! Column counter
INTEGER J             ! Row counter

```

* Define Constants *

CP = 0.24

C = 273.16

K = 0.2854

EPSILON = 0.05

ZERO = 0.0

*****Input Variables*****

*

```

*   WRITE(*,*) 'What is the temperature at 850 mb?(C)'
*   READ(*,100) T850
*   WRITE(*,*) 'What is the Dew Point at 850 mb?(C)'
*   READ(*,100) TD850
*   WRITE(*,*) 'What is the temperature at 500 mb?(C)'
*   READ(*,100) T500
*****
*           Find the variables at the LCL                                     *
*****
      DO 53 J=1,JE
        DO 52 I=1,IE
          T850(I,J) = T850(I,J) - C
          TD850(I,J) = TD850(I,J) - C
          TLCL(I,J)=(TD850(I,J)-((0.212+0.001571*TD850(I,J)-
&          0.000436*T850(I,J))*(T850(I,J)-TD850(I,J))) + C)
          T850(I,J) = T850(I,J) + C
          TD850(I,J) = TD850(I,J) + C
          PLCL(I,J) = 850.0*((TLCL(I,J)/T850(I,J))**(1.0/K))
          IF(TLCL(I,J).GE.C)THEN
            E(I,J) = (10.0**((23.832241 - (5.02808*LOG10(TLCL(I,J)))
&            - (1.3816*(10.0**(-7))*
&            (10.0**((11.334 - (0.0303998*TLCL(I,J))))))
&            + (8.1328*(10.0**(-3))*
&            (10.0**((3.49149 - (1302.8844/TLCL(I,J))))))
&            - (2949.076/TLCL(I,J))))))
            L(I,J) = (597.3 - (0.564*(TLCL(I,J) - C)))
          ELSE
            E(I,J) = (10.0**((3.56654*LOG10(TLCL(I,J))) -
&            (0.0032098*TLCL(I,J)) - (2484.956/TLCL(I,J))
&            + 2.0702294))
            L(I,J) = (597.3 - (0.574*(TLCL(I,J) - C)))
          ENDIF
          WLCL(I,J) = ((0.62197*E(I,J))/(PLCL(I,J)-E(I,J)))
          THETA_D(I,J)=(TLCL(I,J)*((850.0/(PLCL(I,J)-E(I,J))**(K))))
          THETA_SE(I,J)=THETA_D(I,J)*(EXP((L(I,J)*WLCL(I,J)/
&          (CP*TLCL(I,J))))
*****
*           Find the Temp of the parcel at 500mb.                             *
*****
          TP = (C - 5.0)
          DELTA_T = 0.05
          EP = (10.0**((3.56654*LOG10(TP)) - (0.0032098*TP)
&          - (2484.956/TP) + 2.0702294))

```

```

        LP = (597.3 - (0.574*(TP - C)))
        WP = ((0.62197*EP)/(500.0-EP))
        THETAP = (TP*((850.0/(500.0 - EP))**(K)))
        THETA_EP = THETAP*(EXP((LP*WP)/(CP*TP)))
        ERR = (THETA_EP - THETA_SE(I,J))
        IF(ABS(ERR).LT.EPSILON)THEN
            TP500(I,J) = TP
        ELSE
109      TP2 = TP + DELTA_T
            EP = (10.0**((3.56654*LOG10(TP2)) - (0.0032098*TP2)
            &      - (2484.956/TP2) + 2.0702294))
            LP = (597.3 - (0.574*(TP2 - C)))
            WP = ((0.62197*EP)/(500.0-EP))
            THETAP = (TP2*((850.0/(500.0 - EP))**(K)))
            THETA_EP = THETAP*(EXP((LP*WP)/(CP*TP2)))
            ERR_P = (THETA_EP - THETA_SE(I,J))
            IF(ABS(ERR_P).LT.EPSILON)THEN
                TP500(I,J) = TP2
            ELSE
            &      IF((ERR.LT.ZERO.AND.ERR_P.GT.ZERO).OR.
                (ERR.GT.ZERO.AND.ERR_P.LT.ZERO))THEN
                DELTA_T = (0.5*(DELTA_T))
                GOTO 109
            ELSE
                IF(ABS(ERR_P).LT.ABS(ERR))THEN
                    TP = TP2
                    ERR = ERR_P
                    GOTO 109
                ELSE
                    DELTA_T = (-1.0*(DELTA_T))
                    GOTO 109
                ENDIF
            ENDIF
        ENDIF
    ENDIF
ENDIF

```

* Calculate the SSI *

```

*****
        SSI(I,J) = (T500(I,J) - TP500(I,J))
*      SSI(I,J) = (INT(SSSI(I,J)*100.0 +0.5))/100.0
52    CONTINUE
53    CONTINUE

```

```

      RETURN
      END
*
*****
*
* This program was written to transform the u and v components of
* the wind from grid relative to earth relative coordinates. It
* was written for thesis work by 2LT Christian Wohlwend, AFIT/ENP.
*
* Last Modified: 29 OCT 97
*****
*
SUBROUTINE ROT1 (U850,V850,U500,V500)
  PARAMETER(IE=10,JE=10)
  REAL    U850(IE,JE)
  REAL    V850(IE,JE)
  REAL    U500(IE,JE)
  REAL    V500(IE,JE)
  REAL    LON(IE,JE)
  REAL    LON1(IE),LON2(IE),LON3(IE),LON4(IE),LON5(IE)
  REAL    LON6(IE),LON7(IE),LON8(IE),LON9(IE),LON10(IE)
  REAL    UR8
  REAL    VR8
  REAL    UR5
  REAL    VR5
  REAL    ANGLE
  REAL    LAMBDA
  REAL    CONE
  REAL    PI
  INTEGER I
  INTEGER J
*****
*
* Longitude of each point in the 10 x 10 grid.
*****
  DATA LON1,LON2,LON3,LON4,LON5,LON6,LON7,LON8,LON9,LON10
    &/277.71,278.12,278.52,278.93,279.34,279.74,280.15,280.56,280.96,
    &281.37,277.75,278.16,278.56,278.97,279.38,279.79,280.20,280.60,
    &281.01,281.42,277.79,278.20,278.61,279.01,279.42,279.83,280.24,
    &280.65,281.06,281.47,277.82,278.24,278.65,279.06,279.47,279.88,
    &280.29,280.70,281.11,281.52,277.86,278.28,278.69,279.10,279.51,
    &279.92,280.33,280.74,281.16,281.57,277.90,278.32,278.73,279.14,
    &279.56,279.97,280.38,280.79,281.20,281.62,277.94,278.36,278.77,

```

```

&279.19,279.60,280.01,280.43,280.84,281.25,281.67,277.98,278.40,
&278.81,279.23,279.65,280.06,280.48,280.89,281.30,281.72,278.02,
&278.44,278.86,279.27,279.69,280.11,280.52,280.94,281.35,281.77,
&278.06,278.48,278.90,279.32,279.74,280.15,280.57,280.99,281.40,
&281.82/

```

```

*
```

```

PI = 4.0*ATAN(1.0)
DO 58 I=1,IE
  LON(I,1)=LON1(I)*PI/180
  LON(I,2)=LON2(I)*PI/180
  LON(I,3)=LON3(I)*PI/180
  LON(I,4)=LON4(I)*PI/180
  LON(I,5)=LON5(I)*PI/180
  LON(I,6)=LON6(I)*PI/180
  LON(I,7)=LON7(I)*PI/180
  LON(I,8)=LON8(I)*PI/180
  LON(I,9)=LON9(I)*PI/180
  LON(I,10)=LON10(I)*PI/180

```

```

58  CONTINUE

```

```

CONE = SIN(25*PI/180)
LAMBDA = 265*PI/180

```

```

*****

```

```

*
```

```

*
```

```

*   Calculate winds in earth relative coordinates instead of a model
*   relative coordinate system.

```

```

*
*
```

```

*****

```

```

DO 60 J = 1,JE
  DO 59 I = 1,IE
    UR8 = U850(I,J)
    VR8 = V850(I,J)
    UR5 = U500(I,J)
    VR5 = V500(I,J)
    ANGLE = CONE*(LON(I,J) - LAMBDA)
    U850(I,J) = UR8*COS(ANGLE) - VR8*SIN(ANGLE)
    V850(I,J) = VR8*COS(ANGLE) + UR8*SIN(ANGLE)
    U500(I,J) = UR5*COS(ANGLE) - VR5*SIN(ANGLE)
    V500(I,J) = VR5*COS(ANGLE) + UR5*SIN(ANGLE)

```

```

59  CONTINUE

```

```

60  CONTINUE

```

```

  RETURN
END

```

```

*
*****
*
* This program is designed to calculate the Neumann-Pfeffer
* Thunderstorm Index for the grid. The code was written by
* C.J. Neumann in 1970/71 and was modified for thesis work by
* 2LT Christian Wohlwend, AFIT/ENP.
*
* Last Modified: 29 OCT 97
*****
*
SUBROUTINE NP70 (U850,V850,U500,V500,RH_AVE,SSI,DAY,MO,
&      N1,N2,N3,N4,N5,N6)
PARAMETER(IE=10,JE=10,KE=5,LE=36)
REAL    U850(IE,JE)
REAL    V850(IE,JE)
REAL    U500(IE,JE)
REAL    V500(IE,JE)
REAL    RH_AVE(IE,JE)
REAL    SSI(IE,JE)
REAL    UV850
REAL    UV500
REAL    RHF
REAL    SIF
REAL    CP
REAL    PROB
REAL    C(KE,LE)
REAL    SMLRH(KE)
REAL    FZ
REAL    X(2)
REAL    Y(2)
*    INTEGER KTIME(IE,JE)
INTEGER MO
INTEGER I
INTEGER J
INTEGER K
INTEGER L
INTEGER M
INTEGER N1(IE,JE)
INTEGER N2(IE,JE)
INTEGER N3(IE,JE)
INTEGER N4(IE,JE)
INTEGER N5(IE,JE)

```

```

    INTEGER N6(IE,JE)
    INTEGER DAY
    INTEGER DY
*   INTEGER TIME

    DATA SMLRH/12.0,15.0,22.0,35.0,19.0/

101  FORMAT(F13.7)

    OPEN(17, FILE = '~/Thesis/programs/const.dat', STATUS = 'OLD')

    DO 103 K = 1,KE
      DO 102 L = 1,LE
        READ(17,101) C(K,L)
102   CONTINUE
103   CONTINUE
*
    K = MO - 4
    IF((K.EQ.5).OR.(K.EQ.2))THEN
      IF(DAY.EQ.30)THEN
        K = K + 1
        DAY = 1
      ELSE
        DAY = DAY + 1
      ENDIF
    ELSE
      IF(DAY.EQ.31)THEN
        K = K + 1
        DAY = 1
      ELSE
        DAY = DAY + 1
      ENDIF
    ENDIF
    IF((K.LT.1).OR.(K.GT.5))THEN
      WRITE(*,*) 'THIS PROGRAM IS ONLY OPERATIONAL FOR MAY
THROUGH
&SEPTEMBER.'
99   STOP
    ENDIF
    IF((K.GE.1).AND.(K.LE.3))THEN
      WRITE(*,*) 'CHANGE THE LIMITS OF K AND RERUN THE PROGRAM.'
98   STOP
    ENDIF

```

```

DO 105 J = 1,JE
DO 104 I = 1,IE
  X(1) = U850(I,J)
  Y(1) = V850(I,J)
  X(2) = U500(I,J)
  Y(2) = V500(I,J)
DO 61 M = 1,2
  IF(M.EQ.1)L=1
  IF(M.EQ.2)L=11
  FZ = C(K,L) + C(K,L+1)*X(M)+C(K,L+2)*Y(M)+C(K,L+3)*X(M)
&      *Y(M)+C(K,L+4)*X(M)*X(M)+C(K,L+5)*Y(M)*Y(M)+C(K,L+6)
&      *X(M)*X(M)*X(M)+C(K,L+7)*X(M)*X(M)*Y(M)+C(K,L+8)*
&      X(M)*Y(M)*Y(M)+C(K,L+9)*Y(M)*Y(M)*Y(M)
  FZ = FIXFZ(FZ,M,K,X,Y)
  IF(M.EQ.1)UV850=FZ
  IF(M.EQ.2)UV500=FZ
61  CONTINUE
  IF((RH_AVE(I,J)-SMLRH(MO)).LT.(0.0))THEN
    RHF = 0.01
  ELSE
    L = 21
    RHF = C(K,L) + C(K,L+1)*RH_AVE(I,J) + C(K,L+2)*
&      RH_AVE(I,J)*RH_AVE(I,J) + C(K,L+3)*RH_AVE(I,J)*
&      RH_AVE(I,J)*RH_AVE(I,J)
  ENDIF
  L = 25
  SIF = C(K,L) + C(K,L+1)*SSI(I,J) +
&      C(K,L+2)*SSI(I,J)*SSI(I,J)
  UV850 = ADJUST(UV850)
  UV500 = ADJUST(UV500)
  RHF = ADJUST(RHF)
  SIF = ADJUST(SIF)
  L = 28
  DY = NBRDA(MO,DAY)
  CP = C(K,L)+C(K,L+1)*DY+C(K,L+2)*DY*DY
  L = 31
  PROB = C(K,L)+C(K,L+1)*UV850+C(K,L+2)*UV500+C(K,L+3)*RHF+
&      C(K,L+4)*SIF+C(K,L+5)*CP
*  CALL ISTART(X,Y,1,DAY,PROB,TIME)
  N1(I,J) = INT(UV850*100.0 + 0.5)
  N2(I,J) = INT(UV500*100.0 + 0.5)
  N3(I,J) = INT(RHF*100.0 + 0.5)
  N4(I,J) = INT(SIF*100.0 + 0.5)

```



```

        N5(I,J) = INT(PROB*100.0 + 0.5)
        N6(I,J) = INT(CP*100.0 + 0.5)
*       KTIME(I,J) = TIME
        IF(N5(I,J).LT.5) N5(I,J) = 5
        IF(N5(I,J).GT.95) N5(I,J) = 95
104    CONTINUE
105    CONTINUE
        CLOSE(17)
        RETURN
    END
*
*****
*
*       This function fixes the results for 850mb and 500mb wind
*       functions in the case of strong easterly winds
*****
    FUNCTION FIXFZ(FZOLD,M,MON,X,Y)
        REAL    ERR
        REAL    Y(2)
        REAL    X(2)
        REAL    FZOLD
        INTEGER  M
        INTEGER  MON
*
        IF(M.EQ.1)THEN
            IF(MON.EQ.1)THEN
                ERR = Y(M) + 2.0*X(M) + 38.9
            ELSEIF(MON.EQ.2)THEN
                ERR = Y(M) + 0.3*X(M) + 15.4
            ELSEIF(MON.EQ.3)THEN
                ERR = -Y(M) + 1.6*X(M) + 30.4
            ELSEIF(MON.EQ.4)THEN
                ERR = Y(M) + 2.3*X(M) + 25.0
            ELSE
                GO TO
75
            ENDDIF
            IF(ERR.LT.0.)THEN
                GO TO 70
            ELSE
                GO TO 75
            ENDDIF
        ELSE

```

```

      IF(MON.EQ.1)THEN
        ERR = Y(M) + 0.7*X(M) + 22.3
      ELSEIF(MON.EQ.2)THEN
        ERR = Y(M) + 5.0*X(M) + 78.9
      ELSEIF(MON.EQ.3)THEN
        GOTO 75
      ELSEIF(MON.EQ.4)THEN
        ERR = Y(M) + 4.0*X(M) + 59.7
      ELSE
        GOTO 75
      ENDIF
      IF(ERR.LT.0.)THEN
        GO TO 70
      ELSE
        GO TO 75
      ENDIF
    ENDIF
70  FIXFZ = 0.01
    RETURN
75  FIXFZ = FZOLD
    RETURN
  END
*
*****
*
*   This function adjusts probability to within allowable range.
*
*****
FUNCTION ADJUST(V)
  REAL  V
*
  IF(V.LE.0.)THEN
    ADJUST = 0.01
  ELSEIF((V-0.99).LE.0.)THEN
    ADJUST = V
  ELSE
    ADJUST = 0.99
  ENDIF
  RETURN
END
*
```

```

*****
*
*   This function computes the day number.
*
*****

FUNCTION NBRDA(MONTH,KDA)
  INTEGER MONTH
  INTEGER KDA
  INTEGER MONDA(12)
  DATA MONDA/0,31,59,90,120,151,181,212,243,273,304,334/
  NBRDA = MONDA(MONTH) + KDA
  RETURN
END

*
*****
*
*   This calculates the tstm start time.
*
*****

SUBROUTINE ISTART(V,W,LEV,X,Y,TIME)
  PARAMETER(LAE=35,IE=2)
  REAL    C(LAE)
  REAL    Y
  REAL    V(IE)
  REAL    W(IE)
  REAL    X
  REAL    S
  REAL    B
  INTEGER  IN
  INTEGER  JN
  INTEGER  LA
  INTEGER  LEV
  INTEGER  TIME
*
93  FORMAT(F13.7)
  OPEN(11,FILE='~/Thesis/programs/c.dat',STATUS='OLD')
  IF(Y.LT.0.4)THEN
    TIME = 0
    GOTO 95
  ENDIF

  DO 94 LA = 1,LAE
    READ(11,93) C(LA)
94  CONTINUE
    S = C(1)+C(2)*Y+C(3)*Y*Y+C(4)*Y*Y*Y+

```

```

& C(5)*X+C(6)*X*Y+C(7)*X*Y*Y+C(8)*X*X+
& C(9)*X*X*Y+C(10)*X*X*X+C(11)*W(LEV)+C(12)*W(LEV)*
& Y+C(13)*W(LEV)*Y*Y+C(14)*W(LEV)*X+C(15)*
& W(LEV)*X*Y+C(16)*W(LEV)*X*X+C(17)*W(LEV)*W(LEV)+C(18)*
& W(LEV)*W(LEV)*Y+C(19)*W(LEV)*W(LEV)*X+C(20)*W(LEV)*
& W(LEV)*W(LEV)+C(21)*V(LEV)+C(22)*V(LEV)*Y+C(23)*V(LEV)*
& Y*Y+C(24)*V(LEV)*X+C(25)*V(LEV)*X*Y+C(26)*
& V(LEV)*X*X+C(27)*V(LEV)*W(LEV)+C(28)*V(LEV)*W(LEV)*Y+
& C(29)*V(LEV)*W(LEV)*X+C(30)*V(LEV)*W(LEV)*W(LEV)+C(31)*
& V(LEV)*V(LEV)+C(32)*V(LEV)*V(LEV)*Y+C(33)*V(LEV)*V(LEV)*
& X+C(34)*V(LEV)*V(LEV)*W(LEV)+C(35)*V(LEV)*V(LEV)*V(LEV)
IF(S.LT.10.0)S = 10.0
IF(S.GT.22.0)S = 22.0
IN = INT(S)
B = FLOAT(IN)
JN = INT(((S-B)*60.0) + 0.5)
IF((JN-60).GE.0)THEN
  JN = 0
  IN = IN + 1
  TIME = IN*100 + JN
ELSE
  TIME = IN*100 + JN
ENDIF
CLOSE(11)
95 RETURN
END
*
*****
*
* This determines if the observed winds are beyond the 99
* percentile range of the dependant data.
*****
FUNCTION NTEST(U,V,LEV,M)
PARAMETER(ME=5)
REAL CT8(ME),ST8(ME),A8(ME),B8(ME),XH8(ME),YK8(ME)
REAL CT5(ME),ST5(ME),A5(ME),B5(ME),XH5(ME),YK5(ME)
REAL XPRIME
REAL YPRIME
REAL U
REAL V
REAL SUM
INTEGER LEV
INTEGER M

```

*

DATA CT8/0.84897,0.89180,0.98686,0.84989,0.83772/
DATA ST8/0.52844,0.45243,0.16160,0.52696,0.54610/
DATA A8/33.79,30.58,25.88,26.77,35.78/
DATA B8/24.06,21.78,18.58,19.26,24.93/
DATA XH8/-0.120,1.902,2.146,0.061,-2.573/
DATA YK8/0.596,3.257,4.941,4.359,1.887/
DATA CT5/0.82511,0.98741,0.97630,0.83962,0.83772/
DATA ST5/0.56497,0.15816,0.21644,0.54317,0.46020/
DATA A5/45.06,33.46,28.04,30.72,40.06/
DATA B5/34.26,25.64,23.18,22.89,27.15/
DATA XH5/12.336,5.065,2.048,0.995,2.560/
DATA YK5/-1.539,0.511,1.700,2.202,0.268/

*

IF(LEV.EQ.1)THEN
 XPRIME = (U-XH8(M))*CT8(M)+(V-YK8(M))*ST8(M)
 YPRIME = (V-YK8(M))*CT8(M)-(U-XH8(M))*ST8(M)
 SUM = (XPRIME*XPRIME)/(A8(M)*A8(M))+(YPRIME*YPRIME)/
& (B8(M)*B8(M))
 IF((SUM - 1.0).LE.(0.0))THEN
 GOTO 30
 ELSE
 GOTO 40
 ENDIF
ELSE
 XPRIME = (U-XH5(M))*CT5(M)+(V-YK5(M))*ST5(M)
 YPRIME = (V-YK5(M))*CT5(M)-(U-XH5(M))*ST5(M)
 SUM = (XPRIME*XPRIME)/(A5(M)*A5(M))+(YPRIME*YPRIME)/
& (B5(M)*B5(M))
 IF((SUM - 1.0).LE.(0.0))THEN

GOTO 30
 ELSE

GOTO 40
 ENDIF
ENDIF
30 NTEST = 0
 RETURN
40 NTEST = 1
 RETURN
END

*

```

*
*****
*
* Last Modified: 31 OCT 97
*
*****
*
SUBROUTINE POINT (N5,COF,TTS,KCOF,KTTS)
  PARAMETER(IE=10,JE=10)
  REAL COF
  REAL TTS
  INTEGER N5(IE,JE)
  INTEGER KCOF
  INTEGER KTTS
*
  COF = (FLOAT(N5(3,4)) + FLOAT(N5(4,4)) + FLOAT(N5(3,5)) +
& FLOAT(N5(4,5)))/4.0
  TTS = (FLOAT(N5(5,5)) + FLOAT(N5(6,5)) + FLOAT(N5(5,6)) +
& FLOAT(N5(6,6)))/4.0
  IF(COF.GE.40.0)THEN
    KCOF = 1
  ELSE
    KCOF = 0
  ENDIF
  IF(TTS.GE.40.0)THEN
    KTTS = 1
  ELSE
    KTTS = 0
  ENDIF
  RETURN
END
*
*2345678901234567890123456789012345678901234567890123456789012

```

File c.dat used in program

```
+0.1273831E+2
-0.5524785E+2
+0.1678743E+2
-0.3044658E+1
+0.1428297E+0
+0.4120300E+0
-0.5984368E-1
-0.1020633E-2
-0.8332961E-3
+0.2010301E-5
+0.1091247E+1
-0.2395890E+0
+0.8079287E+0
-0.9742853E-2
-0.3330773E-2
+0.2572378E-4
+0.3275030E-2
-0.1128065E-5
+0.3928772E-4
-0.3878205E-3
+0.3856991E-1
+0.2283849E+0
-0.1152510E+1
-0.1318092E-2
+0.5700343E-2
-0.2110866E-6
+0.5209711E-2
+0.5253384E-4
+0.4564636E-5
-0.6700146E-3
+0.1260419E-1
+0.9910755E-2
-0.1220748E-3
+0.1705095E-3
-0.4914740E-4
99999
```

File const.dat used in program

```
+0.1787416E+0 +0.1074020E-1 +0.1365651E-1 +0.4523660E-3
-0.1802959E-3 +0.3397793E-3 -0.1051838E-4 -0.3954366E-4
+0.3376410E-4 +0.1677435E-5 +0.1206249E+0 +0.1080646E-1
+0.1001964E-1 +0.2794513E-3 -0.1012098E-3 +0.1964561E-3
-0.1929388E-5 -0.1095389E-4 -0.6512555E-5 -0.1931907E-5
+0.1037449E+0 -0.1196854E-1 +0.4832994E-3 -0.3570444E-5
+0.4273235E+0 -0.7480216E-1 +0.3056700E-2 -0.5430778E+0
+0.6855607E-2 -0.1053707E-4 -0.1589528E+0 +0.5503053E+0
+0.3738171E+0 +0.3233246E+0 +0.5656907E+0 +0.2053246E-1
+0.3326784E+0 +0.2172438E-1 +0.2162950E-1 +0.3762057E-3
-0.6835820E-3 +0.2579027E-3 +0.1179004E-5 +0.1437934E-5
-0.3373770E-4 -0.2199710E-4 +0.2927882E+0 +0.2638450E-1
+0.1023307E-1 +0.3206674E-3 +0.7055071E-4 +0.1576005E-3
-0.3090318E-4 -0.1422489E-4 +0.5588606E-5 -0.9225416E-5
+0.1350110E+0 -0.1999291E-1 +0.8150660E-3 -0.6342578E-5
+0.6102192E+0 -0.8066767E-1 +0.2403756E-2 -0.1323037E+0
+0.1070858E-2 +0.1208962E-4 -0.5556250E+0 +0.6102450E+0
+0.4851770E+0 +0.3646010E+0 +0.3541640E+0 +0.6391500E+0
+0.4307867E+0 +0.4366697E-1 +0.1055475E-1 -0.3983282E-4
-0.3116466E-3 -0.1888946E-2 -0.5616631E-4 +0.7757704E-4
-0.5417381E-4 +0.3519052E-4 +0.4145883E+0 +0.3166340E-1
-0.7151265E-3 +0.5390950E-3 +0.4251009E-4 -0.5091109E-4
-0.2425546E-4 +0.1581160E-4 -0.2172134E-4 -0.1060904E-4
-0.1029031E+0 -0.2906759E-2 +0.4229306E-3 -0.3308301E-5
+0.6177575E+0 -0.6421018E-1 +0.1310411E-2 +0.9355280E+0
-0.3771816E-2 +0.6918595E-5 -0.5553775E+0 +0.6370509E+0
+0.4154169E+0 +0.4982033E+0 +0.4217904E+0 +0.2361394E+0
+0.3627524E+0 -0.3272211E-1 +0.1085207E-1 -0.5623188E-4
+0.1038914E-2 -0.3726892E-3 -0.3354727E-4 -0.1055251E-3
-0.6772392E-5 +0.1606764E-4 +0.3932798E+0 +0.3119719E-1
+0.2545731E-2 +0.1592548E-3 +0.9662810E-4 +0.2887853E-4
-0.3745136E-4 -0.1717338E-4 -0.1704165E-4 +0.4082921E-5
+0.2562494E+1 -0.1702073E+0 +0.3551389E-2 -0.2161341E-4
+0.5271789E+0 -0.3530199E-1 -0.1094883E-2 -0.4163536E+0
+0.1394724E-1 -0.4493190E-4 -0.4622971E+0 +0.6391629E+0
+0.4061392E+0 +0.4244231E+0 +0.5676596E+0 +0.6062162E-1
+0.2816768E+0 +0.1256518E-1 +0.5804331E-2 +0.1096534E-3
-0.2671097E-3 +0.1469291E-4 -0.1099520E-4 +0.2925611E-5
+0.3228711E-5 -0.3225703E-5 +0.2527479E+0 +0.1084204E-1
+0.3136786E-2 +0.1899334E-3 -0.2175208E-3 -0.3547892E-4
-0.5449895E-5 -0.4427336E-5 +0.6122512E-5 +0.5412232E-5
+0.1736004E+0 -0.1918291E-1 +0.6220713E-3 -0.4414412E-5
+0.4078606E+0 -0.6376678E-1 +0.2571961E-2 +0.3758034E+1
-0.2287890E-1 +0.3598785E-4 -0.6182956E+0 +0.5269289E+0
+0.6065540E+0 +0.5538999E+0 +0.4831459E+0 +0.1294910E+1
```


Appendix B. Example Control Card for Meso-Eta Variable Extraction

This code is a hexadecimal control card that is used to extract the NPTI variables from the Meso-Eta model. It is used with the program `unpkgrib1.x` in order to degrid the desired variables. The control card must be present in the same directory as the program and called `unpkgrib1.dat`. To change the variables and levels extracted from the model column three must be changed. It is a hexadecimal description of the variable and the level it is on. To decipher this number please reference NCEP Office Note 388 (Dey 1996) and the comments at the beginning of the `unpkgrib1.x` code.

10000~/Thesis/A970828.dat

~/Thesis/A970828out.dat

00001C02	0755D4C0	21640352	61081C0F	00011800	00000000	0
00001C02	0755D4C0	216401F4	61081C0F	00011800	00000000	0
00001C02	0755D4C0	226401F4	61081C0F	00011800	00000000	0
00001C02	0755D4C0	22640352	61081C0F	00011800	00000000	0
00001C02	0755D4C0	11640352	61081C0F	00011800	00000000	0
00001C02	0755D4C0	34640258	61081C0F	00011800	00000000	0
00001C02	0755D4C0	34640271	61081C0F	00011800	00000000	0
00001C02	0755D4C0	3464028A	61081C0F	00011800	00000000	0
00001C02	0755D4C0	346402A3	61081C0F	00011800	00000000	0
00001C02	0755D4C0	346402BC	61081C0F	00011800	00000000	0
00001C02	0755D4C0	346402D5	61081C0F	00011800	00000000	0
00001C02	0755D4C0	346402EE	61081C0F	00011800	00000000	0
00001C02	0755D4C0	34640307	61081C0F	00011800	00000000	0
00001C02	0755D4C0	34640320	61081C0F	00011800	00000000	0
00001C02	0755D4C0	0B6401F4	61081C0F	00011800	00000000	0
00001C02	0755D4C0	0B640352	61081C0F	00011800	00000000	0
FFFFFFFF	00000000	00000000	00000000	00000000	00000000	0

Appendix C. NPTI with Meso-Eta Data

This chart shows the calculated NPTI for Cape Canaveral and the associated observations. Also included is the standard deviation for the calculated average of the NPTI for Cape Canaveral.

<u>Date</u>	<u>NPTI (%)</u>	<u>Obs.</u>	<u>Std. Dev.</u>
970816	57.50	1	1.732051
970818	54.50	1	1.290994
970819	47.25	1	0.957427
970820	42.25	1	0.957427
970822	40.75	1	8.995369
970823	53.25	1	0.5
970824	33.00	1	7.615773
970825	55.75	1	2.217356
970826	37.00	1	5.773503
970828	12.25	0	0.957427
970829	35.75	0	4.112988
970830	48.75	1	0.5
970831	52.50	1	1.0
970902	49.25	1	0.5
970903	52.50	1	1.290994
970904	40.75	1	0.5
970905	19.75	0	0.957427
970906	05.00	0	0.57735
970907	12.25	0	2.753785
970908	06.25	0	3.40343
970910	41.25	1	0.957427
970911	45.50	1	1.290994
970912	34.00	1	2.160247
970913	30.75	1	0.5
970914	15.75	0	1.5
970915	11.75	1	3.095696
970922	05.00	1	0.816497
970923	21.75	1	0.5
970924	19.00	1	2.44949
970926	39.50	1	0.57735
970929	28.75	0	2.986079
970930	16.25	0	0.957427

Appendix D. Code for Statistics Calculations

This is the code used to calculate the statistics for the two-by-two contingency tables.

```
PROGRAM STATS
  REAL    HR
  REAL    TS
  REAL    TSN
  REAL    POD
  REAL    FAR
  REAL    BIAS
  REAL    OUT
  REAL    R
  REAL    BS(92)
  REAL    BSS
  REAL    KSS
  REAL    HSS
  INTEGER PER(2)
  INTEGER A
  INTEGER B
  INTEGER C
  INTEGER D
  INTEGER I
  INTEGER J
  INTEGER N
  INTEGER DA
  INTEGER H
  INTEGER RES(92)
  INTEGER DATE(92)
  CHARACTER*20 DB
*
111  FORMAT(I6,I2,2X,F5.2)
112  FORMAT(I6,4X,I1)
    OPEN(12,FILE = 'KTTS.dat',STATUS = 'OLD')
    OPEN(15,FILE = 'statistics5', STATUS = 'UNKNOWN')
*
    DO 10 J = 1,92
      READ(12,112) DATE(J), RES(J)
*      READ(13,112) DT(J),RE(J)
10  CONTINUE
*
    M = 5
```

```

DO 40 L = 1,2
BSS = 0.0
A = 0
B = 0
C = 0
D = 0
PER(1) = 30
per(2) = 20
OPEN(11,FILE = 'KTTS_OUT',STATUS = 'OLD')
DO 30 I = 1,67
  READ(11,111) DA, H, OUT
  IF(H.EQ.15)THEN
    DO 20 J = 1,92
      IF(DA.EQ.DATE(J))THEN
        IF(RES(J).EQ.1)THEN
          R = 95.0
        ELSE
          R = 5.0
        ENDIF
        BS(J) = (OUT - R)*(OUT - R)
        IF((OUT.GE.PER(L)).AND.(RES(J).EQ.1))THEN
          A = A + 1
        ELSEIF((OUT.GE.PER(L)).AND.(RES(J).EQ.0))THEN
          B = B + 1
        ELSEIF((OUT.LT.PER(L)).AND.(RES(J).EQ.1))THEN
          C = C + 1
        ELSEIF((OUT.LT.PER(L)).AND.(RES(J).EQ.0))THEN
          D = D + 1
        ELSE
          GOTO 20
        ENDIF
        BSS = BSS + BS(J)
      ELSE
        GOTO 20
      ENDIF
20  CONTINUE
    ENDIF
30  CONTINUE
  N = A + B + C + D
  HR = ((FLOAT(A) + FLOAT(D))/FLOAT(N))*100.0
  TS = (FLOAT(A)/(FLOAT(A) + FLOAT(B) + FLOAT(C)))*100.0
  TSN = (FLOAT(D)/(FLOAT(D) + FLOAT(B) + FLOAT(C)))*100.0
  POD = (FLOAT(A)/(FLOAT(A) + FLOAT(C)))*100.0

```

```

    PODN = (FLOAT(D)/(FLOAT(B) + FLOAT(D)))*100.0
    FAR = (FLOAT(B)/(FLOAT(A) + FLOAT(B)))*100.0
    FARN = (FLOAT(C)/(FLOAT(C) + FLOAT(D)))*100.0
    BIAS = ((FLOAT(A) + FLOAT(B))/(FLOAT(A) + FLOAT(C)))
    HSS = 2*((FLOAT(A)*FLOAT(D))-(FLOAT(B)*FLOAT(C)))/
&    ((FLOAT(A) + FLOAT(C))*(FLOAT(C) + FLOAT(D))
&    +(FLOAT(A) + FLOAT(B))*(FLOAT(B) + FLOAT(D)))
    KSS = ((FLOAT(A)*FLOAT(D))-(FLOAT(B)*FLOAT(C)))/
&    ((FLOAT(A) + FLOAT(C))*(FLOAT(B) + FLOAT(D)))
    BSS = BSS/N
    IF(BIAS.GT.(1.0))THEN
        DB = ', OVERFORECASTING'
    ELSEIF(BIAS.LT.(1.0))THEN
        DB = ', UNDERFORECASTING'
    ELSE
        DB = ', UNBIASED'
    ENDIF
    WRITE(15,*) 'KTTS statistics from output of contingency table.'
    WRITE(15,*) ' with a percent of', per(L), '%'
    WRITE(15,*) ' A =',A,', B =',B,', C =',C,', D =',D,', N =',N
    WRITE(15,*) ' HIT RATE =',HR,'% '
    WRITE(15,*) ' THREAT SCORE =',TS,'% '
    WRITE(15,*) ' THREAT SCORE NO =',TSN,'% '
    WRITE(15,*) ' PROB. OF DETECTION =',POD,'% '
    WRITE(15,*) ' PROB. OF DET. NO =',PODN,'% '
    WRITE(15,*) ' FALSE-ALARM RATE =',FAR,'% '
    WRITE(15,*) ' FALSE-ALARM RATE NO =',FARN,'% '
    WRITE(15,*) ' BIAS =',BIAS,DB
    WRITE(15,*) ' HSS =',HSS
    WRITE(15,*) ' KSS =',KSS
    WRITE(15,*) ' BSS =',BSS
    WRITE(15,*) "
        close (11)
40  CONTINUE
END
*23456789012345678901234567890123456789012345678901234567890123456789012

```

Appendix E. Segmented Climatological Statistical Results

This is the statistical output to the segmented data from the 20 years of climatology. It is divided into the four major quadrants for comparison of the NPTI's forecast ability in each wind direction.

1) Northeast Statistics

KTTS statistics from output of contingency table with 40% as the NPTI cutoff.

A = 40, B = 73, C = 80, D = 580, N = 773
HIT RATE = 80.2070%
THREAT SCORE = 20.7254%
THREAT SCORE NO = 79.1269%
PROB. OF DETECTION = 33.3333%
FALSE-ALARM RATE = 64.6018%
BIAS = 0.941667, UNDERFORECASTING

KTTS statistics from output of contingency table with 45% as the NPTI cutoff.

A = 30, B = 46, C = 90, D = 607, N = 773
HIT RATE = 82.4062%
THREAT SCORE = 18.0723%
THREAT SCORE NO = 81.6958%
PROB. OF DETECTION = 25.0000%
FALSE-ALARM RATE = 60.5263%
BIAS = 0.633333, UNDERFORECASTING

KTTS statistics from output of contingency table with 50% as the NPTI cutoff.

A = 22, B = 27, C = 98, D = 626, N = 773
HIT RATE = 83.8292%
THREAT SCORE = 14.9660%
THREAT SCORE NO = 83.3555%
PROB. OF DETECTION = 18.3333%
FALSE-ALARM RATE = 55.1020%
BIAS = 0.408333, UNDERFORECASTING

KTTS statistics from output of contingency table with 55% as the NPTI cutoff.

A = 14, B = 19, C = 106, D = 634, N = 773
HIT RATE = 83.8292%
THREAT SCORE = 10.07194%
THREAT SCORE NO = 83.5310%
PROB. OF DETECTION = 11.6667%
FALSE-ALARM RATE = 57.5758%
BIAS = 0.275000, UNDERFORECASTING

2) Northwest Statistics

KTTS statistics from output of contingency table with 40% as the NPTI cutoff.

A = 101, B = 87, C = 51, D = 185, N = 424

HIT RATE = 67.4528%

THREAT SCORE = 42.2594%

THREAT SCORE NO = 57.2755%

PROB. OF DETECTION = 66.4474%

FALSE-ALARM RATE = 46.2766%

BIAS = 1.23684, OVERFORECASTING

KTTS statistics from output of contingency table with 45% as the NPTI cutoff.

A = 77, B = 65, C = 75, D = 207, N = 424

HIT RATE = 66.9811%

THREAT SCORE = 35.4839%

THREAT SCORE NO = 59.6542%

PROB. OF DETECTION = 50.6579%

FALSE-ALARM RATE = 45.7746%

BIAS = 0.934211, UNDERFORECASTING

KTTS statistics from output of contingency table with 50% as the NPTI cutoff.

A = 60, B = 45, C = 92, D = 227, N = 424

HIT RATE = 67.6887%

THREAT SCORE = 30.4569%

THREAT SCORE NO = 62.3626%

PROB. OF DETECTION = 39.4737%

FALSE-ALARM RATE = 42.8571%

BIAS = 0.690789, UNDERFORECASTING

KTTS statistics from output of contingency table with 55% as the NPTI cutoff.

A = 47, B = 33, C = 105, D = 239, N = 424

HIT RATE = 67.4528%

THREAT SCORE = 25.4054%

THREAT SCORE NO = 63.3952%

PROB. OF DETECTION = 30.9211%

FALSE-ALARM RATE = 41.2500%

BIAS = 0.526316, UNDERFORECASTING

3) Southeast Statistics

KTTS statistics from output of contingency table with 40% as the NPTI cutoff.

A = 206, B = 241, C = 103, D = 526, N = 1076

HIT RATE = 68.0297%

THREAT SCORE = 37.4545%

THREAT SCORE NO = 60.4598%

PROB. OF DETECTION = 66.6667%

FALSE-ALARM RATE = 53.9150%

BIAS = 1.44660, OVERFORECASTING

KTTS statistics from output of contingency table with 45% as the NPTI cutoff.

A = 165, B = 183, C = 144, D = 584, N = 1076

HIT RATE = 69.6097%

THREAT SCORE = 33.5366%

THREAT SCORE NO = 64.1054%

PROB. OF DETECTION = 53.3981%

FALSE-ALARM RATE = 52.5862%

BIAS = 1.12621, OVERFORECASTING

KTTS statistics from output of contingency table with 50% as the NPTI cutoff.

A = 129, B = 132, C = 180, D = 635, N = 1076

HIT RATE = 71.0037%

THREAT SCORE = 29.2517%

THREAT SCORE NO = 67.0539%

PROB. OF DETECTION = 41.7476%

FALSE-ALARM RATE = 50.5747%

BIAS = 0.844660, UNDERFORECASTING

KTTS statistics from output of contingency table with 55% as the NPTI cutoff.

A = 96, B = 93, C = 213, D = 674, N = 1076

HIT RATE = 71.5613%

THREAT SCORE = 23.8806%

THREAT SCORE NO = 68.7755%

PROB. OF DETECTION = 31.0680%

FALSE-ALARM RATE = 49.2063%

BIAS = 0.611650, UNDERFORECASTING

4) Southwest Statistics

KTTS statistics from output of contingency table with 40% as the NPTI cutoff.

A = 628, B = 399, C = 83, D = 167, N = 1277

HIT RATE = 62.2553%

THREAT SCORE = 56.5766%

THREAT SCORE NO = 25.7319%

PROB. OF DETECTION = 88.3263%

FALSE-ALARM RATE = 38.8510%

BIAS = 1.44444, OVERFORECASTING

KTTS statistics from output of contingency table with 45% as the NPTI cutoff.

A = 573, B = 328, C = 138, D = 238, N = 1277

HIT RATE = 63.5082%

THREAT SCORE = 55.1492%

THREAT SCORE NO = 33.8068%

PROB. OF DETECTION = 80.5907%

FALSE-ALARM RATE = 36.4040%

BIAS = 1.26723, OVERFORECASTING

KTTS statistics from output of contingency table with 50% as the NPTI cutoff.

A = 504, B = 276, C = 207, D = 290, N = 1277

HIT RATE = 62.1770%

THREAT SCORE = 51.0638%

THREAT SCORE NO = 37.5162%

PROB. OF DETECTION = 70.8861%

FALSE-ALARM RATE = 35.3846%

BIAS = 1.09705, OVERFORECASTING

KTTS statistics from output of contingency table with 55% as the NPTI cutoff.

A = 440, B = 212, C = 271, D = 354, N = 1277

HIT RATE = 62.1770%

THREAT SCORE = 47.6706%

THREAT SCORE NO = 42.2939%

PROB. OF DETECTION = 61.8847%

FALSE-ALARM RATE = 32.5153%

BIAS = 0.917018, UNDERFORECASTING

Appendix F. Entire Climatological Statistic Results

Overall

Percent	HR	TS	TSN	POD	PODN	FAR	FARN	Bias
5	40.36	40.36	0	100	0	59.64	0	2.4779
6	48.84	43.87	14.77	99.06	14.87	55.95	4.1	2.2488
7	49.34	44.08	15.65	98.97	15.76	55.71	4.25	2.2347
8	50.13	44.47	16.97	98.97	17.09	55.32	3.93	2.215
9	50.89	44.76	18.44	98.59	18.62	54.96	4.87	2.1887
10	51.31	44.87	19.33	98.22	19.57	54.76	5.81	2.1709
11	52.07	45.24	20.64	98.12	20.9	54.37	5.73	2.1502
12	52.67	45.55	21.64	98.12	21.92	54.05	5.48	2.1352
13	53.39	45.91	22.88	98.03	23.19	53.66	5.44	2.1155
14	54.15	46.25	24.28	97.75	24.65	53.26	5.83	2.0911
15	54.64	46.44	25.23	97.46	25.67	52.99	6.26	2.0732
16	55.51	46.88	26.76	97.28	27.26	52.5	6.33	2.0479
17	56.42	47.37	28.3	97.18	28.84	51.97	6.2	2.0235
18	57.22	47.71	29.83	96.71	30.5	51.51	6.8	1.9944
19	57.9	48.06	31.04	96.53	31.77	51.09	6.89	1.9737
20	58.58	48.32	32.41	95.96	33.29	50.68	7.58	1.9455
21	59.49	48.8	34.01	95.68	35.01	50.1	7.71	1.9174
22	59.83	48.89	34.77	95.21	35.9	49.88	8.28	1.8995
23	60.14	49.01	35.38	94.93	36.59	49.68	8.57	1.8864
24	60.7	49.22	36.22	94.37	37.93	49.29	9.13	1.861
25	61.12	49.31	37.48	93.71	39.07	49	9.82	1.8376
26	61.77	49.63	38.66	93.33	40.41	48.55	10.04	1.8141
27	62.75	50.15	40.42	92.86	42.38	47.84	10.23	1.7803
28	63.77	50.72	42.24	92.39	44.41	47.07	10.38	1.7455
29	64.57	51	43.88	91.36	46.44	46.42	11.18	1.7052
30	65.4	51.49	45.33	90.99	48.09	45.74	11.25	1.677
31	65.78	51.37	46.41	89.58	49.68	45.36	12.43	1.6394
32	66.2	51.36	47.44	88.45	51.14	44.94	13.25	1.6066
33	66.65	51.35	48.54	87.23	52.73	44.47	14.08	1.5709
34	67.37	51.63	49.94	86.29	54.57	43.76	14.53	1.5343
35	68.47	52.16	51.96	85.16	57.18	42.63	14.93	1.4845
36	68.89	52.1	52.98	83.85	58.77	42.09	15.68	1.4479
37	69.31	52.18	53.85	83	60.04	41.57	16.07	1.4207
38	70.1	52.5	55.35	81.88	62.13	40.6	16.48	1.3784
39	70.41	52.44	56.07	80.85	63.34	40.13	16.99	1.3502
40	70.29	51.72	56.42	78.87	64.49	39.96	18.15	1.3136
41	70.63	51.56	57.28	77.46	66.01	39.34	18.76	1.277
42	70.63	50.61	58	74.55	67.98	38.83	20.21	1.2188
43	70.9	50.1	58.88	72.39	69.89	38.07	21.09	1.169
44	70.97	49.47	59.45	70.42	71.35	37.55	21.91	1.1277

Overall cont.

Percent	HR	TS	TSN	POD	PODN	FAR	FARN	BIAS
45	70.86	48.7	59.72	68.54	72.43	37.29	22.71	1.093
46	71.2	48.44	60.52	67.04	74.02	36.42	23.15	1.0545
47	71.28	47.8	61.03	65.16	75.41	35.8	23.81	1.015
48	70.63	46.14	60.76	62.35	76.24	36.03	25.05	0.9746
49	70.37	45.12	60.82	60.38	77.13	35.89	25.79	0.9418
50	70.56	44.54	61.44	58.59	78.65	35	26.27	0.9014
51	70.37	43.33	61.69	56.15	79.99	34.5	27.06	0.8573
52	70.48	42.68	62.17	54.46	81.32	33.64	27.48	0.8207
53	70.1	41.25	62.16	52.02	82.34	33.41	28.28	0.7812
54	70.25	40.58	62.67	50.33	83.74	32.32	28.64	0.7437
55	70.06	39.69	62.72	48.83	84.43	32.02	29.08	0.7183
56	70.14	39.06	63.07	47.42	85.51	31.11	29.38	0.6883
57	69.84	37.86	63.05	45.54	86.28	30.81	29.93	0.6582
58	69.76	37.02	63.23	44.04	87.17	30.1	30.28	0.63
59	69.69	35.69	63.55	41.69	88.63	28.73	30.8	0.585
60	69.23	34.2	63.37	39.62	89.26	28.6	31.4	0.5549
61	68.78	32.62	63.21	37.46	89.96	28.37	31.99	0.523
62	68.44	31.27	63.14	35.59	90.66	27.95	32.47	0.4939
63	68.13	29.92	63.11	33.71	91.42	27.33	32.91	0.4639
64	67.87	28.56	63.13	31.83	92.25	26.46	33.33	0.4329
65	67.49	27.04	63.03	29.86	92.95	25.87	33.8	0.4028
66	67.49	26.48	63.18	29.01	93.52	24.82	33.93	0.3859
67	67.15	25.19	63.06	27.42	94.03	24.35	34.31	0.3624
68	67.18	24.3	63.32	26.1	94.98	22.13	34.49	0.3352
69	66.84	23.04	63.19	24.6	95.43	21.56	34.84	0.3136
70	66.69	21.8	63.28	23	96.25	19.41	35.12	0.2854
71	66.43	20.75	63.19	21.78	96.63	18.6	35.39	0.2676
72	66.28	20.11	63.15	21.03	96.89	17.95	35.55	0.2563
73	65.86	18.97	62.89	19.81	97.01	18.22	35.87	0.2423
74	65.52	18.01	62.69	18.78	97.14	18.37	36.13	0.23
75	65.37	17.13	62.69	17.75	97.59	16.74	36.32	0.2131
76	65.14	16.36	62.59	16.9	97.78	16.28	36.51	0.2019
77	64.72	15.21	62.34	15.68	97.9	16.5	36.82	0.1878
78	64.15	13.69	61.99	14.08	98.03	17.13	37.23	0.17
79	63.66	12.5	61.67	12.86	98.03	18.42	37.56	0.1577
80	63.09	11.05	61.32	11.32	98.09	19.87	37.94	0.1418
81	62.68	9.7	61.1	10.05	98.28	20.15	38.24	0.1258
82	62.49	9.26	60.99	9.48	98.35	20.47	38.38	0.1192
83	62.22	8.36	60.87	8.54	98.54	20.18	38.57	0.107
84	62.03	7.56	60.81	7.7	98.79	18.81	38.73	0.0948

Overall cont. 2

Percent	HR	TS	TSN	POD	PODN	FAR	FARN	BIAS
85	61.92	6.86	60.82	6.95	99.11	15.91	38.85	0.0826
86	61.69	6.3	60.68	6.38	99.11	17.07	38.99	0.077
87	61.58	5.76	60.65	5.82	99.3	15.07	39.09	0.0685
88	61.27	5.019	60.46	5.07	99.3	16.92	39.28	0.061
89	61.18	4.66	60.45	4.69	99.43	15.25	39.34	0.0554
90	61.01	4.19	60.33	4.23	99.43	16.67	39.46	0.0507
91	60.89	3.91	60.26	3.94	99.43	17.65	39.53	0.0479
92	60.86	3.55	60.28	3.57	99.62	13.64	39.58	0.0413
93	60.63	2.99	60.15	3	99.62	15.79	39.72	0.0357
94	60.55	2.71	60.12	2.72	99.68	14.71	39.77	0.0319

May

Percent	HR	TS	TSN	POD	PODN	FAR	FARN	Bias
25	71.08	45.87	61.7	90.98	63.75	51.95	4.95	1.8934
26	71.74	46.44	62.57	90.98	64.65	51.32	4.89	1.8689
27	73.29	47.84	64.62	90.98	66.77	49.77	4.74	1.8115
28	75.06	49.33	67.06	90.16	69.49	47.87	4.96	1.7295
29	75.72	49.07	68.3	86.89	71.6	47	6.32	1.6393
30	76.82	50	69.83	86.07	73.41	45.6	6.54	1.582
31	77.04	49.51	70.37	83.61	74.62	45.16	7.49	1.5246
32	77.92	50.25	71.59	82.79	76.13	43.89	7.69	1.4754
33	77.26	48.5	71.07	79.51	76.44	44.57	8.99	1.4344
34	79.03	50.52	73.31	79.51	78.85	41.92	8.74	1.3689
35	79.03	49.74	73.54	77.05	79.76	41.61	9.59	1.3197
36	80.35	51.1	75.28	76.23	81.87	39.22	9.67	1.2541
37	81.02	51.41	76.24	74.59	83.38	37.67	10.1	1.1967
38	81.02	50.86	76.37	72.95	83.99	37.32	10.61	1.1639
39	81.24	50.58	76.78	71.31	84.89	36.5	11.08	1.123
40	81.46	50.3	77.17	69.67	85.8	35.61	11.53	1.082
41	82.12	50.91	78.05	68.85	87.01	33.86	11.66	1.041
42	83	51.57	79.25	67.21	88.82	31.09	11.98	0.9754
43	82.34	49.37	78.67	63.93	89.12	31.58	12.98	0.9344
44	81.9	47.1	78.42	59.84	90.03	31.13	14.12	0.8689
45	81.9	46.41	78.53	58.2	90.63	30.39	14.53	0.8361
46	82.56	46.62	79.43	56.56	92.15	27.37	14.8	0.7787
47	82.34	45.58	79.27	54.92	92.45	27.17	15.24	0.7541
48	81.68	43.54	78.66	52.46	92.45	28.09	15.93	0.7295
49	81.68	43.15	78.72	51.64	92.75	27.59	16.12	0.7131
50	81.24	40.97	78.43	48.36	93.35	27.16	16.94	0.6639

May cont.

Percent	HR	TS	TSN	POD	PODN	FAR	FARN	BIAS
51	81.24	39.29	78.64	45.08	94.56	27.16	17.63	0.5984
52	80.79	36.96	78.36	41.8	95.17	23.88	18.39	0.5492
53	80.13	34.31	77.83	38.52	95.47	24.19	19.18	0.5082
54	80.13	33.33	77.94	36.89	96.07	22.41	19.49	0.4754
55	79.91	32.09	77.8	35.25	96.37	21.82	19.85	0.4508
56	79.47	29.55	77.54	31.97	96.98	20.41	20.54	0.4016
57	79.03	27.48	77.22	29.51	97.28	20	21.08	0.3689
58	78.15	23.85	76.54	25.41	97.58	20.51	21.98	0.3197
59	77.48	21.54	76	22.95	97.58	22.22	22.54	0.2951
60	77.48	20.93	76.06	22.13	97.89	20.59	22.67	0.2787
61	76.82	18.6	75.52	19.67	97.89	22.58	23.22	0.2541
62	76.6	17.19	75.41	18.03	98.19	21.43	23.53	0.2295
63	76.38	15.08	75.35	15.57	98.79	17.39	23.95	0.1885
64	76.16	13.6	75.23	13.93	99.09	15	24.25	0.1639
65	75.5	11.2	74.72	11.48	99.09	17.65	24.77	0.1393
66	75.28	10.4	74.55	10.66	99.09	18.75	24.94	0.1311
67	75.06	9.6	74.38	9.84	99.09	20	25.11	0.123
68	75.06	9.6	74.38	9.84	99.09	20	25.11	0.123
69	75.06	8.13	74.49	8.2	99.7	9.09	25.34	0.0902
70	74.83	7.32	74.32	7.38	99.7	10	25.51	0.082
71	74.83	7.32	74.32	7.38	99.7	10	25.51	0.082
72	74.83	7.32	74.32	7.38	99.7	10	25.51	0.082
73	74.61	6.5	74.16	6.56	99.7	11.11	25.68	0.0738
74	74.61	5.74	74.22	5.74	100	0	25.78	0.0574
75	74.61	5.74	74.22	5.74	100	0	25.78	0.0574

June

	Percent	HR	TS	TSN	POD	PODN	FAR	FARN	Bias
	25	63.85	54.46	36.33	96.92	37.23	44.58	6.25	1.7489
	26	65.03	55.28	38.41	96.92	39.36	43.73	5.93	1.7225
	27	65.82	55.84	39.79	96.92	40.78	43.15	5.74	1.7049
	28	66.21	56.01	40.69	96.48	41.84	42.82	6.35	1.6872
	29	66.99	56.36	42.47	95.59	43.97	42.13	7.46	1.652
	30	67.58	56.81	43.49	95.59	45.04	41.67	7.3	1.6388
	31	67.58	56.58	43.88	94.71	45.74	41.58	8.51	1.6212
	32	67.98	56.88	44.56	94.71	46.45	41.26	8.39	1.6123
	33	68.57	56.99	46.13	93.39	48.58	40.62	9.87	1.5727
	34	68.76	57.03	46.64	92.95	49.29	40.4	10.32	1.5595
	35	70.53	58.33	49.83	92.51	52.84	38.78	10.24	1.511
	36	71.51	59.04	51.67	92.07	54.96	37.8	10.4	1.4802
	37	71.91	59.26	52.49	91.63	56.03	37.35	10.73	1.4626
	38	73.67	60.7	55.63	91.19	59.57	35.51	10.64	1.4141
	39	74.07	60.95	56.44	90.75	60.64	35.02	10.94	1.3965
	40	74.07	60.48	57	88.99	62.06	34.63	12.5	1.3612
	41	73.87	60.06	56.96	88.11	62.41	34.64	13.3	1.348
	42	73.87	59.57	57.51	86.34	63.83	34.23	14.69	1.3128
	43	74.07	59.38	58.23	85.02	65.25	33.68	15.6	1.2819
	44	74.26	59.44	58.68	84.58	65.96	33.33	15.84	1.2687
	45	74.66	59.56	59.56	83.7	67.38	32.62	16.3	1.2423
	46	75.05	59.68	60.44	82.82	68.79	31.88	16.74	1.2159
	47	75.25	59.49	61.11	81.5	70.21	31.23	17.5	1.185
	48	74.85	58.58	60.98	79.74	70.92	31.18	18.7	1.1586
	49	74.46	57.65	60.84	77.97	71.63	31.13	19.84	1.1322
	50	74.46	56.95	61.42	75.77	73.4	30.36	20.99	1.0881

June cont.

Percent	HR	TS	TSN	POD	PODN	FAR	FARN	BIAS
51	73.87	55.22	61.45	72.25	75.18	29.91	22.91	1.0308
52	73.87	54.61	61.89	70.48	76.6	29.2	23.67	0.9956
53	73.48	53.45	61.86	68.28	77.66	28.9	24.74	0.9604
54	73.48	52.96	62.18	66.96	78.72	28.3	25.25	0.9339
55	73.48	52.63	62.4	66.08	79.43	27.88	25.58	0.9163
56	74.07	52.69	63.54	64.76	81.56	26.13	25.81	0.8767
57	73.48	51.26	63.22	62.56	82.27	26.04	26.81	0.8458
58	74.07	51.65	64.13	62.11	83.69	24.6	26.71	0.8238
59	73.67	50.37	64.08	59.91	84.75	24.02	27.58	0.7885
60	72.69	48.33	63.32	57.27	85.11	24.42	28.78	0.7577
61	72.69	47.74	63.61	55.95	86.17	23.49	29.15	0.7313
62	72.5	46.77	63.73	54.19	87.23	22.64	29.71	0.7004
63	72.1	45.17	63.78	51.54	88.65	21.48	30.56	0.6564
64	71.71	43.97	63.64	49.78	89.36	20.98	31.15	0.63
65	69.94	40	62.41	44.93	90.07	21.54	32.98	0.5727
66	70.33	40.08	62.99	44.49	91.13	19.84	32.9	0.5551
67	69.94	38.8	62.86	42.73	91.84	19.17	33.42	0.5286
68	69.55	36.73	63.01	39.65	93.62	16.67	34.16	0.4758
69	68.57	34.16	62.44	36.56	94.33	16.16	35.12	0.4361
70	67.39	30.54	61.93	32.16	95.74	14.12	36.32	0.3744
71	66.99	29.11	61.82	30.4	96.45	12.66	36.74	0.348
72	66.21	27.12	61.35	28.19	96.81	12.33	37.39	0.3216
73	65.62	25.85	60.94	26.87	96.81	12.86	37.81	0.3084
74	65.23	24.68	60.75	25.55	97.16	12.12	38.15	0.2907
75	64.64	23.08	60.44	23.79	97.52	11.48	38.62	0.2687

July

Percent	HR	TS	TSN	POD	PODN	FAR	FARN	Bias
25	64.37	57.11	32.21	96.07	33.45	41.52	10.28	1.6429
26	65.26	57.63	34.11	95.71	35.54	40.84	10.53	1.6179
27	65.61	57.79	35	95.36	36.59	40.53	11.02	1.6036
28	66.31	58.21	36.54	95	38.33	39.95	11.29	1.5821
29	67.02	58.72	37.87	95	39.72	39.41	10.94	1.5679
30	67.2	58.67	38.61	94.29	40.77	39.17	12.03	1.55
31	67.9	58.92	40.52	93.21	43.21	38.44	13.29	1.5143
32	67.72	58.41	40.97	91.79	44.25	38.37	15.33	1.4893
33	68.25	58.81	41.94	91.79	45.3	37.92	15.03	1.4786
34	68.78	59.03	43.27	91.07	47.04	37.35	15.63	1.4536
35	68.61	58.6	43.49	90	47.74	37.31	16.97	1.4357
36	69.31	59.06	44.94	89.64	49.48	36.62	16.96	1.4143
37	69.49	59	45.6	88.93	50.52	36.32	17.61	1.3964
38	69.67	59.05	46.08	88.57	51.22	36.08	17.88	1.3857
39	70.02	59.23	46.88	88.21	52.26	35.68	18.03	1.3714
40	70.19	59.28	47.35	87.86	52.96	35.43	18.28	1.3607
41	70.72	59.61	48.45	87.5	54.36	34.84	18.32	1.3429
42	70.02	58.33	48.33	85	55.4	34.97	20.9	1.3071
43	71.08	59	50.45	84.29	58.19	33.71	20.85	1.2714
44	71.78	59.18	52.24	82.86	60.98	32.56	21.52	1.2286
45	72.13	59.28	53.12	82.14	62.37	31.95	21.83	1.2071
46	71.78	58.66	52.94	81.07	62.72	32.04	22.75	1.1929
47	71.6	58.07	53.2	79.64	63.76	31.8	23.75	1.1679
48	71.25	56.99	53.56	77.14	65.51	31.43	25.4	1.125
49	71.25	56.65	53.95	76.07	66.55	31.07	25.97	1.1036
50	71.43	56.45	54.62	75	67.94	30.46	26.42	1.0786

July cont.

Percent	HR	TS	TSN	POD	PODN	FAR	FARN	Bias
51	71.25	55.83	54.85	73.57	68.99	30.17	27.21	1.0536
52	71.78	56.04	55.92	72.86	70.73	29.17	27.24	1.0286
53	71.6	55.4	56.13	71.43	71.78	28.83	27.97	1.0036
54	71.96	55.34	57.03	70.36	73.52	27.84	28.23	0.975
55	72.49	55.68	57.95	70	74.91	26.87	28.09	0.9571
56	72.49	55.56	58.06	69.64	75.26	26.69	28.24	0.95
57	72.49	55.17	58.4	68.57	76.31	26.15	28.66	0.9286
58	73.19	55.69	59.57	68.21	78.05	24.8	28.43	0.9071
59	73.02	54.87	59.84	66.43	79.44	24.08	29.19	0.875
60	72.66	54	59.74	65	80.14	23.85	29.88	0.8536
61	72.49	53.29	59.9	63.57	81.18	23.28	30.45	0.8286
62	72.13	52.41	59.8	62.14	81.88	23.01	31.09	0.8071
63	71.78	51.22	59.9	60	83.28	22.22	31.91	0.7714
64	71.96	50.93	60.45	58.93	84.67	21.05	32.12	0.7464
65	72.13	51.08	60.7	58.93	85.02	20.67	32.03	0.7429
66	71.78	50.16	60.59	57.5	85.71	20.3	32.6	0.7214
67	71.25	48.9	60.34	55.71	86.41	20	33.33	0.6964
68	70.72	47.47	60.19	53.57	87.46	19.35	34.12	0.6643
69	70.37	46.67	60	52.5	87.8	19.23	34.55	0.65
70	70.37	45.81	60.47	50.71	89.55	17.44	34.94	0.6143
71	70.02	44.81	60.37	49.29	90.24	16.87	35.41	0.5929
72	70.19	44.77	60.7	48.93	90.94	15.95	35.4	0.5821
73	69.49	43.09	60.32	46.79	91.64	15.48	36.17	0.5536
74	68.25	40.79	59.37	44.29	91.64	16.22	37.23	0.5286
75	67.2	38.61	58.67	41.79	92	16.43	38.17	0.5

August

Percent	HR	TS	TSN	POD	PODN	FAR	FARN	Bias
25	51.3	46.78	14.85	91.14	16.01	50.99	32.88	1.8598
26	51.13	46.39	15.32	90.04	16.67	51.1	36.62	1.8413
27	51.65	46.35	16.96	88.93	18.63	50.82	34.48	1.8081
28	52.51	46.8	18.45	88.93	20.26	50.31	32.61	1.7897
29	53.21	46.75	20.59	87.45	22.88	49.89	32.69	1.7454
30	53.73	46.92	21.71	87.08	24.18	49.57	32.11	1.7269
31	54.42	46.98	23.55	85.98	26.47	49.13	31.93	1.69
32	54.25	46.34	24.36	84.13	27.78	49.22	33.59	1.6568
33	55.29	46.58	26.7	83.03	30.72	48.51	32.86	1.6126
34	55.63	46.44	27.89	81.92	32.35	48.25	33.11	1.583
35	57.19	47	31.01	80.81	36.27	47.1	31.9	1.5277
36	56.5	45.91	31.04	78.6	36.93	47.54	33.92	1.4982
37	57.19	46.3	32.14	78.6	38.24	47.01	33.14	1.4834
38	56.85	45.15	33.06	75.65	40.2	47.17	34.92	1.4317
39	57.02	44.89	33.87	74.54	41.5	46.98	35.2	1.4059
40	56.67	43.82	34.56	71.96	43.14	47.15	36.54	1.3616
41	57.02	43.25	36.08	69.74	45.75	46.76	36.94	1.31
42	57.37	42.25	38.04	66.42	49.35	46.27	37.6	1.2362
43	57.71	41.9	39.15	64.94	51.31	45.85	37.7	1.1993
44	57.71	40.92	40.2	62.36	53.59	45.66	38.35	1.1476
45	56.5	38.93	39.81	59.04	54.25	46.67	40.07	1.107
46	57.19	38.56	41.47	57.2	57.19	45.8	39.86	1.0554
47	57.02	37.69	41.92	55.35	58.5	45.85	40.33	1.0221
48	56.5	36.13	42.3	52.4	60.13	46.21	41.21	0.9742
49	55.29	33.85	42.02	48.71	61.11	47.41	42.64	0.9262
50	55.81	33.59	43.08	47.6	63.07	46.69	42.39	0.893

August cont.

Percent	HR	TS	TSN	POD	PODN	FAR	FARN	Bias
51	56.33	32.98	44.37	45.76	65.69	45.85	42.24	0.845
52	56.67	32.61	45.18	44.65	67.32	45.25	42.13	0.8155
53	56.85	31.22	46.34	41.7	70.26	44.61	42.36	0.7528
54	56.5	29.49	46.82	38.75	72.22	44.74	42.89	0.7011
55	55.63	27.68	46.56	36.16	72.88	45.86	43.69	0.6679
56	55.63	26.65	47.11	34.32	74.51	45.61	43.84	0.631
57	55.63	25.36	47.76	32.1	76.47	45.28	44.02	0.5867
58	54.94	23.53	47.69	29.52	77.45	46.31	44.63	0.5498
59	55.29	21.34	49.11	25.83	81.37	44.88	44.67	0.4686
60	54.25	18.77	48.84	22.51	82.35	46.96	45.45	0.4244
61	53.73	16.56	49.05	19.56	83.99	48.04	45.89	0.3764
62	53.03	14.24	49.06	16.61	85.29	50	46.41	0.3321
63	52.86	13.38	49.16	15.5	85.95	50.59	46.54	0.3137
64	52.51	11.33	49.45	12.92	87.58	52.05	46.83	0.2694
65	52.69	9.9	50.09	11.07	89.54	51.61	46.8	0.2288
66	52.86	9.33	50.46	10.33	90.52	50.88	46.73	0.2103
67	52.51	7.74	50.54	8.49	91.5	53.06	46.97	0.1808
68	53.21	7.53	51.35	8.12	93.14	48.84	46.63	0.1587
69	52.86	6.21	51.34	6.64	93.79	51.35	46.85	0.1365
70	53.38	5.94	51.96	6.27	95.1	46.88	46.61	0.1181
71	53.03	4.58	51.95	4.8	95.75	50	46.82	0.0959
72	53.03	4.24	52.04	4.43	96.08	50	46.84	0.0886
73	52.69	3.53	51.85	3.69	96.08	54.55	47.03	0.0812
74	52.69	3.53	51.85	3.69	96.08	54.55	47.03	0.0812
75	53.55	3.6	52.73	3.69	97.71	41.18	46.61	0.0627

September

	Percent	HR	TS	TSN	POD	PODN	FAR	FARN	Bias
	25	57.22	39.84	40.31	91.52	41.85	58.63	8.33	2.2121
	26	57.97	40.27	41.36	91.52	42.93	58.17	8.14	2.1879
	27	59.85	41.21	44.13	90.91	45.92	57.02	8.15	2.1152
	28	61.35	41.81	46.49	89.7	48.64	56.08	8.67	2.0424
	29	62.48	42.36	48.19	89.09	50.54	55.32	8.82	1.9939
	30	64.35	43.62	50.78	89.09	53.26	53.92	8.41	1.9333
	31	64.54	43.07	51.54	86.67	54.62	53.87	9.87	1.8788
	32	65.85	43.65	53.57	85.45	57.07	52.84	10.26	1.8121
	33	66.42	43.53	54.68	83.64	58.7	52.41	11.11	1.7576
	34	67.35	43.51	56.39	81.21	61.14	51.62	12.11	1.6788
	35	69.61	44.9	59.6	80	64.95	49.43	12.13	1.5818
	36	69.61	43.94	60.1	76.97	66.3	49.4	13.48	1.5212
	37	69.79	43.31	60.73	74.55	67.66	49.17	14.43	1.4667
	38	72.23	45.39	63.9	74.55	71.2	46.29	13.82	1.3879
	39	72.61	44.91	64.73	72.12	72.83	45.66	14.65	1.3273
	40	72.05	42.91	64.61	67.88	73.91	46.15	16.31	1.2606
	41	72.42	42.13	65.49	64.85	75.82	45.41	17.21	1.1879
	42	72.05	39.68	65.75	59.39	77.72	45.56	18.98	1.0909
	43	72.23	37.29	66.74	53.33	80.71	44.65	20.59	0.9636
	44	72.05	36.05	66.82	50.91	81.52	44.74	21.26	0.9212
	45	72.05	34.65	67.18	47.88	82.88	44.37	21.99	0.8606
	46	72.42	33.78	67.9	45.45	84.51	43.18	22.44	0.8
	47	73.17	32.55	69.18	41.82	87.23	40.52	23.02	0.703
	48	71.86	28.91	68.22	36.97	87.5	42.99	24.41	0.6485
	49	72.23	28.16	68.84	35.15	88.86	41.41	24.65	0.6
	50	72.8	27.14	69.73	32.73	90.76	38.64	24.94	0.5333

September Cont.

Percent	HR	TS	TSN	POD	PODN	FAR	FARN	Bias
51	72.05	24.75	69.21	29.7	91.03	40.24	25.72	0.497
52	72.05	22.8	69.53	26.67	92.39	38.89	26.25	0.4364
53	71.11	20.21	68.83	23.64	92.39	41.79	27.04	0.4061
54	71.86	19.79	69.76	22.42	94.02	37.29	27	0.3576
55	71.48	17.84	69.6	20	94.57	37.74	27.5	0.3212
56	71.67	17.03	69.92	18.79	95.38	35.42	27.63	0.2909
57	71.11	15.38	69.51	16.97	95.38	37.78	28.07	0.2727
58	70.92	14.36	69.43	15.76	95.65	38.1	28.31	0.2545
59	71.29	13.56	69.94	14.55	96.74	33.33	28.37	0.2182
60	71.48	12.64	70.25	13.33	97.55	29.03	28.49	0.1879
61	70.54	9.77	69.57	10.3	97.55	34.62	29.19	0.1576
62	70.36	8.67	69.05	9.09	97.83	34.78	29.41	0.1394
63	69.98	7.51	69.23	7.88	97.83	38.1	29.69	0.1273
64	69.42	5.23	68.89	5.45	98.1	43.75	30.17	0.0967
65	69.42	4.12	69.01	4.24	98.64	41.67	30.33	0.0727
66	69.42	3.55	69.07	3.64	98.91	40	30.4	0.0606
67	69.23	2.38	69	2.42	99.18	42.86	30.61	0.0424
68	69.61	2.41	69.38	2.42	99.73	20	30.49	0.0303
69	69.61	2.41	69.38	2.42	99.73	20	30.49	0.0303
70	69.61	2.41	69.38	2.42	99.73	20	30.49	0.0303
71	69.42	1.81	69.25	1.82	99.73	25	30.62	0.0242
72	69.23	1.2	69.11	1.21	99.73	33.33	30.75	0.0182
73	69.04	0.6	68.99	0.61	99.73	50	30.89	0.0121
74	69.04	0.6	68.99	0.61	99.73	50	30.89	0.0121
75	69.04	0.6	68.99	0.61	99.73	50	30.89	0.0121

These tables represent the NPTI statistics for each threshold percentile. They are divided by month to correspond to figures 5 – 16. These tables will allow any percentile to be chosen as the threshold and view the statistics calculated for that percentile. This is a summation of the climatological data sets statistics.

Appendix G. Example Output from the NPTI Code

Output from the NPTI code in the ten-by-ten matrix around Cape Canaveral. The probability calculated from each part of the NPTI is shown as well as the total thunderstorm probability forecast. This example is for the 28th of August, 1997.

August 28, 1997

Probability from 850-mb winds

37	36	33	30	28	27	26	25	24	24
35	34	32	30	29	27	26	24	24	23
32	32	32	31	30	28	26	24	23	23
31	31	31	30	29	27	26	25	24	23
29	30	29	29	28	27	26	25	24	24
28	29	28	28	27	27	26	25	25	25
28	29	29	28	27	26	26	25	25	26
28	29	30	28	26	26	25	25	25	26
27	29	30	28	26	26	26	25	25	25
27	28	29	28	27	26	25	25	24	25

Probability from 500-mb winds

40	41	43	45	47	49	52	55	57	59
40	42	44	46	48	50	53	55	58	60
42	43	45	47	49	51	54	57	59	61
43	45	47	49	51	53	55	57	60	62
45	46	48	51	53	55	57	58	60	63
46	48	50	52	54	56	58	59	61	63
48	49	51	53	55	57	59	60	61	63
50	51	53	55	56	58	59	60	62	63
52	53	55	56	57	58	59	60	61	62
54	55	56	57	57	58	59	59	60	62

Probability from relative humidity

9	9	10	10	9	8	8	8	8	9
8	7	6	5	4	4	4	4	4	5
5	4	3	3	3	3	3	3	3	3
3	3	3	3	3	3	3	4	5	5
3	3	3	3	3	3	3	4	6	8
4	3	3	3	3	3	3	3	5	9
6	4	4	3	3	3	3	3	4	8
9	7	5	4	3	3	3	3	4	6
12	11	8	6	5	4	4	4	4	5
18	17	14	11	9	8	6	5	5	5

Probability from Showalter Stability Index

30	28	27	23	20	19	19	18	19	19
27	26	25	23	21	20	19	18	17	17
27	26	26	25	24	23	21	21	21	21
28	28	27	27	26	25	24	23	24	26
30	29	30	30	29	26	25	24	25	26
29	30	31	31	29	26	24	23	24	26
29	30	31	32	30	26	22	21	24	26
28	29	31	32	30	24	22	20	22	25
28	28	30	30	28	23	21	20	21	23
30	29	29	28	26	24	23	22	22	23

Probability from climatology

34	34	34	34	34	34	34	34	34	34
34	34	34	34	34	34	34	34	34	34
34	34	34	34	34	34	34	34	34	34
34	34	34	34	34	34	34	34	34	34
34	34	34	34	34	34	34	34	34	34
34	34	34	34	34	34	34	34	34	34
34	34	34	34	34	34	34	34	34	34
34	34	34	34	34	34	34	34	34	34
34	34	34	34	34	34	34	34	34	34
34	34	34	34	34	34	34	34	34	34

Total NPTI Probability

16	15	14	10	8	7	7	8	8	9
13	12	11	9	8	6	6	6	6	7
11	11	11	10	10	9	8	7	8	9
11	11	12	12	11	10	10	10	11	13
11	12	13	13	13	11	11	11	13	15
11	12	13	14	13	12	11	11	13	16
12	13	15	14	13	11	10	10	12	16
14	14	16	16	14	11	10	10	11	14
15	16	17	16	14	11	10	9	10	13
19	20	19	18	15	13	12	10	11	12

KTTS Probability = 12.25

Bibliography

- Bauman, William H., M. L. Kaplan, and S. Businger, 1997: Nowcasting Convective Activity for Space Shuttle Landings during Easterly Flow Regimes. *Wea. Forecasting*, **12**, 78-107.
- Black, T. L., 1994: The New NMC Mesoscale Eta Model: Description and Forecast Examples. *Wea. Forecasting*, **9**, 265-278.
- Bluestein, H. B., 1993: *Synoptic-Dynamic Meteorology in Midlatitudes, Volume II: Observations and Theory of Weather Systems*. Oxford University Press, Inc., 426-579.
- Byers, H. R., and H. R. Rodebush, 1948: Causes of Thunderstorms of the Florida Peninsula. *J. Meteor.*, **5**, 275-280.
- Cetola, J. D., 1997: *A Climatology of the Sea Breeze at Cape Canaveral, Florida*. Masters Thesis, Florida State University, 56 pp.
- Dey, Clifford H., 1996: National Centers For Environmental Prediction Office Note 388, *GRIB (edition 1): The WMO Format For The Storage Of Weather Product Information And The Exchange Of Weather Product Messages In Gridded Binary Form*. NCEP Central Operations, 100 pp.
- Duffield, George F., and G. D. Nastrom, 1983: AWS/TR-83/001, *Equations and Algorithms for Meteorological Applications in Air Weather Service*. Air Weather Service, 58 pp.
- Everitt, B. S., 1992: *The Analysis of Contingency Tables*. 2nd ed., Chapman & Hall, 164 pp.
- Haltiner, G. J., and R. T. Williams, 1980: *Numerical Prediction and Dynamic Meteorology*. 2nd ed., John Wiley & Sons, 477 pp.
- Montz, John M., and R. C. Sloane, 1943: *Elements of Topographic Drawing*. McGraw-Hill Co., Inc., 250 pp.
- NASA Contract Report. CR-205409, 1997: *Evaluation of the 29-km Eta Model for Weather Support to the United States Space Program*. Applied Meteorology Unit, 91 pp.

- Neumann, C. J., 1968: Weather Bureau Technical Memorandum SOS-2, *Frequency and Duration of Thunderstorms at Cape Kennedy, Part I*. Spaceflight Meteorology Group, 26 pp.
- Neumann, C. J., 1970: ESSA Technical Memorandum WBTM SOS-6, *Frequency and Duration of Thunderstorms at Cape Kennedy, Part II (Application to Forecasting)*. Spaceflight Meteorology Group, 32 pp.
- Neumann, C. J., 1971: NOAA Technical Memorandum NWS SOS-8, *Thunderstorm Forecasting at Cape Kennedy, Florida, Utilizing Multiple Regression Techniques*. Spaceflight Meteorology Group, 45 pp.
- Pielke, Roger A., 1974: A Three-Dimensional Numerical Model of the Sea Breeze Over South Florida. *Mon. Wea. Rev.*, **102**, 115-139.
- Roeder, W. P., F. J. Merceret, S. J. Sokol, S. T. Heckman, and G. E. Taylor, 1997: *Operational Meteorological Research Requirements on the Central Florida Atlantic Coast in Support of the United States Space Program*. 45th Weather Squadron, Patrick AFB, FL, 9 pp.
- Staudenmaier, Mike, Jr., 1996: Western Region Technical Attachment No.96-06, *A Description of the Meso Eta Model*. NWSO-Sacramento, 4 pp.
- 1996: Western Region Technical Attachment No. 96-30, *The Initialization Procedure in the Meso Eta Model*. WRH-SSD/NWSFO-Salt Lake City, 5 pp.
- Wilks, D. S., 1995: *Statistical Methods in the Atmospheric Sciences*. Academic Press, 233-283.

Vita

Christian S. Wohlwend was born on 02 December 1973 in Carmichael, California, but he was raised in the small foothill town of El Dorado, California. He entered the Air Force on 29 June 1992, when he arrived at the United States Air Force Academy. He was commissioned through that institution on 29 May 1996, and graduated with a degree in Applied Physics. This degree had a specialization in space and atmospheric physics. This enabled Lieutenant Wohlwend to be posted as a weather officer. His first official assignment was to the Air Force Institute of Technology (AFIT) as a masters student in Meteorology. Following the completion of his AFIT tour, he will be assigned to the 88th Weather Squadron, Wright-Patterson AFB. His assignment will be as a Wing Weather Officer in the base weather station.

Christian was just married to the former Second Lieutenant Kirsten M. Larson, of Jupiter, Florida. They were married on 31 May 1997 after her graduation from the United States Air Force Academy. They currently have no children.

Permanent Address:

5745 Quartz Drive

El Dorado, CA 95623

REPORT DOCUMENTATION PAGE			Form Approved OMB No. 0704-0188	
Public reporting burden for this collection of information is estimated to average 1 hour per response, including the time for reviewing instructions, searching existing data sources, gathering and maintaining the data needed, and completing and reviewing the collection of information. Send comments regarding this burden estimate or any other aspect of this collection of information, including suggestions for reducing this burden, to Washington Headquarters Services, Directorate for Information Operations and Reports, 1215 Jefferson Davis Highway, Suite 1204, Arlington, VA 22202-4302, and to the Office of Management and Budget, Paperwork Reduction Project (0704-0188), Washington, DC 20503.				
1. AGENCY USE ONLY (Leave blank)		2. REPORT DATE March 1998		3. REPORT TYPE AND DATES COVERED Final
4. TITLE AND SUBTITLE Improving Cape Canaveral's Day-2 Thunderstorm Forecasting Using Meso-Eta Numerical Model Output			5. FUNDING NUMBERS	
6. AUTHOR(S) Christian S. Wohlwend, 2LT USAF				
7. PERFORMING ORGANIZATION NAME(S) AND ADDRESS(ES) AFIT/ENP 2950 P. Street Wright-Patterson AFB, OH 45433 Attn: LtCol Mike Walters COMM: (937) 255-3636 x4681 DSN: 785-3636 mwalters@afit.af.mil			8. PERFORMING ORGANIZATION REPORT NUMBER AFIT/GM/ENP/98M-12	
9. SPONSORING/MONITORING AGENCY NAME(S) AND ADDRESS(ES) 45 WS/SYR 1201 Minuteman Street Patrick AFB, FL 32925-3238 Attn: Mr. William Roeder COMM: (407) 853-8410 DSN: 467-8410 william-roeder@pafb.af.mil			10. SPONSORING/MONITORING AGENCY REPORT NUMBER	
11. SUPPLEMENTARY NOTES				
12a. DISTRIBUTION AVAILABILITY STATEMENT Approved for public release; distribution unlimited			12b. DISTRIBUTION CODE A	
13. ABSTRACT (Maximum 200 words) <p>The 45th Weather Squadron (WS) is responsible for the protection of billions of dollars worth of Air Force and NASA equipment from weather hazards. They produce a seven day planning forecast as one tool to support the space launch community. Improving this forecast can potentially save millions of dollars of government funds.</p> <p>This research focuses on the feasibility of improving the day-two thunderstorm forecast by applying Meso-Eta numerical forecasts to the Neumann-Pfeffer Thunderstorm Index (NPTI). The NPTI is currently used by the 45th WS for same-day thunderstorm probability forecasting utilizing the morning radiosonde as input. The perfect prognosis assumption was used when assessing the value of this technique.</p> <p>NPTI thunderstorm probabilities were calculated using input variables extracted from the day-two Meso-Eta. The NPTI output was verified against coincident thunderstorm observations taken at Cape Canaveral Air Station. Accuracy and bias statistics were used to calculate a forecasting skill score versus persistence. Statistically significant positive skill scores were produced, indicating that the proposed method is a potentially useful forecasting tool for day-two thunderstorm probability forecasting. A test of NPTI over 20 years of climatology revealed a moderately accurate forecasting method.</p>				
14. SUBJECT TERMS Meteorology, Numerical Weather Prediction, Meso-Eta Numerical Model, Thunderstorm Forecasting			15. NUMBER OF PAGES 188	
			16. PRICE CODE	
17. SECURITY CLASSIFICATION OF REPORT UNCLASSIFIED	18. SECURITY CLASSIFICATION OF THIS PAGE UNCLASSIFIED	19. SECURITY CLASSIFICATION OF ABSTRACT UNCLASSIFIED	20. LIMITATION OF ABSTRACT UL	